KUNGL
TEKNISKA
HÖGSKOLAN

TRITA-EES-0001
ISSN 1100-1607

On Load Flow Control in Electric Power Systems

Arnim Herbig

Stockholm 2000

Doctoral Dissertation
Royal Institute of Technology
Department of Electric Power Engineering
Electric Power Systems

KTH Högskoletryckeriet, Stockholm 2000

Abstract

This dissertation deals with the control of active power flow, or load flow, in electric power systems.

During the last few years, interest in the possibilities to control the active power flows in transmission systems has increased significantly. There is a number of reasons for this, coming both from the application side—that is, from power system operations—and from the technological side, where advances in power electronics and related technologies have made new system components available.

Load flow control is by nature a multi–input multi–output problem, since any change of load flow in one line will be complemented by changes in other lines. Strong cross–coupling between controllable components is to be expected, and the possibility of adverse interactions between these components cannot be rejected straightaway. Interactions with dynamic phenomena in the power system are also a source of concern.

Three controllable components are investigated in this thesis, namely the controlled series capacitor (CSC), the phase angle regulator (PAR), and the unified power flow controller (UPFC). Properties and characteristics of these devices are investigated and discussed.

A simple control strategy is proposed. This strategy is then analyzed extensively. Mathematical methods and physical knowledge about the pertinent phenomena are combined, and it is shown that this control strategy can be used for a fairly general class of devices. Computer simulations of the controlled system provide insight into the system behavior in a system of reasonable size. The robustness and stability of the control system are discussed as are its limits.

Further, the behavior of the control strategy in a system where the modeling allows for dynamic phenomena are is investigated with computer simulations. It is discussed under which circumstances the control action has beneficial or detrimental effect on the system dynamics.

Finally, a graphical approach for analyzing the effect of controllers on the closed–loop behavior of a system is discussed. The phase root locus technique is presented and its application to power systems illustrated.

TRITA-EES-0001 • ISSN 1100-1607

Acknowledgments

This dissertation covers the work I have carried out at the division of Electric Power Systems, Department of Electric Power Engineering, Royal Institute of Technology, since February 1995.

First, I would like to express my deepest gratitude and appreciation to my supervisor, Professor Göran Andersson. His skilled guidance, valuable comments, stimulating discussions and support throughout this project have been indispensable.

I wish to thank my colleagues at the division of electric power systems for the friendly atmosphere. Special thanks go to the secretary of the division Ms. Lillemor Hyllengren for her help in countless practical matters. I also owe thanks to Mr. Erik Thunberg, without whose help the computer administration would have kept me too busy to write this thesis, Mr. Mehrdad Ghandhari and Mr. Thomas Ackermann, who were always helpful friends and good company for the lunch breaks, Mr. Jonas Persson for his help with SIMPOW, and Dr. Lawrence Jones for his collaboration on papers and discussions on control theory.

Financial support from the Swedish NUTEK REGINA project is gratefully acknowledged.

I owe my utmost and lifelong gratitude to my parents for their unfaltering backing and encouragement and their support through the lows and delight in the highs through the years.

Last, but certainly not least, I would like to thank my fiancée Ms. Juleigh Giddens, who enriches my life in more ways than I can ever hope to express.

Arnim Herbig

Stockholm
February 2000

Acronyms

Acronym	Description
AC	Alternating Current
ANN	Artificial Neural Network
CSC	Controllable Series Capacitor
DC	Direct Current
FACTS	Flexible AC Transmission Systems
GTO	Gate–Turn–Off Thyristor
HVDC	High Voltage Direct Current
KBS	Knowledge Based System
LQG	Linear Quadratic Gaussian
MIMO	Multi–Input Multi–Output
NASA	National Aeronautics and Space Administration
NASREM	NASA/NIST Standard Reference Model for Telerobot Control System Architecture
NIST	National Institute of Standards and Technology
PAR	Phase Angle Regulator
SOFLIC	Self–Organizing Fuzzy Logic Control
UPFC	Unified Power Flow Controller

Contents

List of Figures

List of Tables

To my parents

Chapter 1

Introduction

Electricity is a very convenient and useful energy form. It plays an ever increasing role in our modern industrialized society. Intimately connected to this development is the development of power transmission systems as a means to distribute electrical energy. These power systems today face several changes.

The almost everywhere continuously increasing demand for electrical power makes it desirable to operate power systems closer to their thermal ratings than they currently are. Due to environmental concerns and right–of–way issues, the construction of new power lines is increasingly difficult. The prime responsibility of power system operators is to supply electric power safely and economically to customers. Since the measures necessary for secure operation often contradict those for economical operation, it is necessary to make a trade–off between these two objectives.

1.1 Control of Active Power Flow — Motivation

During the last several years interest in the possibilities to control the (active) power flows in transmission systems has increased significantly. There is a number of reasons for this, originating both from the application side—that is, from the power system operation—and from the technological side, that is, the advent of new system components such as semi–conductor based devices. In many countries the operation of power systems has changed due to higher utilization of the transmission network

and a deregulation of the power market [5]. In certain deregulated environments, transmission capacity becomes a commodity. For the use of transmission capacity, fees have to be paid, and the transmission grid operator depends economically on these fees. With the economic dependence on the grid comes the necessity to be able to control the transmission system as well as possible. The new components that are becoming feasible are to a large extent based on advances in power electronics and related technologies.

There are four main reasons why power flow control is attractive:

1. Overload alleviation. In a meshed power system, a situation where a low impedance line carries much more power than originally designed for, while parallel paths are underutilized, can occur. With power flow control, the stressed line can be relieved, resulting in a better overall utilization of the network.

2. Contractual requirements. These originate usually in either of the two situations described above. The transfer of power in a meshed network is likely to be accompanied by requests of the neighboring utilities that their networks are not influenced in an adverse way.

3. Currently, independent transmission projects are being discussed [6]. The idea is that private companies operate transmission lines and sell transmission capacity or energy to interested parties. In that environment, the load flow will obviously have to be controlled. One possibility is to use HVDC lines, another possibility is load flow control using FACTS devices in an AC network.

4. Loss reduction. Generally, total losses in a system cannot be reduced to such an extent that the installation of power flow controllers is justified. Easily avoidable are only the losses due to reactive power flow, which usually are quite small. A reduction of the losses due to active power flow would require a decrease of the line resistances, which necessitates drastic changes in the conductors.

   However, loss reduction in a particular area of the system is a relevant issue. Power transfers from one point to another will physically flow on a number of parallel paths and thereby impel losses on lines that might belong to another utility, thus causing increased costs for that company. If the latter utility cannot accept these losses, power flow control can be a solution.

The control of active power flow is in its general form by nature a multi–input multi–output (MIMO) problem. Since the active power has to be transferred through a number of paths in the system, any change of active power flow in one line will be complemented by changes in other lines. Strong cross–coupling between controllable components is to be expected, and the possibility of adverse effects between several such components, like hunting phenomena, cannot be rejected straightaway.

Speed is a minor issue for power flow control. The time frame in which an equilibrium should be reached can be measured in terms of seconds or even minutes. That makes it possible to use the same device for the control of dynamic phenomena in a power system as is used for power flow control, since the time frame of those dynamic phenomena is usually at most a few seconds.

1.2 Scope and Organization of this Thesis

In Chapter 2, some background on multivariable control is given. Methods for multivariable control are tentatively ordered in a taxonomy, which is juxtaposed to a scaling of control levels. Some guidelines for the choice of control methods depending on the control level are proposed.

Chapter 3 presents the idea of FACTS devices and discusses the devices used in this investigation. A concise description of a very recently introduced power flow control concept that does not need any high power electronic parts is given. Some other FACTS devices not treated in this thesis are mentioned.

In Chapter 4, multivariable power flow control using CSCs and PARs is investigated. A control scheme is proposed and examined first with an analytical and physical approach depending on a linearization, and then with nonlinear simulations. Limits of this control scheme are discussed.

In Chapter 5, a method for deciding where series capacitors should be located in an electric power system to maximize controllability is introduced. This method is based on an investigation of the sensitivities of the active power flow through one line to changes in series compensation in another or the same line. The validity of this method is checked by nonlinear simulations.

In Chapter 6, the characteristics of an additional FACTS device, the UPFC, are presented. These characteristics have been determined in a

realistic, meshed power system. The most efficient use of the UPFC's control variables is discussed.

Chapter 7 shows that the control scheme proposed for CSCs and PARs can be used in conjunction with the UPFC as well. Further, the possibility to use the shunt part of the UPFC to control bus voltages while load flow is controlled is investigated and discussed.

In Chapter 8, the large signal stability of the proposed control system is examined. Currently available methods for the analysis of the large signal stability of nonlinear systems are presented, and an attempt is made to apply these methods to the control system at hand. The implications of instability of the control system are discussed.

In Chapter 9, the control scheme is tested beyond the algebraic load flow model. One controllable series capacitor is implemented in a four–machine test system that exhibits moderately damped inter–area oscillations. An advantage and a disadvantage of fast and slow load flow control is discussed.

Chapter 10 is outside the topic of load flow control. In this chapter, the counterpart to the well-known Evans gain root locus [7], the phase root locus is introduced. Until recently [8], this concept has been largely ignored. The main differences between these techniques and their application to damping control design are discussed. The principle is illustrated by a power system example.

1.3 Contributions of this Thesis

Some of the work presented here has already been published [1, 2, 3, 4]. The main contributions of this thesis are:

- An overview of available multivariable control methods for control of power systems is given.
- A method for controlling load flow using a class of devices with a certain characteristic, namely monotonicity, is proposed. The method is investigated extensively, with physio-mathematical tools as well as with simulations. While the proposed method is fairly simple, it is robust with respect to system topology.

- The load flow and voltage characteristics of the unified power flow controller in a meshed system are presented.
- Properties of the load flow equations and their implications are developed and discussed.
- The influence of the proposed load flow control on dynamic phenomena is presented. The influence of the controller speed in a relevant situation is explained.
- The phase root locus technique is presented and illustrated. The use of phase root locus together with gain root locus for controller design is explained and demonstrated.

Chapter 2

Multivariable Control Strategies

The desire to control processes, in the broadest sense, has existed for a very long time [9]. In electrical engineering, the first explicit attempts to formalize control problems mathematically go back to James Maxwell. The invention of the negative feedback amplifier by Harold Black in 1927 [10], proposing the sacrifice of some amplification of a high–gain amplifier to reduce the influence of distortion due to noise and component drift, contained the fundamental ideas on which almost all modern controllers are based. The works of Harry Nyquist [11], Hendrick Bode [12], Walter Evans [7], and many others are based on these ideas.

Today, there is a vast amount of control methods, which are more or less suited for the solution of multivariable control problems. Control theory is largely treated as a field of mathematics. Theories for robustness, stability analysis, optimal control, and many other aspects are constantly published. Unfortunately, the connection between these often very theoretical works and practical control problems in engineering is often difficult to determine. It often takes a long time until mathematical progress leads to practical and sound applications in engineering.

Common causes for problems arising in control system design are:

- Controlled objects have their own dynamics, so their outputs cannot be changed instantaneously.

- The state of the controlled system may be affected by uncontrolled external inputs, which are often unpredictable.
- The range of possible adjustments is usually limited.
- Measurements that hold information about the current state are noisy.
- Unforeseen states of the system occur, especially in large scale systems.

This chapter gives an overview of some important control methods, with some tentative classification. A scaling of control levels is juxtaposed, and a preliminary proposition for the choice of control methods depending on the control level is given.

2.1 Short Taxonomy of Available Control Methods

Control methods are often subdivided in two domains. Those are frequently called *intelligent* and *non–intelligent* control. This terminology is somewhat unfortunate, since the term "intelligence" raises certain expectations and is rarely well–defined. Nevertheless, this terminology can be used, if it is clear that a specific definition of the term "intelligence" is used.

An useful definition of intelligence can be found in [13]:

> Central to any control theory is the construction, or identification, of plant models; rather than being based on linear physio–mathematical models, intelligent control derives models of the plant input–output mapping from experiential evidence.

2.1.1 Control Methods Based on Physio–Mathematical Modeling

Classical Control

Conventional feedback control is the oldest and most researched area of control engineering in electrical engineering. The foundations still go back

to Nyquist, Bode and Evans. Properties of this method are (+ = advantage, - = disadvantage)

+ Well–developed criteria for stability etc. exist.
+ Insight of physical properties (bandwidth, loop gain into sensitivity, noise, etc.) is available.
– Multi-variable extensions are clumsy.
– Often is very dependent on correct modeling.

Functional

These methods are extensions of conventional feedback control, which implies that the basic stability criteria are applicable. In practical applications, controller design is mostly performed in the frequency domain. Common to these methods is the approach of selecting the control law from some space of functions.

- $\mathcal{H}_2$ [14] or Linear Quadratic Gaussian (LQG) control is based on the minimization of the 2–norm of the closed–loop system.
  + This method is reasonable for multi–variable problems.
  + Desensitizing methods dealing with parameter uncertainty are available.
  – There are no robustness guarantees.
- $\mathcal{H}_\infty$ [14] control is based on the minimization of the ∞–norm of the closed–loop system.
  + Is reasonable for multi–variable problems.
  + Has guaranteed robustness.
  + Can be used with certain loop shaping techniques.
  – Usually sacrifices much of the performance in the trade–off between performance and robustness.
  – Leads to high–order controllers
- μ–**Synthesis** [15] is based on the investigation of the complex structured singular value.

+ Information on the structure of uncertainties can be incorporated in design.
- Computation of design is difficult, convergence is not guaranteed.
- It leads to high–order controllers.

Fuzzy Logic

Static fuzzy logic control [16, 17, 18] has recently been used with impressive success in electrical engineering. The rigid mathematical modeling (mostly in frequency domain) of conventional feedback control (including function space methods) is replaced by modeling in terms of fuzzy sets.

This modeling is usually not directly produced by any kind of rigid mathematics. Instead, an expert accumulates precise knowledge, obtained from mathematical models and imprecise knowledge. This knowledge is then mapped into fuzzy sets and relations between fuzzy sets.

+ Easy implementation of heuristic, imprecise knowledge.
+ Additional implementation of quantitative knowledge.
+ Interpolation and generalization between roles for situations that are not explicitly contained in the rules.
+ Robustness and ability to deal with complex or poorly defined systems.
- Memory requirements for fuzzy logic controllers that grow exponentially with the dimension of the system variables.
- Acquisition of rules from human experts that frequently leads to incomplete and conservative control strategies.
- No reliable criteria for stability, disturbance analysis etc.
- No online adaption capability.

2.1.2 Control Methods Based on Experiential Evidence

Self–Organizing Fuzzy Logic Control

Self–organizing fuzzy logic control (SOFLIC) [13, 19, 20] can be partitioned in two basic approaches:

1. *Direct adaptive control* addresses the adaptive, nonlinear control problem in which the reference model of ideal closed loop behavior is encapsulated in a performance index that directs the control rule updating process.
2. *Indirect adaptive control* first establishes a parametric model of the plant from input/output data through an identification scheme. After that, a feedback controller is synthesized under the assumption that the identified model represents the true plant parameters.

\+ No need for initial knowledge of the plant dynamics.

\+ Good noise and disturbance rejection capabilities.

\+ Online adaption capability.

– Memory requirements for fuzzy logic controllers that grow exponentially with the dimension of the system variables.

– No reliable criteria for stability, disturbance analysis, etc.

– No ability to deal with non–minimum phase plants.

Artificial Neural Networks

Artificial neural networks (ANN) [13, 21] originate from research on artificial intelligence. They are by design multi–variable systems and very well suited to parallel computation. The modeling of the plant is replaced by a teaching process. Basically, there are three possibilities to teach an ANN:

1. Teaching by a given set of input–output vectors.

2. Teaching by partitioning the output vectors into "good" and "bad" by means of some criterion.

3. Teaching by giving a large set of input vectors and letting the ANN partition appropriate responses (few applications so far; however, a working inverted pendulum exists).

By choosing the structure of the network and the element functions, it is possible to design interpolating as well as extrapolating ANNs.

+ ANNs are suited to highly nonlinear problems.

+ Their response time can be almost arbitrarily shortened by adding more processing units.

+ No plant model is necessary. After a teach–in with experientially derived vector–pairs, the ANN generalizes.

+ ANNs adapt online to changed parameters or control goals.

– There are no fixed design criteria.

– "Trial and error" testing must be used, since there are no possibilities to determine the behavior in a given situation theoretically.

Expert Systems

Expert systems [22, 23] (Knowledge Based Systems, KBS) were first developed to enable a naive user to have access to the capability of an expert in some specialized domain of expertise. They use facts, heuristics, common sense knowledge, and other forms of knowledge together with reasoning methods connecting the implemented knowledge.

In control engineering, expert systems are used for two different classes of control:

1. *Off–line* applications, which are mainly planning and long–term scheduling issues.

2. *On–line* applications, mostly high–level process management and control.

Expert systems have the following advantages and disadvantages:

+ They have modular structure, since the domain knowledge is separate from the inference procedure.
+ Rules can represent superficial experiential and heuristic knowledge as well as algorithmic or model–based knowledge.
+ They are very extensible, since the KBS can easily be changed by changing the knowledge base.
– Expert systems often require a lot of computing time and are therefore not always suitable for real time applications.
– The knowledge elicitation from an human expert leads to conservative control strategies, not necessarily to optimal or even near–optimal solutions.

2.2 Control Architecture

Many attempts to propose standard architectures for control systems have been made. One of the more successful ones is the NIST Real–Time Control System (RCS3) architecture, which is now incorporated in the functional specification of the NASA Space Station Flight Telerobot Server, the NASA/NIST Standard Reference Model for Telerobot Control System Architecture (NASREM)[24]. This architecture is here applied to a fictional power system that should, with the help of devices containing solid state switches, like CSCs, make it possible to direct the power flow according to some kind of criteria. It proposes several *control levels*, depicted in Figure 2.1:

1. **Actuator or Servo Level**

   As the lowest level, this contains the direct control of the hardware. In small, single–variable control systems this usually is the only level. In large–scale, multi–variable systems, this level provides the first abstraction from the physical realities. The equipment then contains an interface to the next higher level. In robotics, this is the control of the actual motors; in power systems this might be the control of the single switching devices in a CSC.

2. **Primitive or Component Level**

   This level provides a convenient, i.e. more generalized, interface. In robotics, this is the control of, for example, a robot arm in a more generalized coordinate system; in power systems, this might be the higher–level control of a single device containing several solid state switches.

3. **Elementary / Subsystem Level**

   This level performs a piecewise decomposition of elementary control commands for a subsystem. In robotics, elementary moves are decomposed into a series of intermediate motion commands that define a path of motion. In power systems, this might be the control of several devices in such a way that a given impedance structure in the net is obtained.

4. **Task Subsystem Level**

   This level decomposes object tasks into appropriate partitions of elementary control actions. In robotics, this is the fixing of a path ensuring that this path is free of obstacles. In power systems, this might be the control of a whole station or plant.

5. **Co–operating Level**

   This level splits up complex tasks involving operations on a number of controlled objects into tasks carried out on single objects. In power systems, this might be the control of several devices or plants in a way that ensures that system voltages and other controlled quantities stay within their specified ranges.

6. **Mission Level**

   This level decomposes an overall mission plan into control commands. Mission plans might be specified in terms of mission goals, priorities, requirements, and/or constraints. In power systems this might be a control scheme that ensures that the power flow is distributed economically within given parameters.

Further layers corresponding to higher command abstractions are possible. Besides, several layers can be condensed in one single device. This partition into six levels should be regarded as a general proposal, not as a strict rule.

Of course, different hierarchical structures are possible. In [25], a partitioning in three levels is proposed:

1. **Primary–Level Control**

   At this level, controllers typically respond only to changes in the local output variables. The main function of primary–level control is to correct for small, fast output deviations that are caused by fast disturbances. Examples for primary–level control are excitation systems for voltage control and governor systems for frequency control. Primary–level control corresponds to level 2 of the NASREM architecture.

2. **Secondary–Level Control**

   At this level, changes within a region are controlled. Interactions with the neighboring regions are assumed to be small. Examples for secondary–level control are adjustments of the speed–changers in governors and control of the terminal voltages of generators. Secondary–level control corresponds to levels 3, 4, and partly 5 of the NASREM architecture.

3. **Tertiary–Level Control**

   At this level, secondary–level controllers are coordinated by incorporating the effects of interactions on the quasi–static changes of the interconnected system over a long time horizon. The main goal of this coordination is to achieve system–wide optimal performance. Tertiary–level control corresponds to levels 5 and 6 in the NASREM architecture.

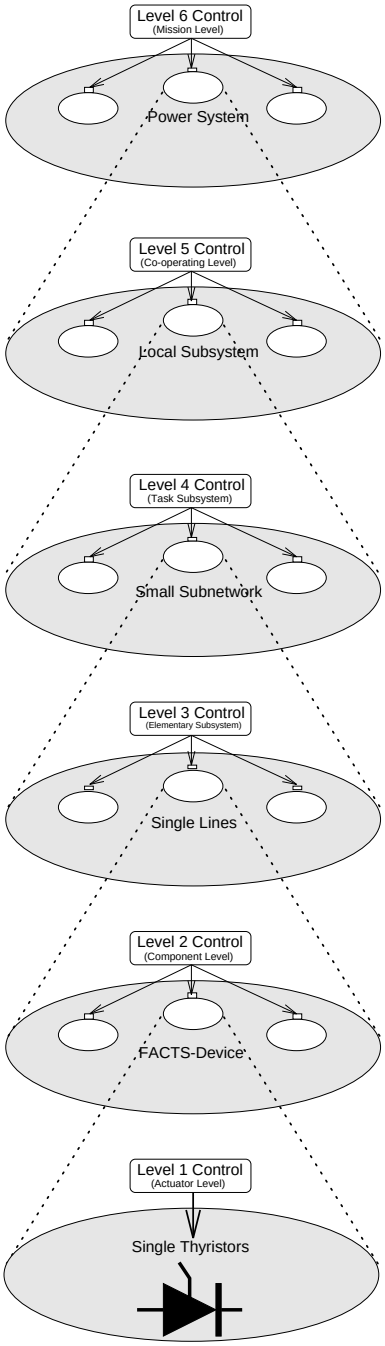

Figure 2.1. Control Levels in an Electric Power System

2.3 Control Methods for the Different Levels of the Architecture

As the control system level in the previous section increases, the requirements in terms of controller speed decrease in general and the formulation of the control problem becomes almost always more and more imprecise. Consequently, the control methods will be different. Attempts to use one control method for the solution of all control problems are bound to fail, as the demands are too different. As a rule, the simplest possible control method should be employed.

Even though it is generally impossible to decide which control method should be used for which application, an outline of the suitability of the different control methods to the architectural levels discussed above can be given. (Which control method should be used for which application largely depends on issues like linearizability, the ability to derive a model, and the amount of knowledge available about possible system states.) Table 2.1 contains such an overview.

2.4 Controllers in Electric Power Systems: Special Considerations

Electric power systems are probably the largest interconnected systems that have been created by mankind. Their beginnings go back to the late nineteenth century [26]. The demand for electric power has been growing ever since, and today, the power system reaches even remote parts in western societies and many developing countries. Still, advanced intelligent control methods are not used to a larger extend. There are several reasons for this:

1. The demands on the reliability of electric power systems are very high. Even short outages incur high costs for the customers, and outages of a longer duration, starting from just a few hours, can lead to severe disruptions for society. For example, after just eight hours without electric power, there is a risk that the supply of drinking water becomes contaminated because the pressure in the pipes is lost [27]. Therefore, utilities are reluctant to implement any control

	Level 1	Level 2	Level 3	Level 4	Level 5	Level 6
Conventional Feedback Control	**very well suited** often single–variable control problems; "traditional", very well researched approach;	**feasible** one or few variables; tight connection to physical reality;	**possible** more variables; more abstract demands on control; generally other methods are better suited;	increasing level of abstraction makes coordinated design difficult;	**not feasible** increasing level of abstraction makes coordinated design difficult;	
Static Fuzzy Logic Control	**well suited** especially if heuristic knowledge should be implemented; however, feedback control is often simpler;	**very well suited** many successful applications with combination of heuristic and qualitative knowledge on this level;	**well suited** control strategies can often easily be expressed in terms of fuzzy sets;	**feasible** if the number of system variables is not too high;	**possible** with a low number of system variables and combination of heuristic and quantitative knowledge is required;	**not feasible** modeling in terms of fuzzy sets usually very difficult; high dimensional system variables;
Self–Organizing Fuzzy Logic Control	**possible** but the cost will usually not be justified; little insight into physical properties;	**well suited** if little initial knowledge of plant dynamics is provided and online adaption is important;	**very well suited** (potentially) very fast; online adaption; generalization capabilities;	**very well suited** especially if adaptive behavior is required as well as heuristic / quantitative knowledge;	**well suited** if adaptive behavior is required as well as heuristic / quantitative knowledge; not to many system variables;	**possible** if there are few system variables and adaptive behavior is required as well as heuristic / quantitative knowledge;
Artificial Neural Networks	**feasible** if control problem is highly nonlinear, plant model is badly defined and fast response time is required;	**well suited** for highly nonlinear systems; systems which are difficult to model;			**well suited** especially if no heuristic / quantitative knowledge available;	**possible** but feasible only when speed has a high priority;
Expert Systems	**not feasible** generally, the complexity of these control problems is to low to justify the cost; real time demands;	**possible** but only for very complex level-3 assignments;	**feasible** if mainly heuristic and algorithmic knowledge of the system is available;		**well suited** complex tasks with high level of abstraction;	**very well suited** very high complexity; low real time demands;

Table 2.1. Control Methods and Architecture Levels

strategy if it is perceived that the consequences of the implementation cannot be predicted reliably.

2. An electric power system is subject to large changes all the time. Load and generation patterns change, the system topology changes, and the way the system is operated changes. The number of possible permutations for the system conditions is extraordinarily high. That makes it impossible to, for example, train a neural network with all possible system conditions, or even to determine its response for all cases. In contrast, modeling–based control systems often offer ways to analyze things like robustness mathematically for a wide range of system conditions.

3. Utilities use a large number of software tools, like voltage stability analysis programs or dynamic security analysis programs, for system planning and increasingly also system operation. Any controller that has a system–wide influence has to be incorporated in these tools. It is far easier and faster to incorporate classical controllers in these programs than to incorporate, for example, neural networks or expert systems.

4. Historically, it has been comparatively easy to meet the rising demand for transmission capacity by building new power lines. In the monopolistic power industry, reliability and the obligation to serve all customers were the driving forces behind system design. The cost for system extensions was simply passed down to the customers. Hence, power systems were built with redundancy and large margins of safety. Advanced control methods were not needed.

Today, the utility industry is facing significant changes. Deregulation of the electricity markets is changing the operation of the power system. More efficient ways to operate the power system are becoming very attractive, since the cost of inefficiencies cannot simply be passed on to the customer; it is expected that the market share of the most efficient provider will rise. While it is quite clear that the demand for electric power will rise for some time to come, it is not self–evident that the peak load on the transmission system will rise. Distributed generation could shift the production of electric power geographically closer to the demand thus alleviating the load on the transmission system.

Whether these changes as a whole will lead to an increased acceptance of advanced intelligent control methods remains to be seen.

Chapter 3

Tools for Control of Active Power Flow

In Section 1.1, reasons for load flow control were given. The active power flow through a transmission line, like the one shown in Figure 3.1, is, neglecting losses, given by the equation

$$P = \frac{U_1 U_2}{X} \sin(\delta_1 - \delta_2) \; . \tag{3.1}$$

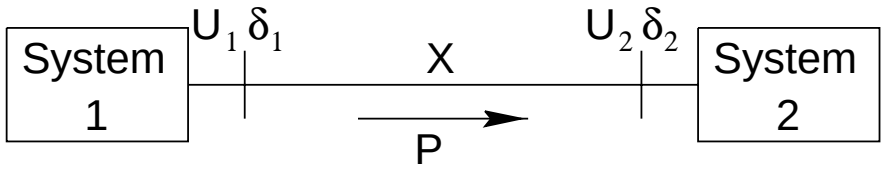

Figure 3.1. Transmission Line

This equation contains five parameters that influence the active power flow:

- U_1, the voltage at the sending end.
- U_2, the voltage at the receiving end.

- X, the line's reactance.
- δ_1, the angle at the sending end.
- δ_2, the angle at the receiving end.

The idea of flexible AC transmission systems, FACTS [28], is to introduce devices, based on power electronics, that can influence those parameters without the introduction of external power generation. Some of these devices will be presented in this chapter.

3.1 Controlled Series Capacitor, CSC

The CSC, as shown in Figure 3.2, is a reactance that is controlled by the thyristor firing angle. For steady–state load flow studies, the CSC can be

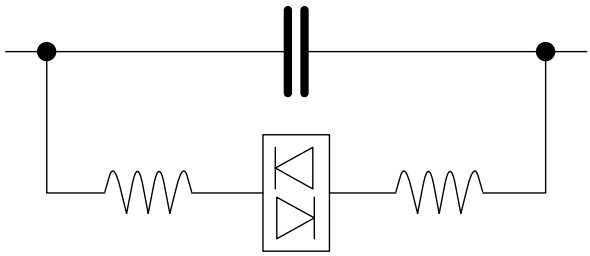

Figure 3.2. Internal Structure of CSC

considered a controllable capacitance, which is connected in series with the transmission line, Figure 3.3.

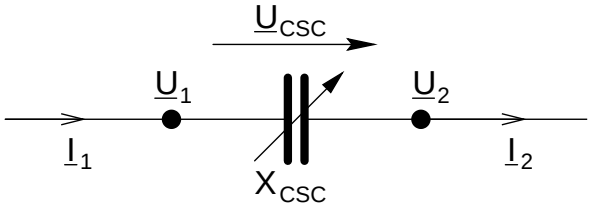

Figure 3.3. Concept of CSC

According to the vector diagram in Figure 3.4, the basic mathematical relations are

$$\underline{I}_1 = \underline{I}_2 = \underline{I}\,, \tag{3.2a}$$

$$\underline{U}_{CSC} = -jX_{CSC}\underline{I}\,. \tag{3.2b}$$

For load flow studies, the CSC influences the line impedance X.

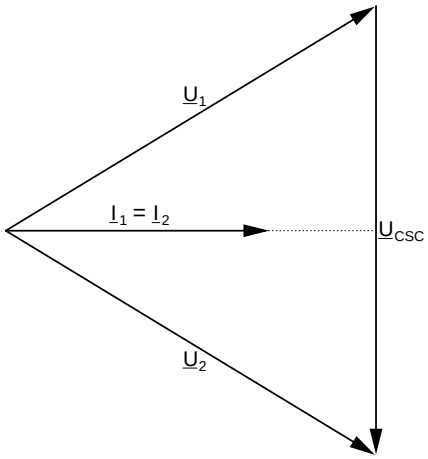

Figure 3.4. CSC Vector Diagram

3.2 Phase Angle Regulator, PAR

The PAR is a transformer with a complex turns ratio. The phase angle difference between the terminal voltages is achieved by connecting a boosting transformer into the transmission line. The power injected into the line must be taken from the network by a shunt transformer. This is shown in Figure 3.5; other designs are also possible.

The controllable parameter of the PAR is the voltage shift angle α. Voltages and current magnitudes of both terminals are equal for an ideal PAR. The operating characteristics and the vector diagram are shown in Figures 3.6 and 3.7, respectively.

Basic mathematical relations are

$$\underline{U}_2 = \underline{U}_1 \cdot e^{j\alpha}\,, \tag{3.3a}$$

$$\underline{I}_2 = \underline{I}_1 \cdot e^{j\alpha}\,. \tag{3.3b}$$

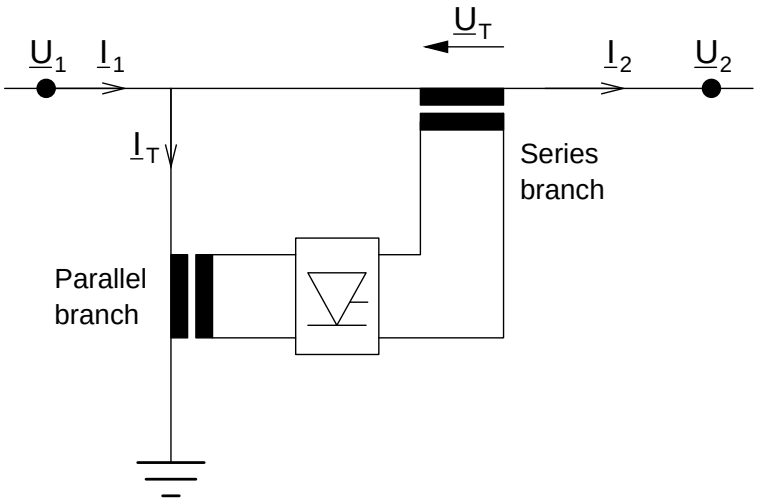

Figure 3.5. PAR Structure

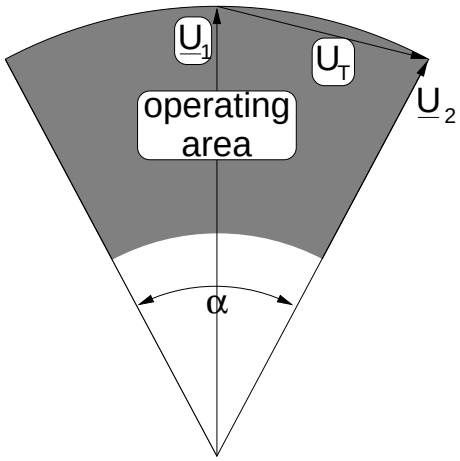

Figure 3.6. PAR Operating Characteristic

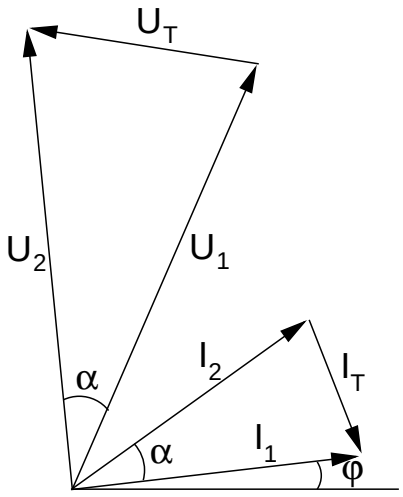

Figure 3.7. PAR Vector Diagram

3.3 Unified Power Flow Controller, UPFC

Figure 3.8 shows the basic technical concept of the UPFC. The UPFC consists of a shunt (or exciting) and a series (or boosting) transformer. Both transformers are connected through two static converters that contain a capacitor as an energy storage device in their DC-link. Any real power injected by the series branch into the system obviously has to be taken from the system by the parallel branch and then transmitted through the DC–circuit to the series branch. This is represented in Figure 3.8 by the current $\underline{I}_T$. Further, the reactive current $\underline{I}_q$ can be controlled so that the parallel branch acts as a controllable reactive shunt susceptance.

Figure 3.9 gives the vector diagram of the UPFC. $\underline{U}_T$ can be at any phase with regard to $\underline{U}_1$; its magnitude is limited by U_{Tmax}, which is a design parameter of the UPFC. Controllable parameters are the phase and the magnitude of $\underline{U}_T$ and the magnitude of $\underline{I}_q$. The operating area is the circle described by U_{Tmax} around $\underline{U}_1$. Control parameters often used for the UPFC are r and γ, given by $U_T = r \cdot U_1 \cdot e^{j\gamma}$

The basic mathematical relations are:

$$\underline{U}_2 = \underline{U}_1 + \underline{U}_T \tag{3.4}$$

$$\angle \underline{I}_q = \angle \underline{U}_1 \pm 90^\circ \tag{3.5}$$

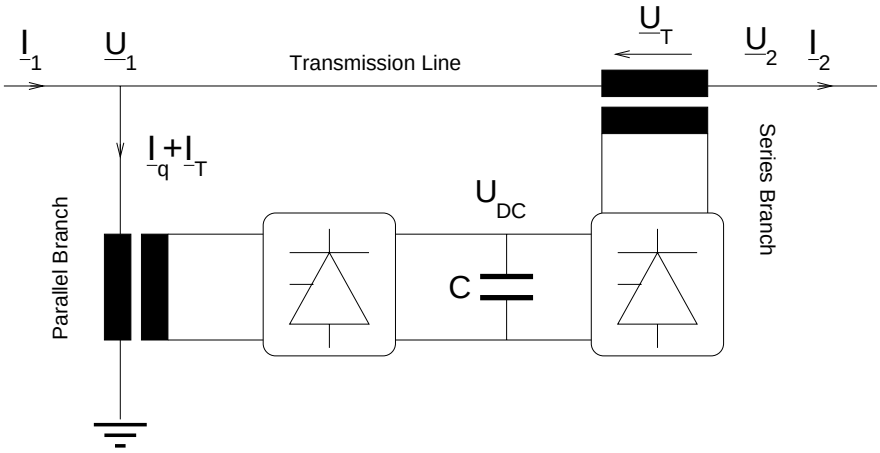

Figure 3.8. Basic Scheme of the UPFC

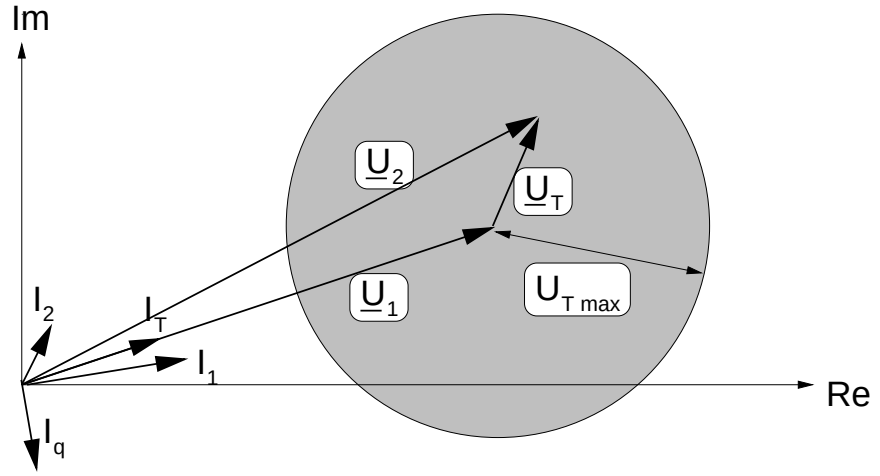

Figure 3.9. UPFC Vector Diagram

$$\angle \underline{I}_T = \angle \underline{U}_1 \tag{3.6}$$

$$I_T = \frac{\Re(\underline{U}_T \cdot \underline{I}_2^*)}{U_1} \tag{3.7}$$

The influence of the presented FACTS devices on the load flow equation (3.1) is illustrated in Figure 3.10.

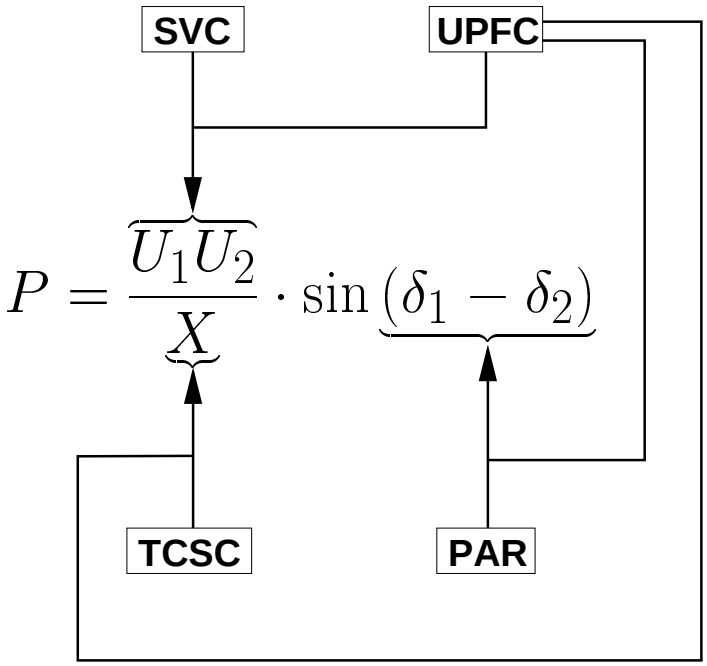

Figure 3.10. Influence of FACTS Devices on Load Flow Equations. SVC is included for completeness.

3.4 Other FACTS Devices

Very recently, a device that utilizes rotary transformers, based on the phase difference between rotor and stator in a stationary electrical machine [29] was introduced. In [30], a configuration using two of these rotary transformers with the same capability as a UPFC, except for the possibility of reactive power injection at the shunt transformer, is presented. ABB's Powerformer technology [31, 32] might even eliminate the

need for fixed transformers. The control system uses hydraulics or electric servo motors, rather than the solid state switching control logic that the UPFC uses. While this system is bound to be slower than a UPFC, the speed should certainly be sufficient for the application discussed in this thesis.

Some other FACTS devices not treated here are

- the static var compensator, SVC [33].
- the static var generator, SVG or STATCOM [34].
- the interphase power controller, IPC [35].
- the superconducting magnetic energy storage, SMES [36].
- high voltage DC transmission, HVDC (only sometimes ranked as a FACTS concept).

Chapter 4

Load Flow Control Using CSC and PAR

This chapter treats two of the FACTS devices described in Chapter 3, namely the controlled series capacitor (CSC) and the phase angle regulator (PAR). These two devices can be treated together since they have, as it will be shown, similar properties on some points crucial for load flow control. A simple control scheme is proposed in Section 4.1.2, and it is shown in Sections 4.1.3 and 4.2.1 that this scheme can *always* be used for two PARs or CSCs in parallel paths. The generalization of that scheme for more than two devices is investigated in Section 4.3, and the relative merits of CSC and PAR are discussed in Section 4.4. Simulations are performed to confirm these analytical results, and a short discussion of the problems that can arise in power systems that are close to their stability limits is provided in Section 4.5.

4.1 Two Series Capacitors

The investigation starts with two CSCs. A simple test system is given, which then is used for a mathematical analysis of a simple control scheme. The results, which are valid for small signals, are then extended in simulations for larger signals. A larger system, for which the analytical results are still valid, is given, and simulations confirm the applicability of the proposed control scheme for large systems.

4.1.1 The Simple Test System

The first investigation is carried out on a test system that models a power system in which active power is transferred from a generation area to a load area. Such a system can be used as a general model for an electric power system with a generation area and a load area, when those two areas are connected by several lines. Some of these lines contain controllable FACTS devices.

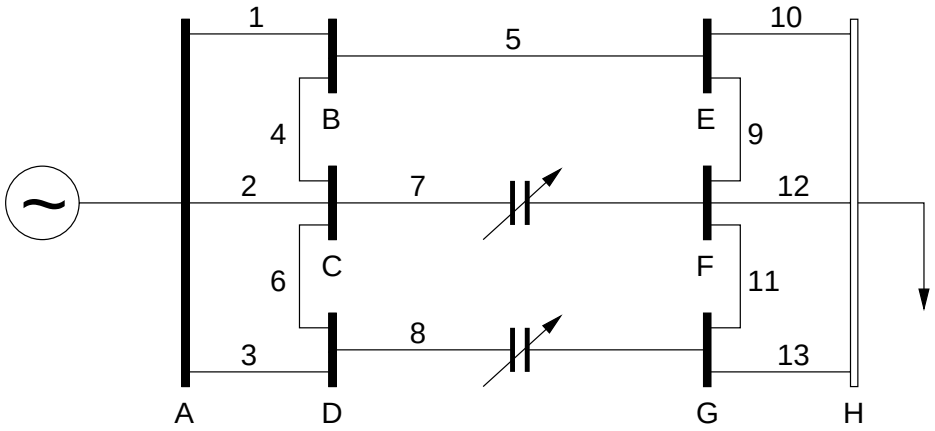

Figure 4.1. Simple Test System

Figure 4.1 shows a simple model fulfilling these requirements. The generation area consists of the nodes A, B, C, and D. A is a slack bus with voltage 1 pu and a reference angle of 0°. The connections of these nodes within the generation area are modeled by the lines 1, 2, 3, 4, and 6. The load area consists of the nodes E, F, G, and H. Node H is a PU node with a voltage of 1 pu and an active power demand of 1 pu. The lines 9, 10, 11, 12, and 13 model the connections within the load area. The two areas are connected by the lines 5, 7, and 8. Lines 7 and 8 contain controllable components, namely CSCs. The bus and line data are given in Tables 4.1 and 4.2. These data result in an active power flow of around 1 pu through the lines 5, 7, and 8.

For this investigation the series compensation will be limited to values between 0% and 70% of the line reactance.

Nr.	Type	V	δ	P_g	Q_g	P_d	Q_d
A	Slack	1	0	–	–	–	–
B–G	PQ	–	–	0	0	0	0
H	PU	1	–	0	–	1	–

Table 4.1. Bus Data

Nr.	R	X
1–4,6,9–13	0.03	0.12
5,7,8	0.03	0.24

Table 4.2. Line Data

4.1.2 Control with Independent Integral Controllers

The first and most simple approach is controlling the series capacitors with independent integral controllers without regard to the cross coupling effects. Integral controllers are appropriate for power flow control, since speed is of little importance. (A reasonable time frame for power flow control is on the order of magnitude of tens of seconds.) It has to be investigated whether the controllers influence each other in a way that might lead to unstable system behavior or hunting phenomena, that is, the controllers oscillating against each other.

Figure 4.2 shows the block diagram of the controlled system.

4.1.3 Mathematical Analysis of the Controlled System

Generally, a power system where the active power flow is controlled with several integrating controllers can be described by

$$w = F(u); \quad u = K \cdot \int_0^t w'(\tau)\, d\tau \quad . \tag{4.1}$$

u is a vector of series compensations (the control variable), w is a vector of load flows, F is the function that connects load flows and series compensations, and w' is the deviation of the load flows from the specified

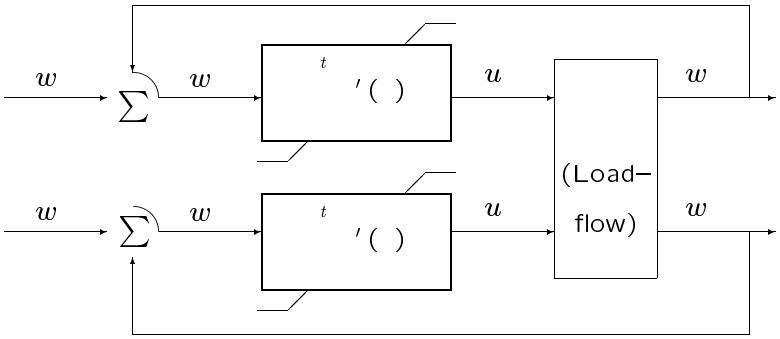

Figure 4.2. Two Integral Controllers; : Active Power Flow : Series Compensation

values. Differentiating Equation (4.1) leads to

$$\frac{dw}{dt} = \frac{dF}{du} \cdot K \cdot w'(t) = \frac{dF}{du} \cdot K \cdot (w^* - w) \quad . \tag{4.2}$$

An equilibrium point is, as expected, at $w = w^*$. The small signal stability of that equilibrium point is determined by the eigenvalues of $-\frac{dF}{du} \cdot K$, where $\frac{dF}{du}$ is a submatrix of the sensitivity matrix describing the sensitivity of the active power flow to the series compensation in the line, $S = \frac{dw}{du}$, [37, 38]. The sensitivity matrix can either be determined analytically (see Appendix C) or by simulations with small perturbations.

The limitations on the series compensation shown in Figure 4.2 are not taken into consideration at this point. These limits are not detrimental to system stability: These limits are nonwindup limits. If the limits are reached in the i-th integrator, $\frac{du}{dt} = 0$, and u is stuck at the limit value as long as the input w_i' is driving u_i beyond the limit value. This effectively implies that one degree of freedom is lost, that is, the system dimension in the sense of dynamics drops by one [39]. Then, u_i is constant, thus the line containing the corresponding i-th controlled device is effectively uncontrolled. Of course, the limits influence the range in which the load flow can be controlled.

Radial Systems

Using a sign convention such that active power flow is considered positive at the current operating state, the diagonal elements of the submatrix of

the sensitivity matrix are always positive, since an increased series compensation in a line increases the load flow in that line. The off–diagonal elements are always negative if the power flow is controlled in several parallel lines connecting a generation area and a load area, since the increase of load flow in one line must be compensated by a decrease of load flow in the other lines. Further, the negative sum of off–diagonal elements in a column is less than or equal to the diagonal element in that column,

$$-\sum_{\substack{i=1\\ i\neq k}}^{n} S_{i,k} \leq S_{k,k} \quad \text{or} \quad \sum_{\substack{i=1\\ i\neq k}}^{n} |S_{i,k}| \leq |S_{k,k}|\,, \tag{4.3}$$

since the change of active power flow in the controlled line is compensated by an inverted change in active power flow in all the other lines. Here, it is assumed that the power transfer capability of these lines is sufficient to carry the compensating power flow. The equal sign in Equation (4.3) represents the case when each line contains a CSC, which leads to loss of controllability since the equation system then is overdetermined and is therefore not of practical interest. Loss of controllability means here that, due to the modeling of the power system with one slack bus and the other buses PU or PQ, the load flow through the lines cannot change independently.

The power system model using the purely algebraic load flow equations instead of more detailed generator and load models is appropriate for investigating load flow control, since, under normal conditions, power systems operate in a quasi–steady state on slow time scales; that is, the system reaches its steady state within a fast time scale. For sufficiently different time scales, the phenomena are de–coupled and different models can be used [40]. In Chapter 9, a more detailed model that is investigated. As mentioned in Section 4.1.2, a reasonable time frame for load flow control is in the order of magnitude of tens of seconds.

With the same sign convention, all K_i have to be positive if the controlled system is to converge. Therefore, the observations above are valid for $\frac{dF}{du} \cdot K$ as well.

The Simple Test System

The stability of the simple test system from Section 4.1.1 depends on the eigenvalues of

$$-\frac{dF}{du} = - \begin{matrix} S_{7,7} & S_{7,8} \\ S_{8,7} & S_{8,8} \end{matrix} \cdot \begin{matrix} K_1 & 0 \\ 0 & K_2 \end{matrix} \quad , \tag{4.4}$$

which, with $\Gamma = K_1 S_{7,7} + K_2 S_{8,8} > 0$, are

$$-\frac{1}{2} \quad \Gamma \pm \quad \overline{\Gamma^2 - 4K_1 S_{7,7} K_2 S_{8,8} + 4K_1 S_{7,8} K_2 S_{8,7}} \quad . \tag{4.5}$$

According to Equation (4.3),

$$4K_1 S_{7,7} K_2 S_{8,8} > 4K_1 S_{7,8} K_2 S_{8,7} \quad , \tag{4.6}$$

and therefore the eigenvalues (4.5) are always negative and real. Small signal stability is thus guaranteed, and (adverse) oscillations are not expected.

4.1.4 Simulation of the Simple Test System with the Integral Controller

Having proven small signal stability, the question remains how the system behaves if the starting value is far from the equilibrium point. Since an analytical treatment of this problem is virtually impossible, it has to be treated using time simulations.

The time simulations were performed from a state given by a certain value of series compensation. The goal was to achieve a defined active power flow. The key in Figures 4.3–4.11 denotes the initial state and the desired state. (0,70)→(0.3405,0.3405) therefore means that starting from line compensations 0% and 70% an active power flow of 0.3405 pu should be achieved in both lines. Lines with lower line number are always mentioned first.

Figures 4.3–4.8 show clearly that the simple test system can safely be controlled with two integral controllers. The trajectories in Figures 4.3–4.6 converge smoothly toward the equilibrium point, and in time domain there are only minor overshoots, which in no case occur in the state variable and the control variable simultaneously.

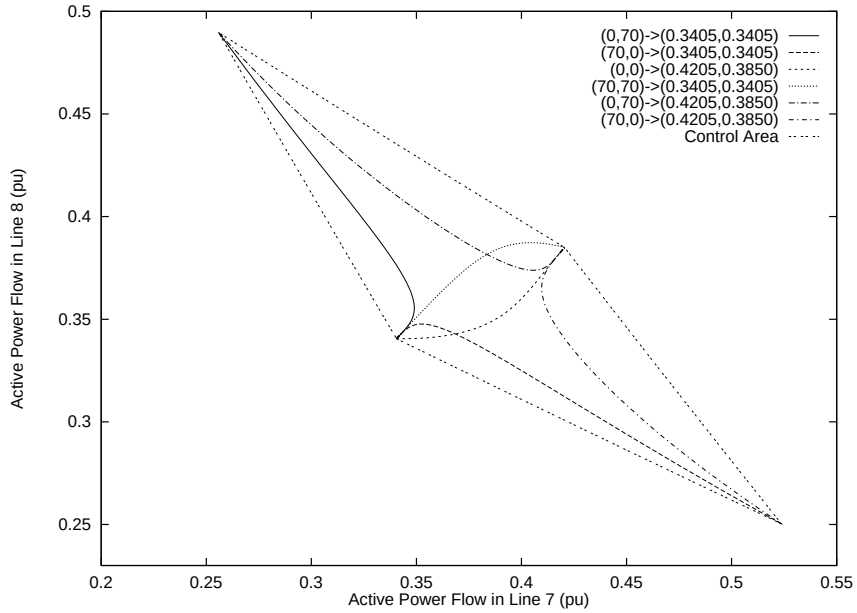

Figure 4.3. Simulations in State Space

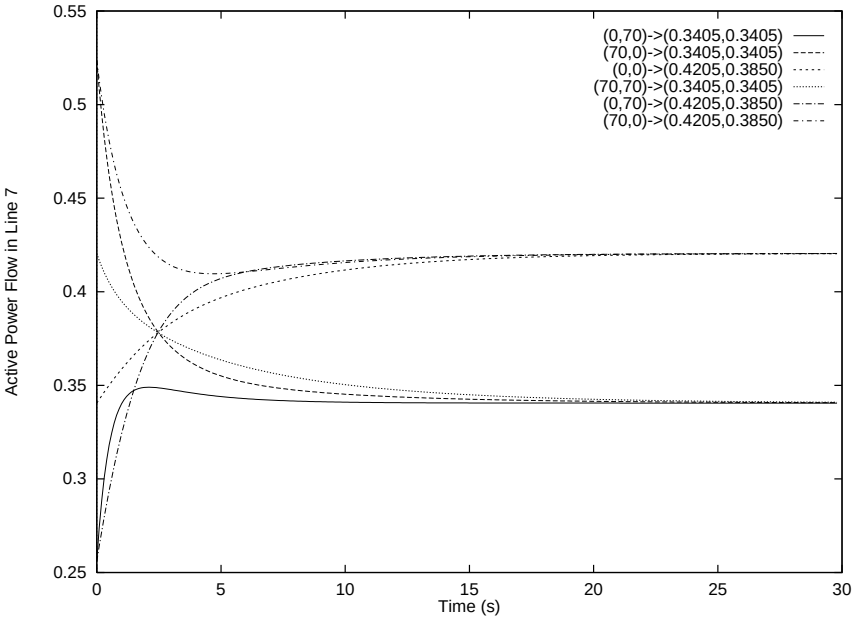

Figure 4.4. Power Flow in Time Domain — Line 7

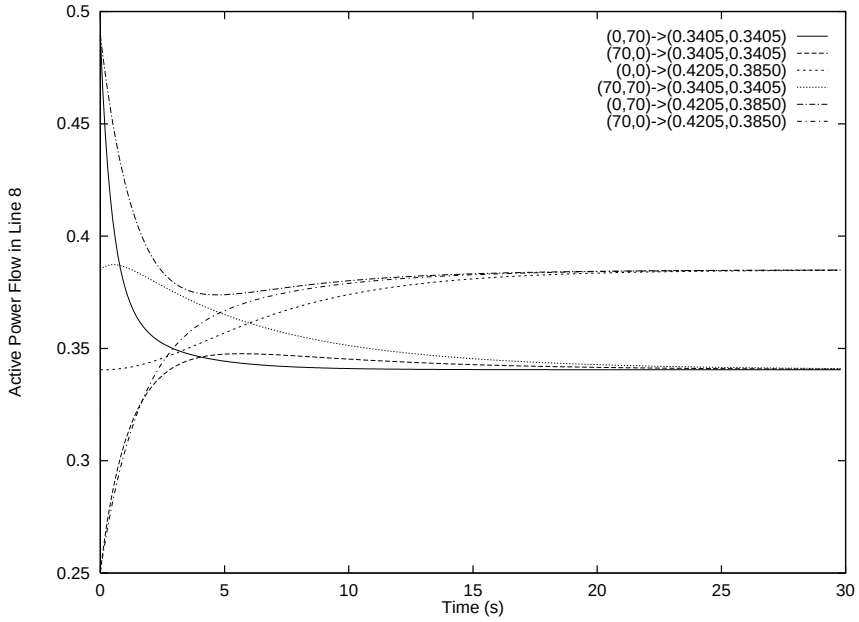

Figure 4.5. Power Flow in Time Domain — Line 8

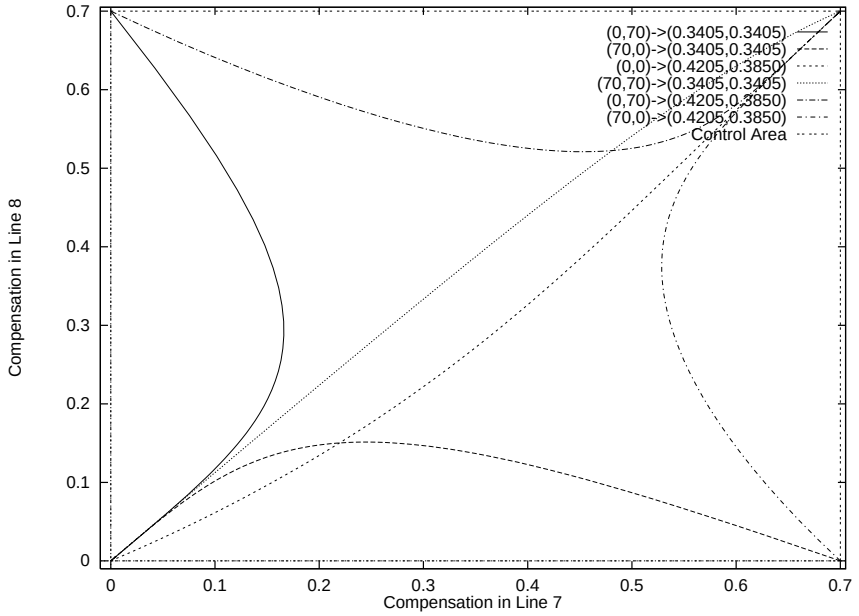

Figure 4.6. Simulations in Control Space

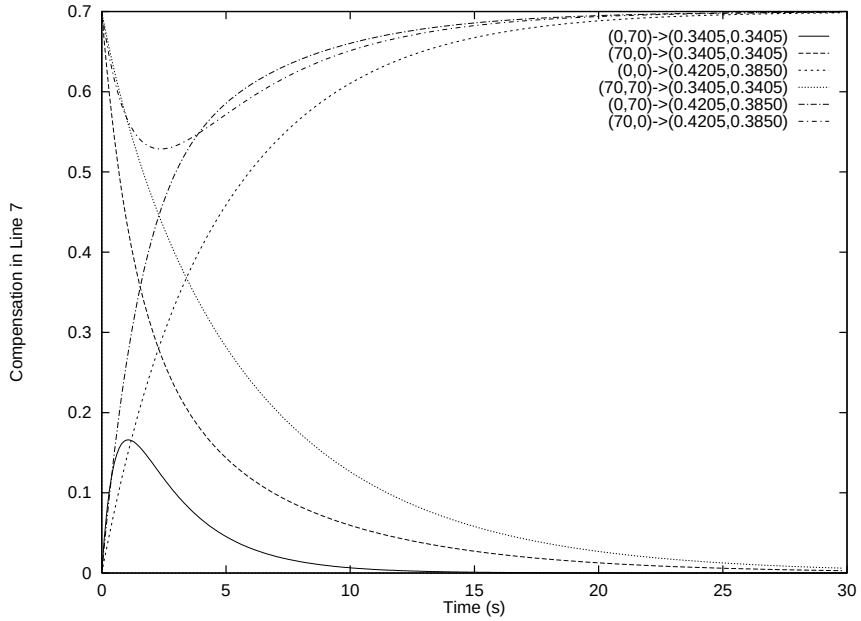

Figure 4.7. Compensation in Time Domain — Line 7

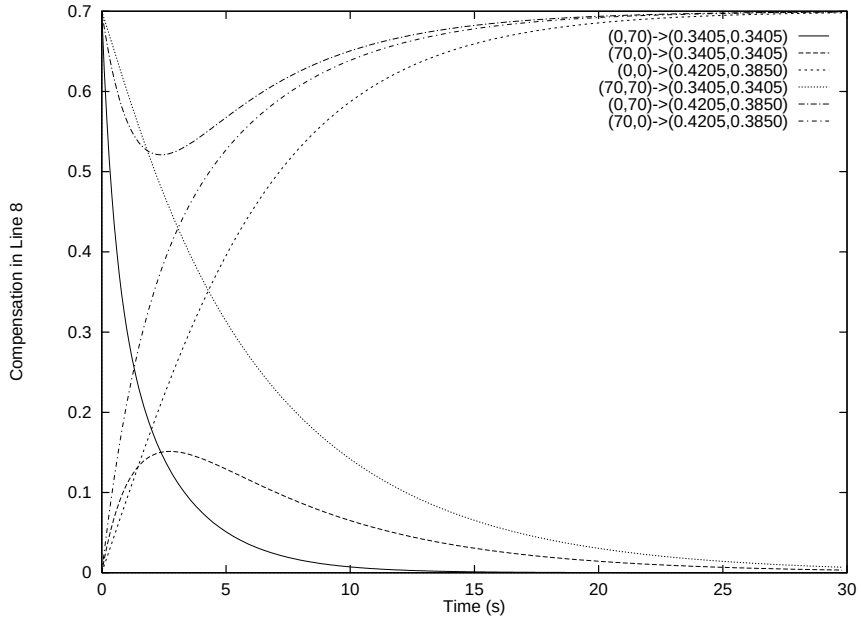

Figure 4.8. Compensation in Time Domain — Line 8

4.1.5 Larger Systems

An equation similar to Equation 4.6 can be obtained irrespective of the system's size, since the crucial property for the validity of Equation 4.6 is the presence of a path for the load flow other than the two controlled lines. As long as such an alternative path exists and the remaining power transferred through that path is within its power transfer capability, small signal stability is guaranteed, if the independent integral controllers are used.

To verify whether this result, which is valid for small perturbations, can be generalized for large signals, a larger system with a different topology is needed. The IEEE 30 Bus System, shown in Figure 4.9, is used here. The system data are given in Appendix B; originally, the data were obtained from [41]. According to the data from [41], there are limits on the generators connected to buses 2, 5, 8, 11, and 13. These limits are *not* considered in the following investigations, because:

- The limits on the generators are limits on the absolute value of the complex power. The production of active power is given as a constant for these generators. Thus, the limits only affect the production of reactive power and consequently the reactive power flow, which is not discussed in this thesis.
- When one or several generators reach their generation limits, the system is not in a desirable state. Generally, reaching the generation limits is an indication of an imbalance in the system that has to be addressed.

Simulation of the IEEE 30 Bus Test System

Figure 4.10 shows the trajectories obtained when controlling lines 30 and 35 in state space. The situation here is almost the same as in the case of the simple test system, the active power flow through these two lines together with line 31 is constant. Convergence is smooth and unproblematic, and there are no signs of adverse interactions.

Figure 4.11 shows the trajectories obtained when controlling lines 2 and 14 in state space. Here, the cut set of lines through which the active power

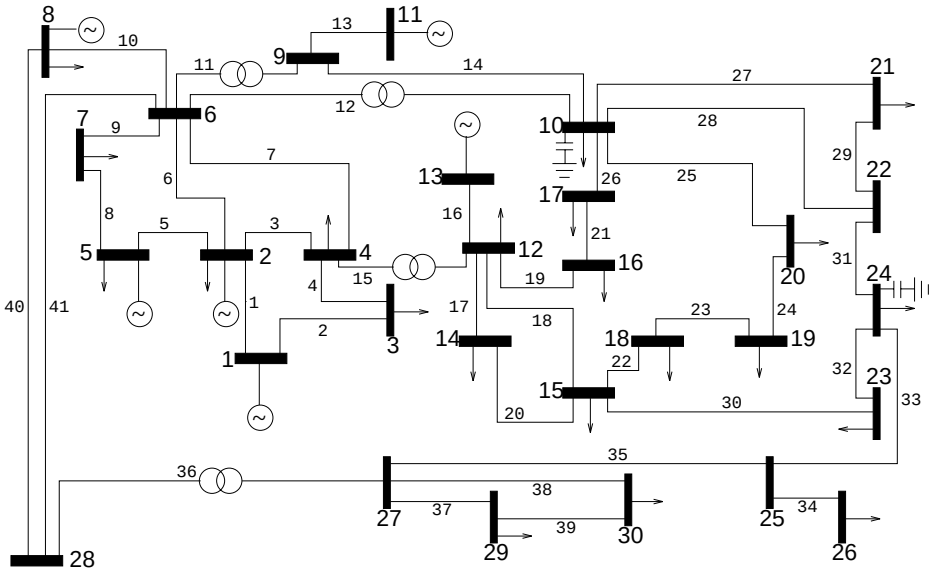

Figure 4.9. IEEE 30 Bus System

flow is constant is considerably larger. Still, there are no convergence or stability problems.

It is worth noting that Figures 4.10 and 4.11 also show how the control area changes shape if the impedance of the parallel paths decreases: In Figure 4.11, the control area is almost rectangular, thus indicating a low impedance of the parallel paths. When controlling lines 30 and 35, the impedance of the alternative path is higher, leading to a "flatter" shape of the control area, that is, the angles at the corners of the control area deviate more from 90°. If there were no parallel path for the load flow, the control area would degenerate to a line, thus making independent control of the load flows in the two lines impossible. That would be exactly the situation in which the eigenvalues in equation 4.5 vanish and small signal stability becomes uncertain.

4.1.6 Robustness of the Control Scheme

All electric power systems are subjected to topological and other changes: Lines are disconnected due to faults or maintenance; the same applies to transformers and other elements. The load pattern is varying. Thus, it

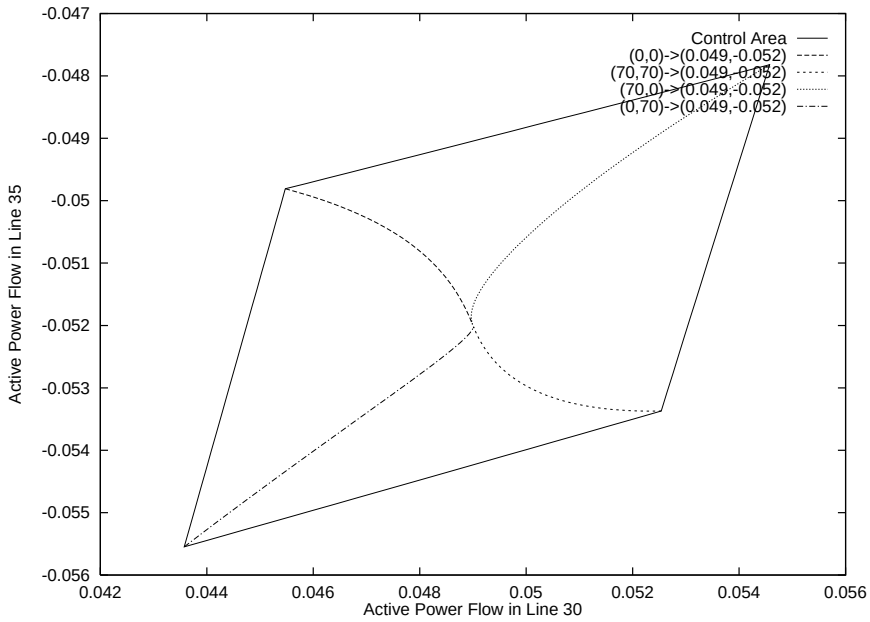

Figure 4.10. Results for Control of Lines 30 and 35

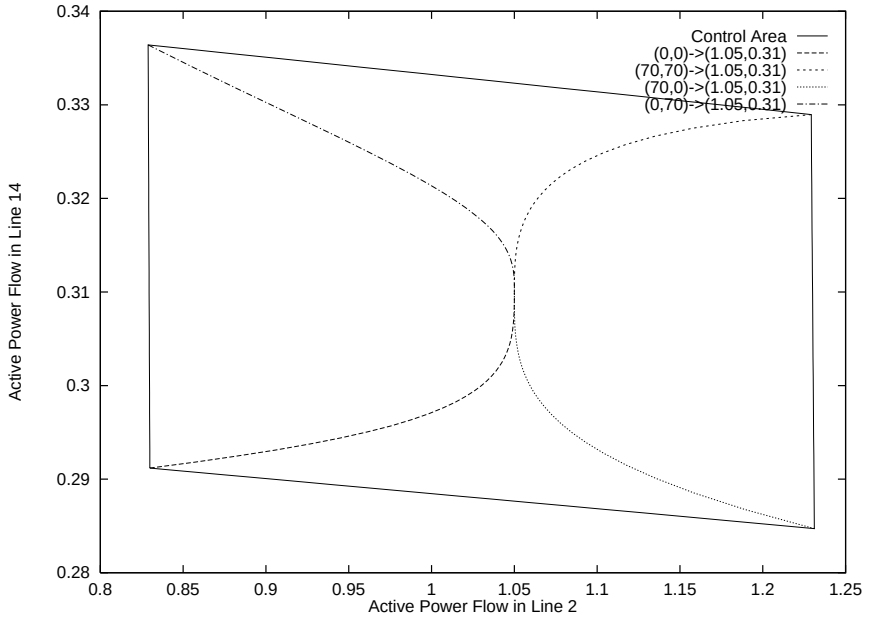

Figure 4.11. Results for Control of Lines 2 and 14

is important that controllers are robust with respect to these and other conceivable changes.

The proposed control scheme uses only local signals. The system's topology is, apart from ensuring controllability, not used in the controller design. Therefore, this control scheme is robust with respect to such changes. As long as the desired state can be reached, that is, the operating point is inside the control area and all lines operate within their power transfer capabilities, that steady state will eventually be reached.

However, provisions have to be made for one case. If the alternate path for the load flow is taken out, the total load flow in the controlled lines is constant. The real part of the eigenvalues (4.5) vanishes. System stability can no longer be determined using a linearization. If such a case occurs, at least one of the controllers should be blocked to avoid adverse oscillations.

4.2 Two Phase Shifters

Phase shifters are, as described in Chapter 3, another possibility to control the active power flow. The analytical investigation for the the small–signal stability of CSCs controlled by independent integral controllers is here extended to PARs. Simulations verify the large–signal stability of this control scheme.

4.2.1 Analytical Investigation

The load flow through a transmission line is, neglecting losses, given by

$$P = \frac{U_1 U_2}{X} \sin(\delta_1 - \delta_2) \,, \tag{4.7}$$

which is the same equation as (3.1). A phase angle regulator changes $\delta_1 - \delta_2$. As long as $-\pi/2 < \delta_1 - \delta_2 < \pi/2$, which is valid for practical cases, the phase angle regulators are, like CSCs, devices with a monotonic characteristic with respect to the load flow in the line those devices are located in. Like the line flow increases with increasing series compensation in the case of the CSC, the line flow increases with increasing difference of phase angles at the buses, that is, an increasing phase angle over the device, in case of the PAR. This fundamental similarity between those

two devices can be used to extend the results obtained for the CSC to the PAR.

The physical background of Equations 4.3–4.6 depends only on the monotonicity of the line flow with respect to the control variable of the controllable device. Therefore, the small–signal analysis from Section 4.1.3 is directly valid for load flow control with PARs. The same simple control scheme can be used.

4.2.2 Simulations

Large signal stability will be confirmed by simulations. Again, the IEEE 30 bus test system in Figure 4.9, without generator limits, is used.

Figure 4.12 shows the load flows in lines 2 and 14 controlled by PARs in these lines, when the phase angle is varied from $-10°$ to $10°$. Starting from each corner of the control area, the load flows converge smoothly without oscillations or overshoot. The control area is considerably larger than the one obtained using CSCs with compensations between 0% and 70%; the load flow in line 14 can even be reversed. The control variables, depicted in Figure 4.13, converge equally smoothly towards the equilibrium point. The large signal stability for this case is thus verified.

Load flow control for other lines leads to similar results; the controllers move the system to the specified load flow distribution without any indication of problems. The control area is in all investigated cases larger for a PAR, with a phase angle from $-10°$ to $10°$, than for a CSC with a series compensation from 0% to 70% of the line impedance.

4.3 More Than Two CSCs or PARs

For two series capacitors or two phase shifters, an analytical proof of small–signal stability of the proposed control scheme was given in Section 4.1.3. Here, the validity of the control scheme for load flow control with more than two CSCs or PARs is discussed.

4.3.1 Discussion of the Problem

The analytical proof of small–signal stability given in Section 4.1.3 depends on the comparatively simple expression for the eigenvalues of a

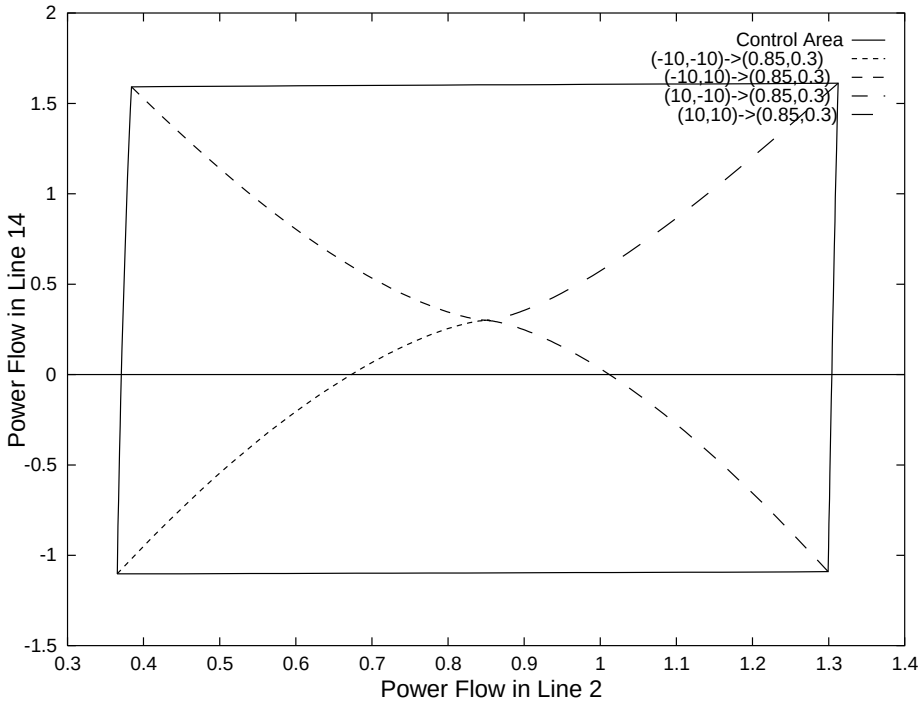

Figure 4.12. Results for Control of Lines 2 and 14 with PAR

2×2–matrix. For n controllable devices in a system, the real parts of the eigenvalues of a $n \times n$–matrix have to be evaluated. This corresponds to finding the zeros of a polynomial of n^{th} order.

For polynomials of 3^{rd} and 4^{th} order, closed form solutions exist. However, these are quite complicated and therefore of little use. For polynomials of order 5 and higher, closed form solutions do not even exist in the general case. Thus, that approach is not feasible.

It is, of course, possible to compute the eigenvalues of larger matrices numerically to find out whether the controlled system with an arbitrarily high number of devices and independent controllers is stable. However, that only shows stability for one particular system with one particular configuration, that is, one combination of controllable devices.

Still, one can argue that a system controlled with the proposed control scheme will in general be stable, as long as there is at least one uncontrolled path with sufficient power transfer capability for the active power

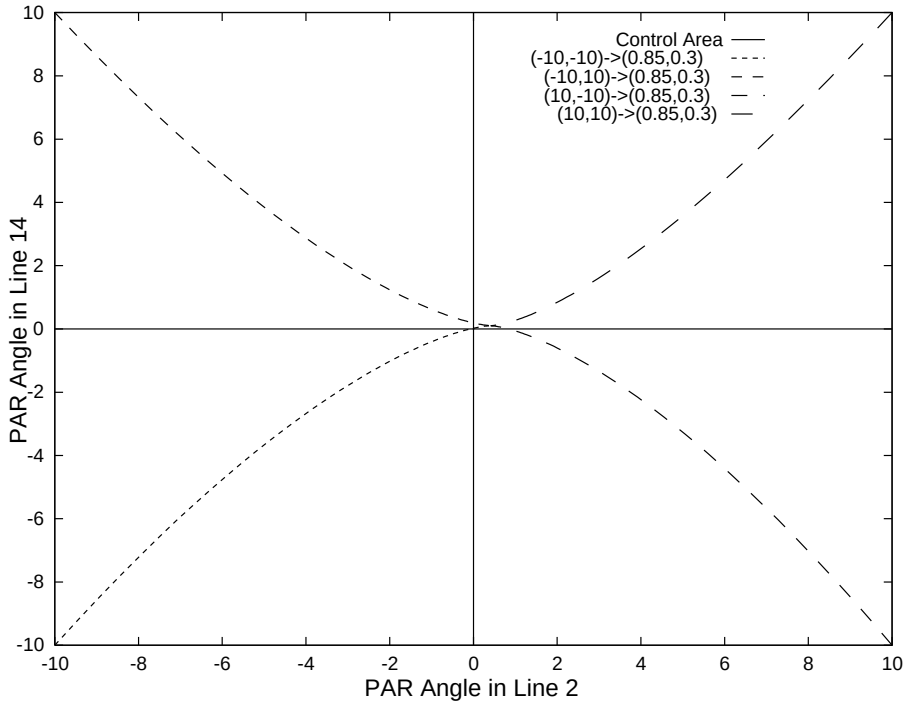

Figure 4.13. Results for Control of Lines 2 and 14 with PAR

flow to each load. These alternative paths will then "compensate" the forced variations in the load flow pattern, thereby providing damping for oscillatory hunting patterns that might develop between the controllers.

For the special case that $K = [k_1, k_2, \ldots, k_n]^T; k_1 = k_2 = \ldots = k_n$, a more formal proof of small–signal stability can be given.

The state equations of the system in Figure 4.14 are, if for now $K = I$,

$$\begin{aligned} \dot{x} &= -F(x) + u \\ v &= x \; . \end{aligned} \tag{4.8}$$

The problem in (4.3) is the function $F(v)$ that connects the settings of the FACTS devices and the load flows in the lines. If this function is replaced by its linearization $S = \frac{dF}{dv}$,

$$\begin{aligned} \dot{x} &= -Sx + u \\ v &= x \end{aligned} \tag{4.9}$$

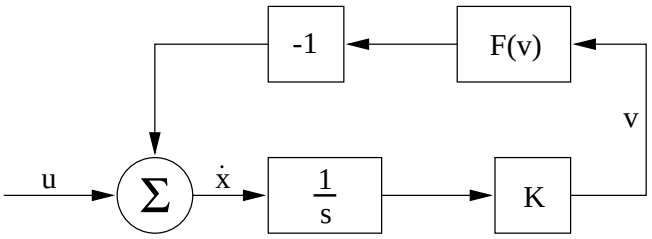

Figure 4.14. The Full Feedback System

is obtained. The stability of this linear system depends on the eigenvalues of $-S$. With the property of the linearization given in 4.3, Gershgorin's theorem [42] can be used to estimate these eigenvalues:

Gershgorin's theorem: *The eigenvalues of the $n \times n$ matrix A lie in the union of n circles in the complex plane, each with center a_{ii} and radius $r_i = \sum_{j \neq i} |a_{ij}|$ (sum of off-diagonal elements in row i). They also lie in the union of n circles, each with center in a_{ii} and radius $r'_i = \sum_{j \neq i} |a_{ji}|$ (sum of off-diagonal elements in column i).*

The Gershgorin–circles for S are centered around the positive diagonal elements S_{ii}. According to (4.3), the radii of those circles are smaller than S_{ii}. Thus the eigenvalues of S are all positive, the eigenvalues of $-S$ are all negative, and (4.9) is stable.

Introducing $K \neq I$ leads to replacing S with KS in (4.9). With $k_i = \text{const.} > 0$, the same argument holds.

4.3.2 Some Simulations

For all simulations the IEEE 30 bus test system, as described in Section 4.1.5, was used.

Figures 4.15 and 4.16 show the results of load flow control in lines 2, 7, and 14 using CSCs in these lines. The simulations start at the eight corners of the control volume, which is obtained for series compensations between 0% and 70% of the line reactances. In each case, the desired load flow is 1.05 pu, 0.87 pu, and 0.32 pu in lines 2, 7, and 14 respectively. Figure 4.15 shows the trajectories in state space, Figure 4.16 the change in the series compensations.

Figures 4.17 and 4.18 show similar results for controlling lines 2, 6, and 7. Again, the simulations start in the corners of the control volume. The set load flow pattern here is 0.99 pu, 0.69 pu, and 0.65 pu in lines 2, 6, and 14 respectively, which, again, is in the middle of the control volume.

Simulation results for the same line combinations, but using PARs, are depicted in Figures 4.19–4.22. The set load flow pattern for controlling lines 2, 7, and 14 was 0.85 pu, 0.91 pu, and 0.26 pu respectively; for controlling lines 2, 6, and 7 these values are 0.9 pu, 0.7 pu, and 0.9 pu. These load flow patterns are near the middle of the control volume obtained for PARs with the capability to vary their phase angle from $-10°$ to $10°$. Figures 4.19 and 4.21 show the variations of line flows; Figures 4.20 and 4.22 show the changes in the phase angles.

None of these results show signs of undamped, or even weakly damped oscillations. Only slight overshoots are visible. The proposed control scheme is obviously usable. Comparing the situations where the power flow is controlled with CSCs to those where PARs are used, it is evident that the control volume using PARs can be much larger. In [38], it has been shown that the rating of a series capacitor is essentially the same as the rating of a phase shifter for the same flow of active power. Thus, the increased control range is also connected to an increase of the power rating of the phase shifter.

4.4 Comparison of PAR and CSC for Load Flow Control

Since the proposed control scheme can be used for both devices, the decision whether CSCs or PARs should be used for load flow control depends on factors other than the overall performance of the controlled system:

Controllability: The control range using PARs is in general larger than the control range using CSCs. In highly loaded lines, CSCs come closer to PARs in that aspect. The rating of the devices is determined by the maximum load flow through the line in which they are located.

Costs: At the present time, both devices are expensive. However, the ongoing research in new materials for semiconductors, here especially

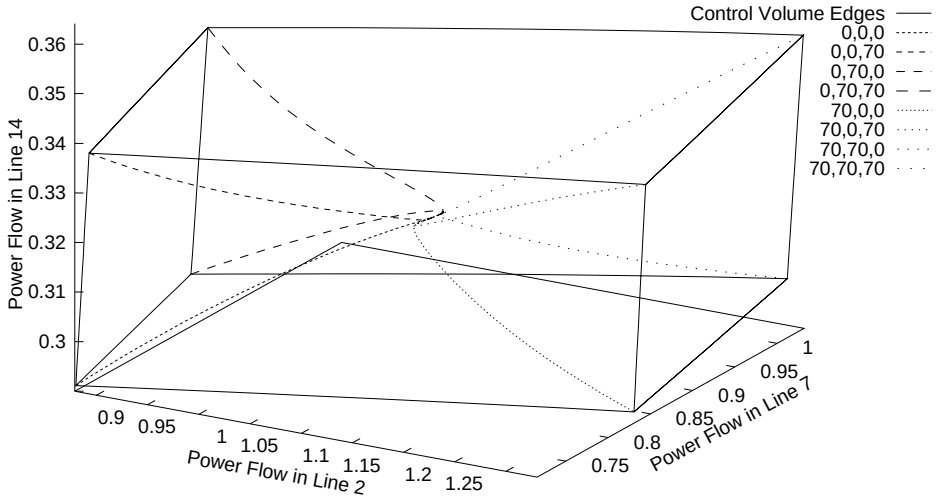

Figure 4.15. Results for Control of Lines 2, 7, and 14 with CSC

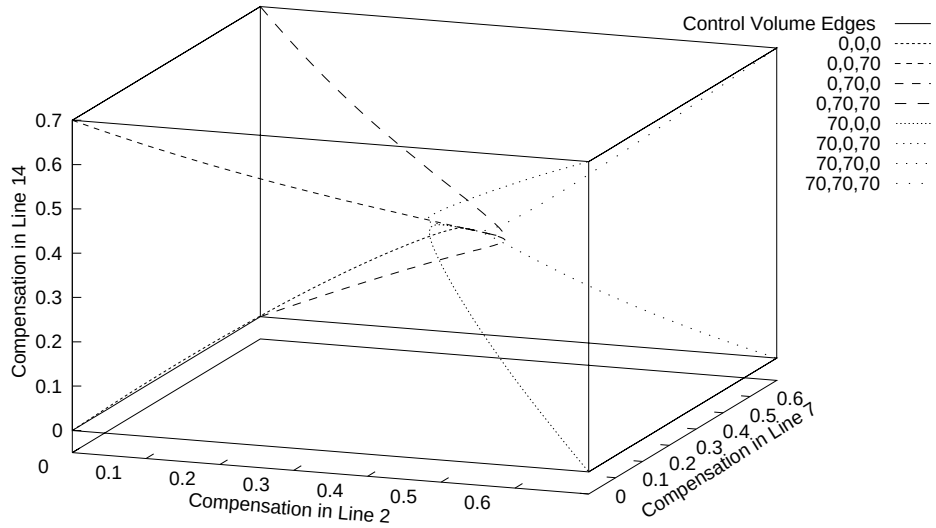

Figure 4.16. Results for Control of Lines 2, 7, and 14 with CSC

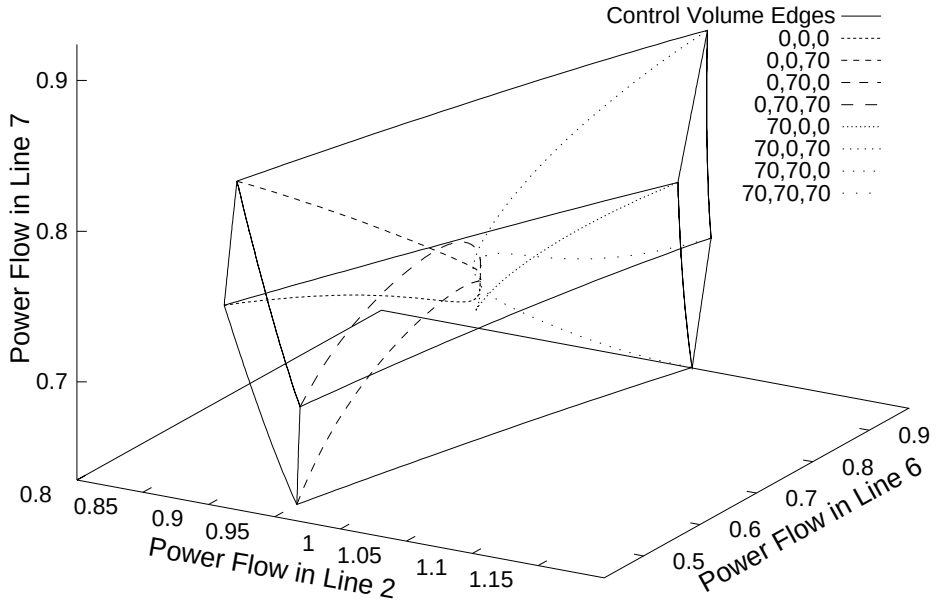

Figure 4.17. Results for Control of Lines 2, 6, and 7 with CSC

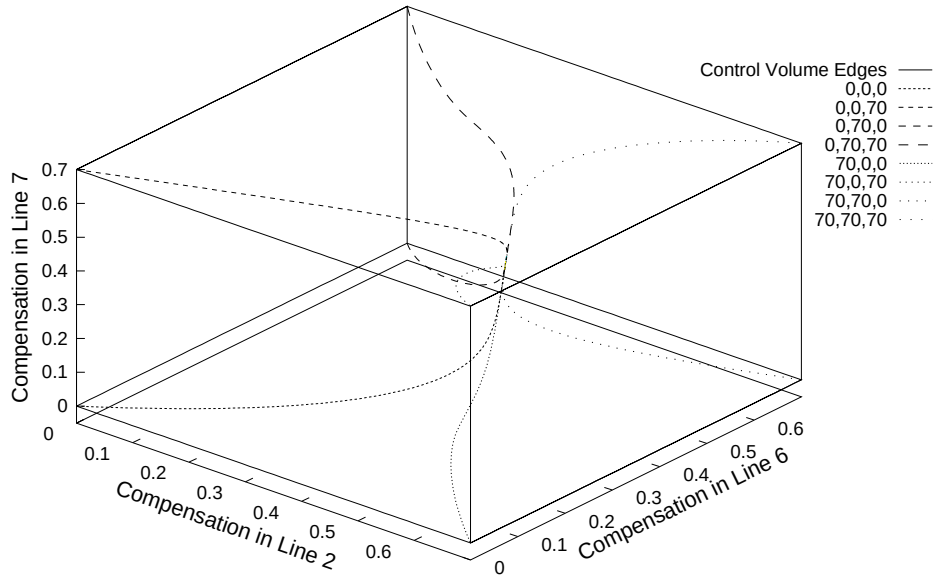

Figure 4.18. Results for Control of Lines 2, 6, and 7 with CSC

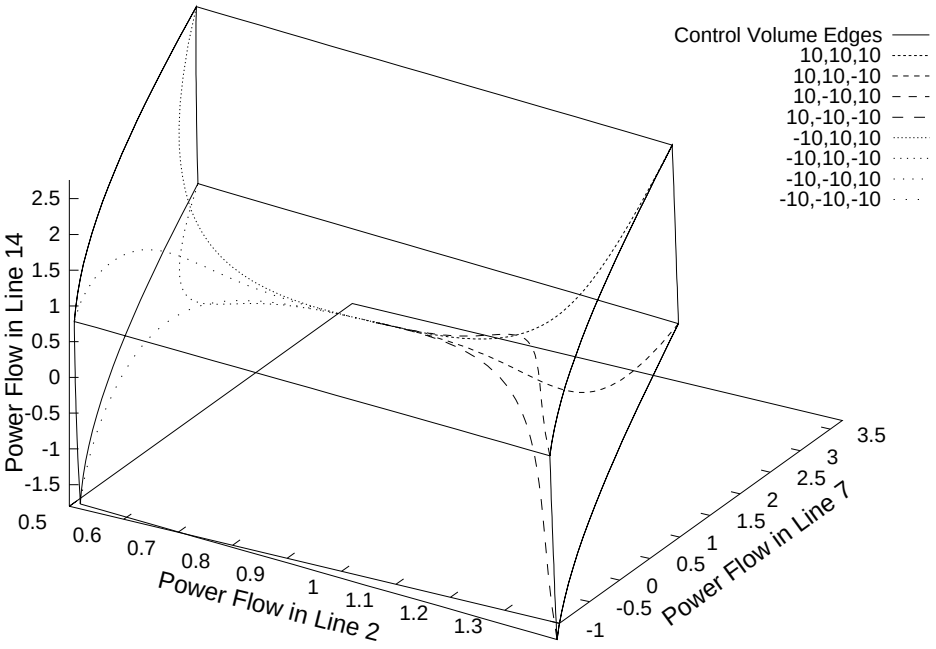

Figure 4.19. Results for Control of Lines 2, 7, and 14 with PAR

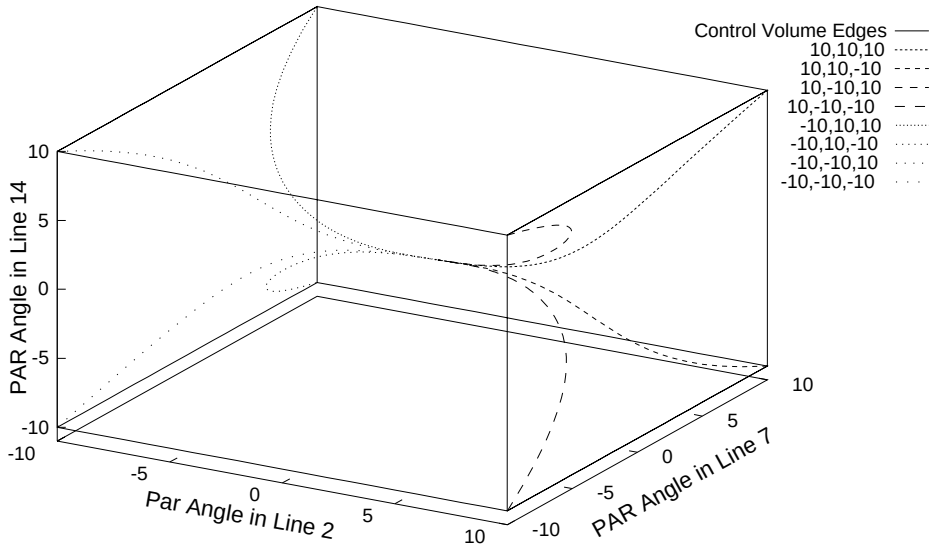

Figure 4.20. Results for Control of Lines 2, 7, and 14 with PAR

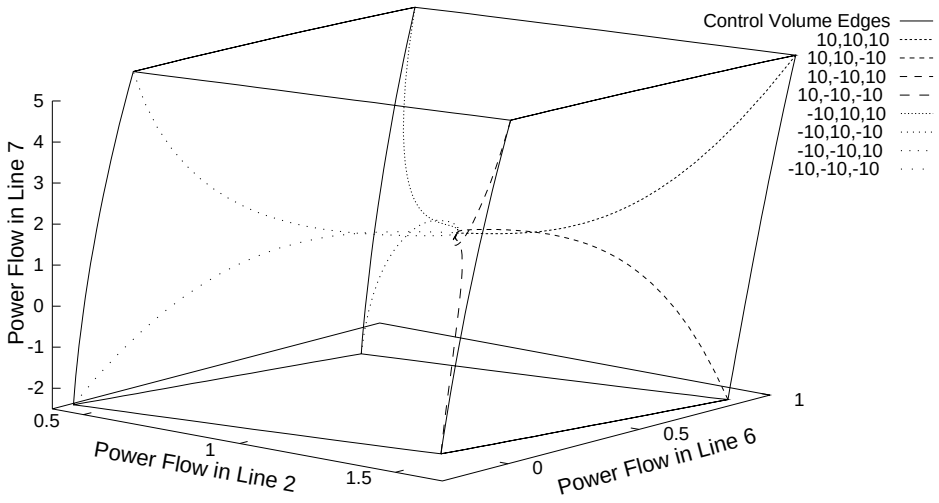

Figure 4.21. Results for Control of Lines 2, 6, and 7 with PAR

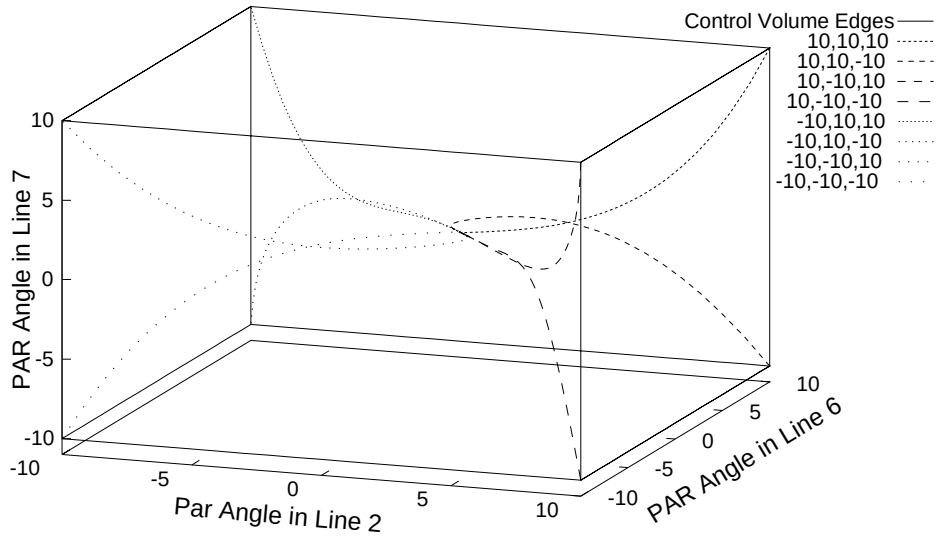

Figure 4.22. Results for Control of Lines 2, 6, and 7 with PAR

silicon carbide (SiC), might lead to considerably lower prices for thyristors, GTOs, and similar components. That could decrease the costs for CSCs considerably; PARs on the other hand contain transformers, which will certainly not become substantially cheaper in the foreseeable future. However, a number of phase shifters with mechanical switches, now able to change their phase angle in steps, are in use. These could be equipped with semiconductor switching gear, thus enabling them to change their phase angle continuously. This would obviously be a cheaper alternative.

Universal Applicability: Both devices have, in research papers, been used to control power system dynamics. The number of papers dealing with the CSC seems quite a bit larger.

Neither of those two devices has an overwhelming advantage over the other. The decision on the appropriate device will have to be made on a case–by–case basis.

4.5 Load Flow Control in Systems Close to Collapse

Typically, AC power systems are operated considerably below the thermal rating of their lines. Limiting for the power transmission is often one type of system instability called voltage collapse, characterized by a slow decrease in bus voltage magnitude as some system parameters, particularly the system load, increase gradually, followed at the collapse by a rapid decrease in voltage magnitude.

The amount of load that the system can supply in a given direction without loss of steady–state stability is often called the loadability margin. It has been shown that the loadability margin can be increased considerably by the use of FACTS devices [43].

However, it is conceivable that, in a system which is already close to its loadability margin, load flow control has a detrimental effect. Parts of the system might be pushed beyond the loadability margin, causing a voltage collapse situation. For highly loaded systems, such a situation can be considered during the design of the load flow control. However, it cannot be ruled out that a system which normally has a large loadability

margin suddenly suffers a dramatic decrease of loadability margin, or even becomes directly unstable, due to contingencies, unusual load patterns, or loss of generators.

The proposed control scheme does not in itself deal with these issues, since it only provides a way to achieve a desired load flow pattern in the electric power system. The desired load flow pattern can be determined by contractual requirements, optimal system operation, or system security; see Figure 4.23. Voltage stability issues have to be addressed in the determination of the desired load flow pattern.

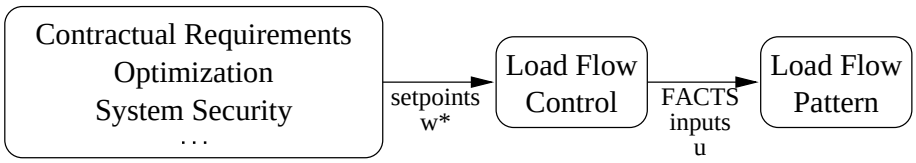

Figure 4.23. Higher Level Controller for Setting Control Inputs

Chapter 5

On the Placement of CSCs

So far, few FACTS devices are installed in existing power systems. Since these devices are meant to be employed in large AC power systems, there is a need to develop tools to investigate their optimal location in a given system. This chapter addresses the optimal location of these devices for load flow control.

It is not quite obvious which location of a FACTS device is optimal to control the load flow in a given line. CSCs, for example, are most effective in highly loaded lines [38]. Placed in a highly loaded line, a CSC may well have a larger effect on another, lightly loaded, line than when it is installed in the latter. Besides, it is desirable to find a method that allows consideration of other criteria than load flow, like cost, system stability, or optimal placement for oscillation damping.

5.1 Definitions

Sign Convention

The active power flow W through a line k connecting buses i and j is considered positive if active power is transmitted from bus i to bus j; it is considered negative if active power is transmitted from bus j to bus i:

$$W_k \quad \begin{array}{l} > 0 \Longrightarrow \text{Power transmission from bus } i \text{ to bus } j \\ < 0 \Longrightarrow \text{Power transmission from bus } j \text{ to bus } i \end{array} \tag{5.1}$$

Sensitivity

The sensitivity of an output variable α to a control variable β can be defined in two ways:

$$\hat{S}_{\alpha}^{\beta} = \frac{\partial \alpha}{\partial \beta} \tag{5.2}$$

or

$$S_{\alpha}^{\beta} = \frac{\partial \alpha}{\partial \beta} \cdot \frac{\beta}{\alpha} \tag{5.3}$$

When investigating the sensitivities of active power flows in lines k to series capacities in lines l, S_w , the definition given in Equation (5.3), sometimes also called relative sensitivity, has some advantages:

- S_w is dimensionless. Therefore the sensitivities for different voltage levels are commensurable.
- The possible series compensation in a line is usually not limited by the absolute size of the capacitor, but the limit is relative to the series reactance of the line. This is taken into account when using the definition given in Equation (5.3).
- For the control of active power flow, the absolute value of the active power flow is of interest. With this definition, the sign of the entry in the sensitivity matrix corresponds to the change of the absolute value of the active power flow.

Further, only the definition given in Equation (5.3) will be used, that is,

$$S_w = \frac{\partial W_k}{\partial x_l} \cdot \frac{x_l}{W_k} \ . \tag{5.4}$$

The first fraction in this definition is essentially the sensitivity of the line flows to the series compensation in a line. These sensitivities can be determined by simulation of small perturbations in x_l; they can also be determined analytically; see Appendix C.

5.2 Placing one CSC

Using the definitions above, the investigation starts with the simplest case, that is, the placement of one device in the system.

5.2.1 Controllability

The sensitivity S_w is a direct measure for the controllability of the active power flow in line k by a controllable series capacitor in line l.

Example: If we want to raise the active power flow in line 33 of the IEEE 30 bus test system, the sensitivity for a CSC in the same line is $S_{w_{33\ 33}} = 0.128$. Since the diagonal entry in the sensitivity matrix is not the largest entry in this row, a CSC in another line will result in a larger control range. In Figure 5.1, the control ranges of the active power flow in line 33 by CSCs in line 33, 7, and 5 are shown. These control ranges have been determined using a full nonlinear load flow. The corresponding entries in the sensitivity matrix are $S_{w_{33\ 33}} = 0.128$, $S_{w_{33\ 5}} = 0.151$, and $S_{w_{33\ 7}} = 0.396$.

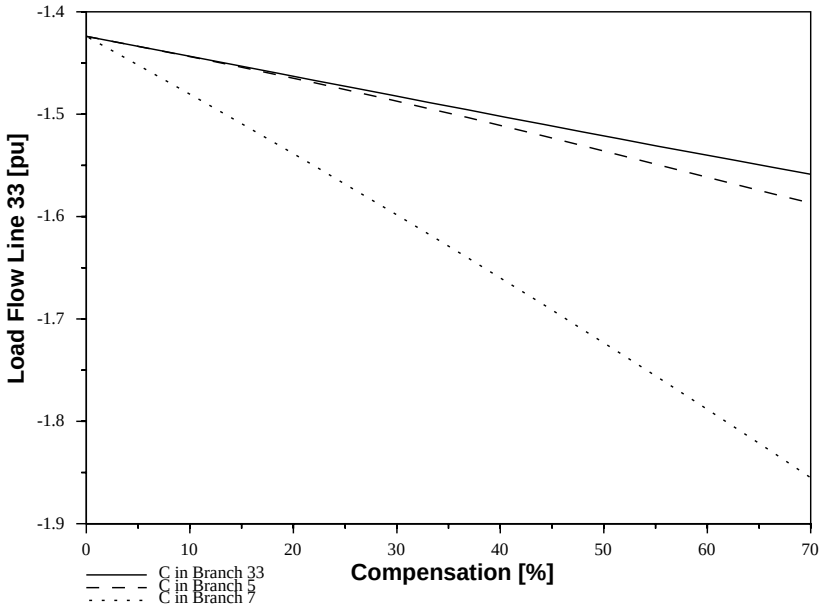

Figure 5.1. Change of Active Power Flow in Line 33

5.2.2 Cross Coupling

The cross coupling, that is, the effect that a CSC in one line has on the active power flow in another line, is determined by the off-diagonal

elements in the sensitivity matrix.

Example: The CSC in line 7 from the previous example has considerable stronger side effects on some other lines than the CSC in line 33. Two examples from the sensitivity matrix are

1. $S_{w_8\ 33} = 0.000$ whereas $S_{w_8\ 7} = 0.191 \Longrightarrow$ strong rise in active power flow in line 8 with rising series compensation in line 7
2. $S_{w_{21}\ 33} = 0.000$ whereas $S_{w_{21}\ 7} = -0.564 \Longrightarrow$ line 21 alleviated with rising series compensation in line 7.

The simulation results, again from a full nonlinear load flow computation, shown in Figures 5.2 and 5.3 confirm these predictions.

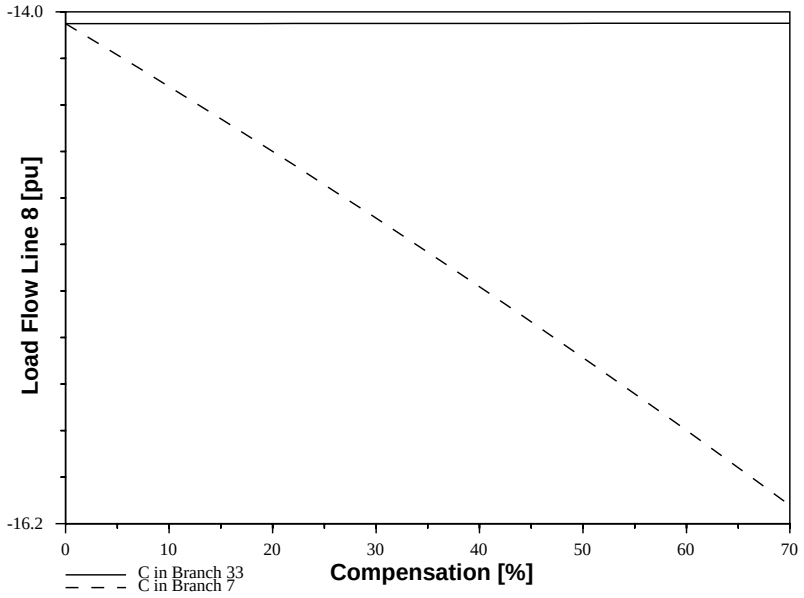

Figure 5.2. Influence of CSC in Lines 7 or 33 on Load Flow in Line 8

5.2.3 Load Alleviation

If the goal is to decrease the active power flow in a line k to a value that is lower than the load flow in the original system, the CSC will always

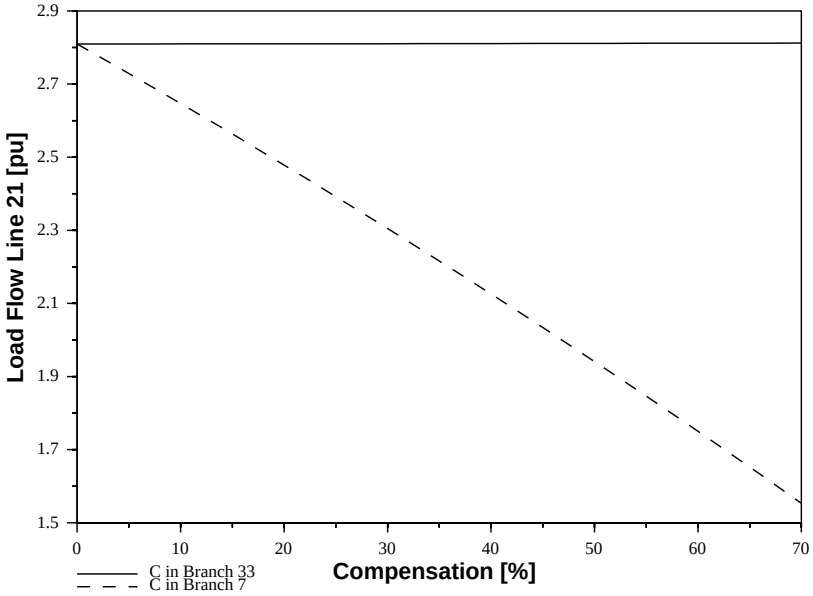

Figure 5.3. Influence of a CSC in Lines 7 or 33 on Load Flow in Line 21

have to be in a line different from the line where the line load, that is, the active power flow through the line, should be alleviated since a CSC can only increase the active power flow in the line in which it is situated. Suitable lines are lines l for which S_w is negative.

Example: The minimum value of row 9 in the sensitivity matrix is $S_{w_{9\,5}} = -0.804$. Therefore a CSC in line 5 is optimal for alleviating line 9. The next best choice would be a CSC in line 1, but since $S_{w_{9\,1}} = -0.088$ the effect will be much weaker. Simulation results are shown in Figure 5.4 and confirm these predictions.

5.3 Placing Several CSCs

In order to control the active power flow in more than one line, more than one CSC will be needed in the power system. Since these devices influence more than only one branch, they might have detrimental or augmentative effects on each other. The sensitivity matrix can be used as a tool for

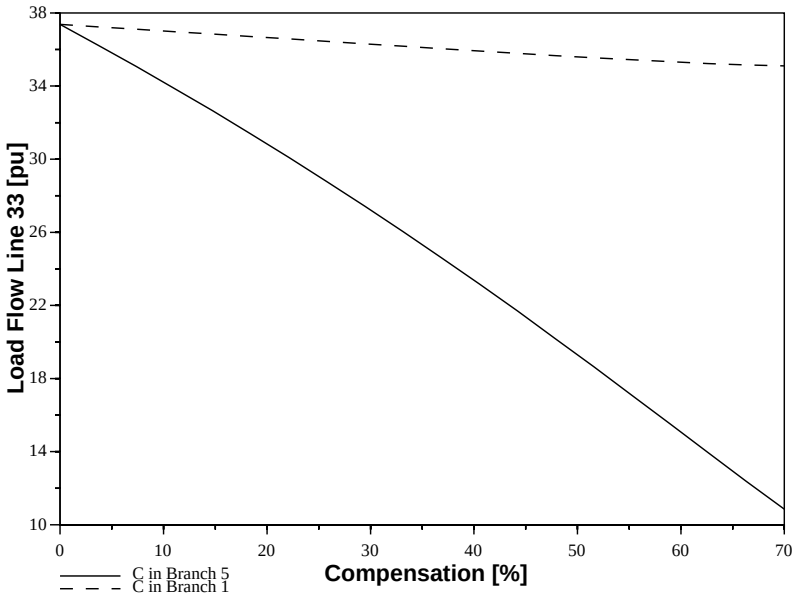

Figure 5.4. Change of Active Power Flow in Line 33

investigating these effects. Of interest are the row sums in the sensitivity matrix corresponding to the lines in which the CSCs are located.

5.3.1 Method

The proposed algorithm for the placement of the CSCs devices is quite straightforward:

1. Compute the sensitivity matrix S for the system.
2. Define some objective function that returns a scalar value proportional to the "desirability" of a particular configuration.
3. For each combination of device placements, compute this scalar value. Store the successive values in a list.
4. Sort the list.
5. Return the first m elements of the list, that is, those elements that have the largest "desirability" or optimality. This delivers the m best placements.

The objective function in Step 2 should contain the design specifications. Basically, any quantifiable design criterion can be considered. Some possible criteria are:

- Controllability range.
- Minimal cross coupling.
- Minimal cost.
- Change of load flow positive / negative.
- Impact on system stability.
- Possibility of damping oscillation modes.

5.3.2 Computational aspects

In a power system with n lines, there are in principle $N = \binom{n}{k}$ possibilities to place k CSCs. Due to practical limitations, series compensation may not be feasible in all lines; that is, n may be smaller than the number of lines in the system. This means that N line sums have to be computed and evaluated in order to be sure that an optimal placement for the devices is found. This is only feasible for small systems or a small number of series devices. For locating 3 CSCs in the test system, we have 10660 possibilities; for 4 CSCs 101270. This shows that even for comparatively small systems, more advanced methods, will have to be employed.

5.3.3 Validity of the Linearization

The sensitivity matrix is strictly valid only in the operating point for which it has been computed. Therefore, the results we obtain might not be quite reliable. A more thorough investigation of a number of the best results will, however, reveal "the best" possibility.

5.3.4 Examples

The results obtained from the following examples are given in Tables 5.1–5.10 and Figures 5.5–5.14. The tables give the ten "best" possibilities

for each example according to the proposed algorithm with the optimality, that is, the value of the objective function, for each configuration. The figures show the control areas obtained for the first seven of these configurations. The depicted control areas were obtained using nonlinear simulations.

Placing CSCs for Controlling Load Flow in Lines 30 and 35

Lines 30 and 35 are highly interdependent, since all changes in load flow through these lines must be compensated by an inverted change of load flow through line 31.

Maximizing Controllability. To maximize controllability, the expression

$$S_{w30} \times S_{w35} = S_{w30} \cdot S_{w35} - S_{w30} \cdot S_{w35} \tag{5.5}$$

is used to determine the optimality. i and j are the lines containing a CSC. This expression uses the entries of the sensitivity matrix to form two vectors pointing in the directions where the load flow will change in both lines. Each vector corresponds to the change of load flow in both lines by changing the compensation of one CSC. The expression delivers the area of the rhombus these two vectors span, and since the vectors' length is given by the sensitivities of the line flows of the controlled lines, that area is proportional to the expected control area.

Table 5.1 and Figure 5.5 show the results of this procedure. Generally, with decreasing optimality, the control area gets smaller. This validates the proposed method.

Maximizing Controllability Given the Direction of the Change of Load Flow. Often, when controlling load flow, it is given in the design whether the loading of a certain line should increase or decrease from the loading in the uncompensated system. Incorporating this knowledge in the objective function is straightforward; cases where $S_{w30} + S_{w30}$ and $S_{w35} + S_{w35}$ are positive or negative for increase or decrease of load flow respectively, are assigned optimality 0.

Tables 5.2–5.5 and Figures 5.6–5.9 show results that were obtained using this knowledge. A +–sign following a line number means that the load

Nr.	Optimality	Line 1	Line 2
1	0.0604574	14	18
2	0.0524747	14	30
3	0.0492398	7	14
4	0.0491557	18	31
5	0.048942	7	31
6	0.0386885	30	31
7	0.0377679	31	35
8	0.0373054	18	35
9	0.0349903	30	35
10	0.0340536	18	27
⋮	⋮	⋮	⋮

Table 5.1. Controlling Lines 30 and 35. Objective function is given by Equation (5.5).

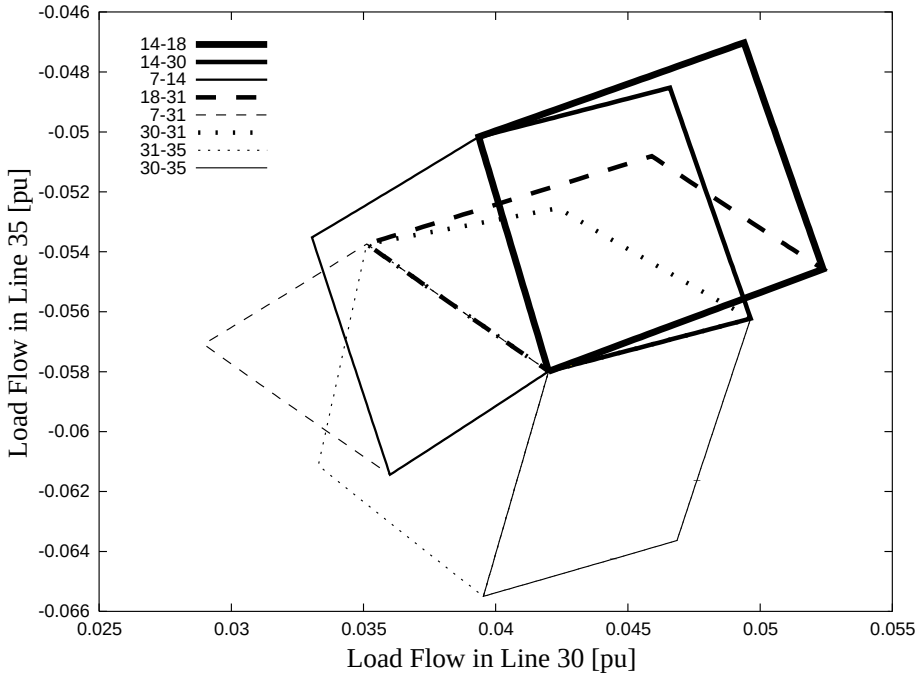

Figure 5.5. Control Areas for Lines 30 / 35

flow in that line should be increased, a -–sign means the load should be decreased.

Again, the approximation agrees with the simulations. It can be observed that even when the load flow in both lines should be increased, it is not the best solution to place the CSCs in lines 30 and 35, as one might expect. Usually, not the whole control area lies within the desired area, which gives an additional reason for checking the results obtained from the optimization.

Placing CSCs for Controlling Load Flow in Lines 2 and 14

To give an example using less interdependent lines, the same investigations are carried out for load flow control in lines 2 and 14. These lines are quite independent; a change of load flow in these lines is compensated by changes of load flow in many other lines.

The optimality is here determined by

$$S_{w_2} \cdot S_{w_{14}} - S_{w_2} \cdot S_{w_{14}} , \tag{5.6}$$

and when it is known whether the load flow should increase or decrease, the signs of $S_{w_{30}} + S_{w_{30}}$ and $S_{w_5} + S_{w_{35}}$ are considered.

The optimal lines according to the proposed algorithm are given in Tables 5.6–5.10; corresponding simulation results for some of these are shown in Figures 5.10–5.14.

Again, the predictions are confirmed, and the predictions have the same limits as in the case where lines 30 and 35 were considered.

5.4 Summary

The usefulness of the sensitivity matrix that links series compensation and load flow for determining the optimal location of CSCs has been investigated in this chapter. Examples for the application of this sensitivity matrix were given and the predictions made in these examples were verified using nonlinear simulations. The simulation results agreed with the predictions, that is, the sensitivity matrix can be used for placing CSCs.

Nr.	Optimality	Line 1	Line 2
1	0.0373054	18	35
2	0.0349903	30	35
3	0.0330902	18	41
4	0.031047	30	41
5	0.0228133	25	35
6	0.0202514	25	41
7	0.0202082	7	30
8	0.016408	7	18
9	0.0151154	32	35
10	0.0134846	1	30
⋮	⋮	⋮	⋮

Table 5.2. Controlling Lines 30+ and 35+. Objective function is given by Equation (5.5).

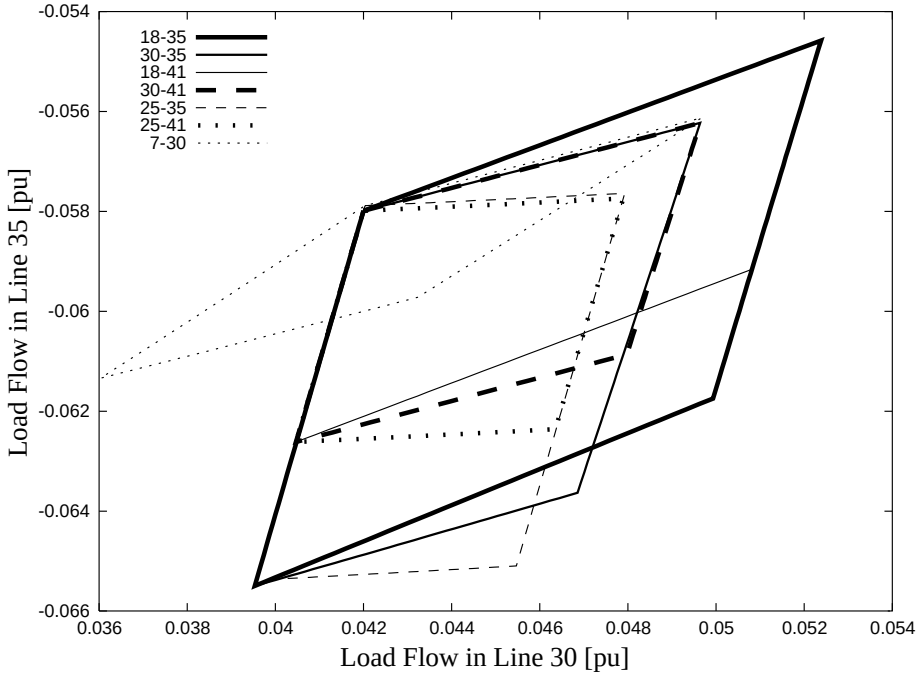

Figure 5.6. Control Areas for Lines 30+ / 35+

Nr.	Optimality	Line 1	Line 2
1	0.048942	7	31
2	0.0377679	31	35
3	0.0339863	7	27
4	0.0335693	31	41
5	0.0263481	27	35
6	0.0245363	7	35
7	0.0234187	27	41
8	0.021741	7	41
9	0.0212706	7	28
10	0.017428	7	25
⋮	⋮	⋮	⋮

Table 5.3. Controlling Lines 30- and 35+. Objective function is given by Equation (5.5).

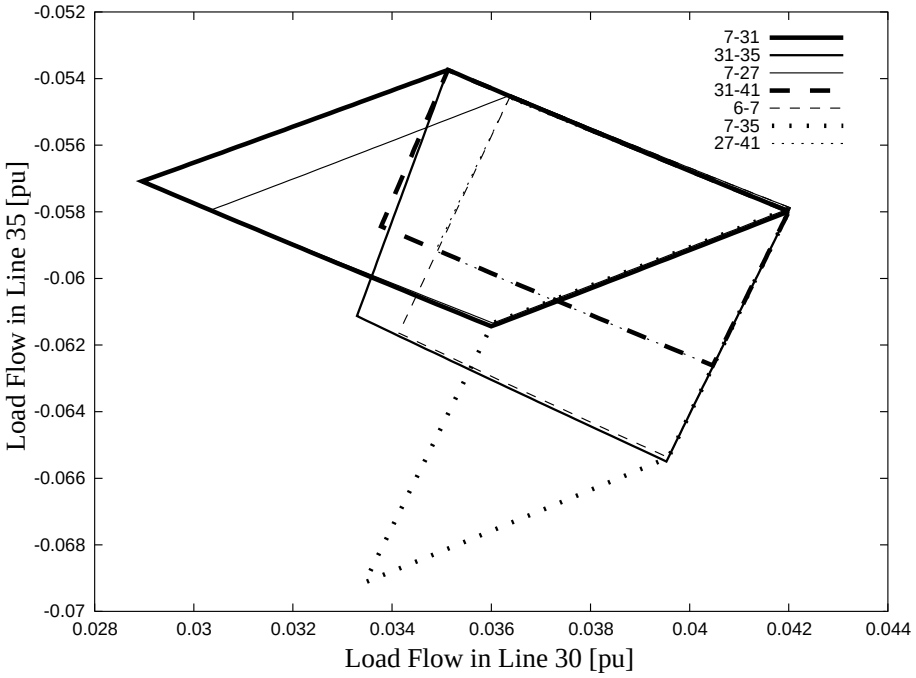

Figure 5.7. Control Areas for Lines 30- / 35+

Nr.	Optimality	Line 1	Line 2
1	0.0604574	14	18
2	0.0524747	14	30
3	0.0491557	18	31
4	0.0386885	30	31
5	0.0340536	18	27
6	0.030479	14	25
7	0.0267661	27	30
8	0.0226085	14	32
9	0.0213323	18	28
10	0.0167759	28	30
⋮	⋮	⋮	⋮

Table 5.4. Controlling Lines 30+ and 35-. Objective function is given by Equation (5.5).

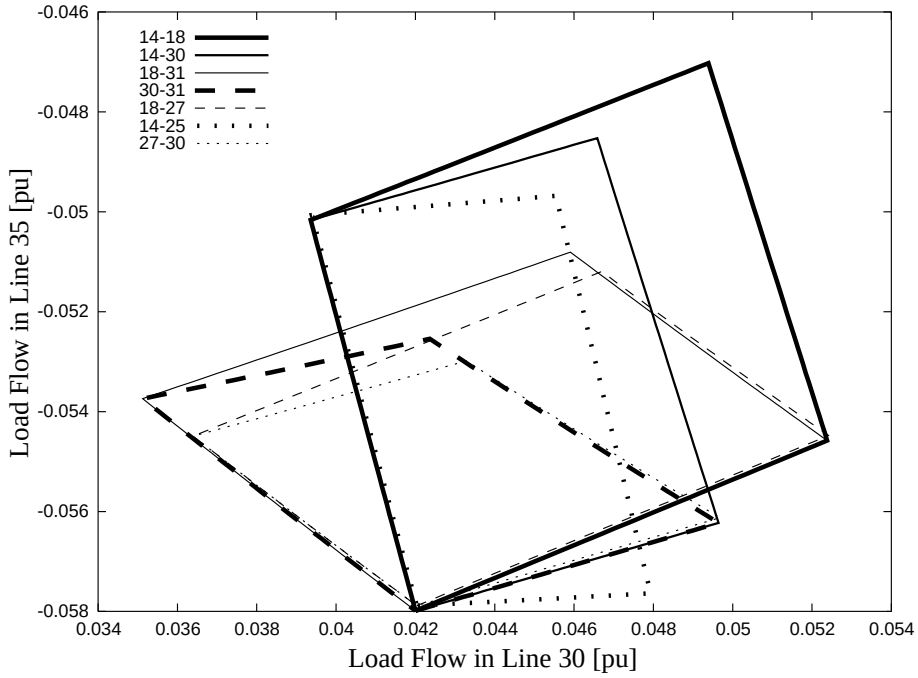

Figure 5.8. Control Areas for Lines 30+ / 35-

Nr.	Optimality	Line 1	Line 2
1	0.0492398	7	14
2	0.0328185	14	31
3	0.0262162	6	31
4	0.0252032	6	14
5	0.0231213	1	31
6	0.0230333	14	27
7	0.0215447	14	35
8	0.0204572	5	31
9	0.0199217	1	14
10	0.019195	14	41
⋮	⋮	⋮	⋮

Table 5.5. Controlling Lines 30- and 35-. Objective function is given by Equation (5.5).

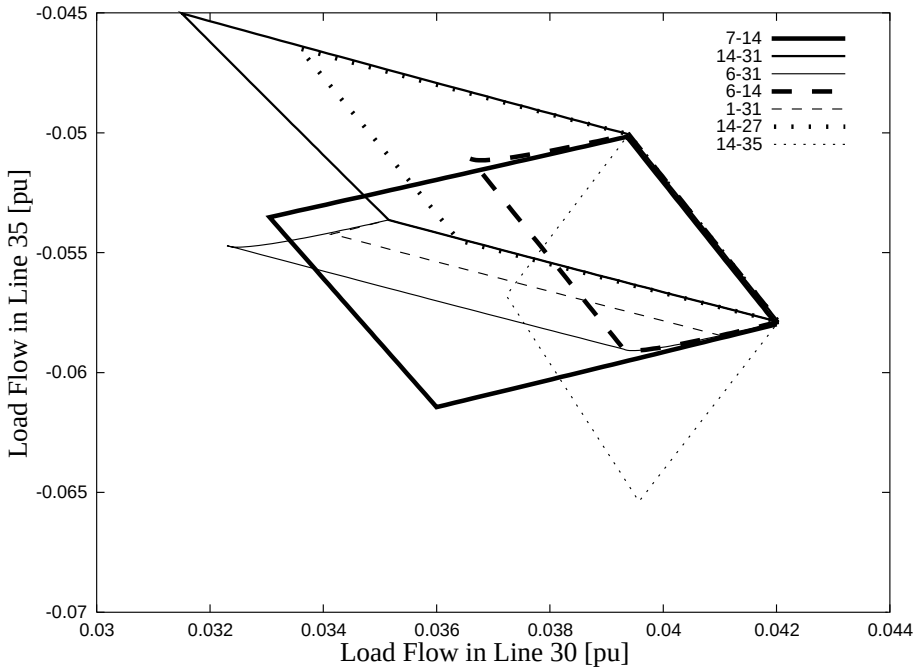

Figure 5.9. Control Areas for Lines 30- / 35-

Nr.	Optimality	Line 1	Line 2
1	0.0939862	2	14
2	0.0541938	1	14
3	0.0315778	2	7
4	0.0235141	3	14
5	0.0232857	6	14
6	0.0187091	4	14
7	0.0180985	1	7
8	0.0162724	5	14
9	0.0124287	2	3
10	0.0105481	2	6
⋮	⋮	⋮	⋮

Table 5.6. Controlling Lines 2 and 14. Objective function is given by Equation (5.6).

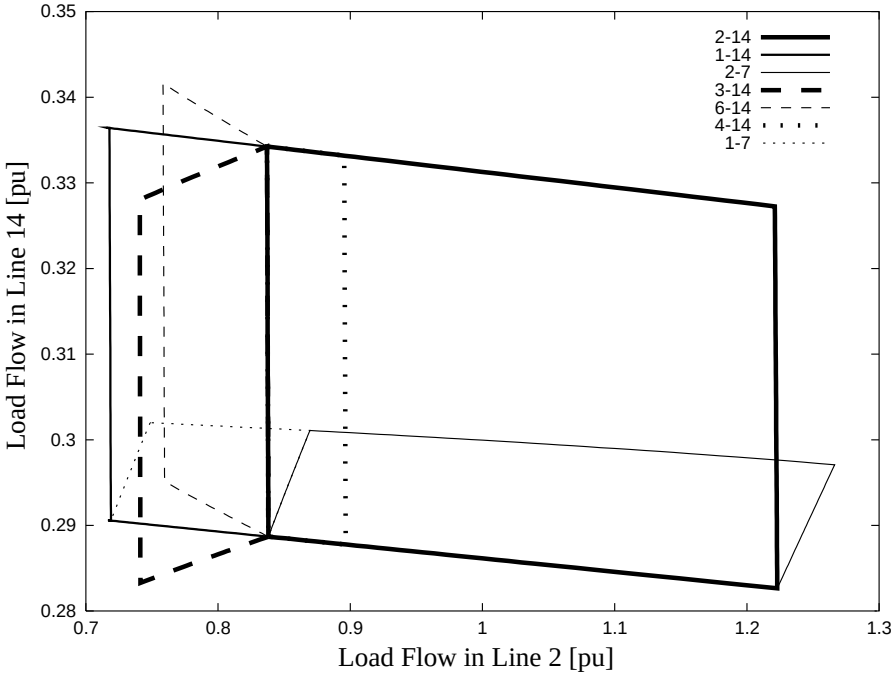

Figure 5.10. Control Areas for Lines 2 / 14

Nr.	Optimality	Line 1	Line 2
1	0.0939862	2	14
2	0.0315778	2	7
3	0.0187091	4	14
4	0.0105481	2	6
5	0.00948566	7	14
6	0.00628546	4	7
7	0.00323646	9	14
8	0.00165353	4	25
9	0.00158732	4	31
10	0.00141527	8	14
⋮	⋮	⋮	⋮

Table 5.7. Controlling Lines 2+ and 14+. Objective function is given by Equation (5.6).

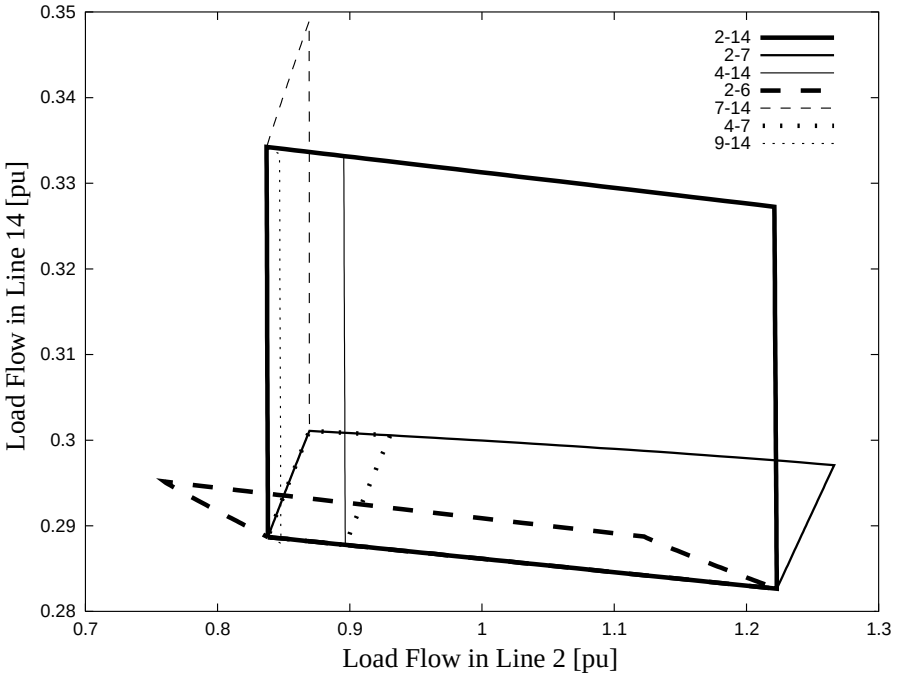

Figure 5.11. Control Areas for Lines 2+ / 14+

Nr.	Optimality	Line 1	Line 2
1	0.0541938	1	14
2	0.0235141	3	14
3	0.0232857	6	14
4	0.0180985	1	7
5	0.0162724	5	14
6	0.00888819	6	7
7	0.00664595	3	7
8	0.00635144	1	6
9	0.00617981	5	7
10	0.00571828	3	6
⋮	⋮	⋮	⋮

Table 5.8. Controlling Lines 2- and 14+. Objective function is given by Equation (5.6).

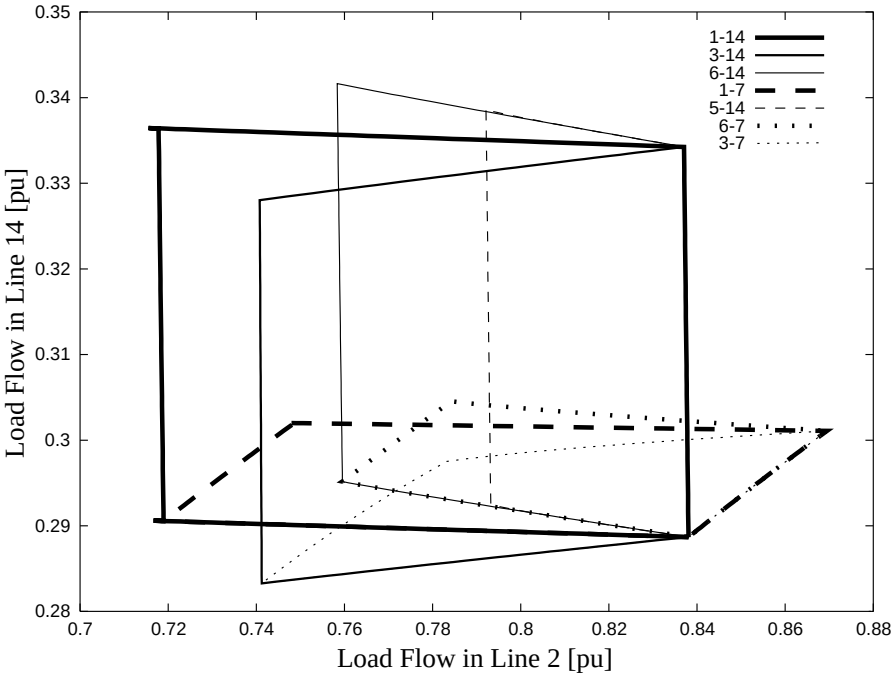

Figure 5.12. Control Areas for Lines 2- / 14+

Nr.	Optimality	Line 1	Line 2
1	0.0124287	2	3
2	0.010494	2	18
3	0.00866081	2	19
4	0.0083066	2	25
5	0.00797399	2	31
6	0.00706032	2	5
7	0.00688266	2	13
8	0.00552254	2	27
9	0.00531568	2	35
10	0.00497611	2	22
⋮	⋮	⋮	⋮

Table 5.9. Controlling Lines 2+ and 14-. Objective function is given by Equation (5.6).

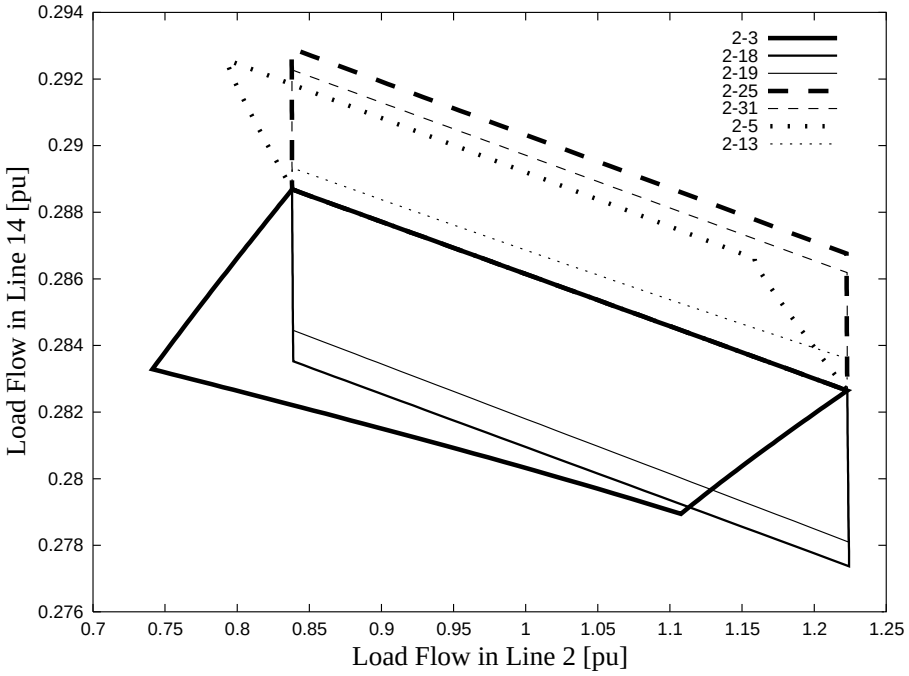

Figure 5.13. Control Areas for Lines 2+ / 14-

Nr.	Optimality	Line 1	Line 2
1	0.00689465	1	3
2	0.00605274	1	18
3	0.00499496	1	19
4	0.00391825	3	5
5	0.00264558	3	18
6	0.00247287	3	4
7	0.00217839	3	19
8	0.00208859	3	25
9	0.00199384	3	31
10	0.00180545	5	18
⋮	⋮	⋮	⋮

Table 5.10. Controlling Lines 2- and 14-. Objective function is given by Equation (5.6).

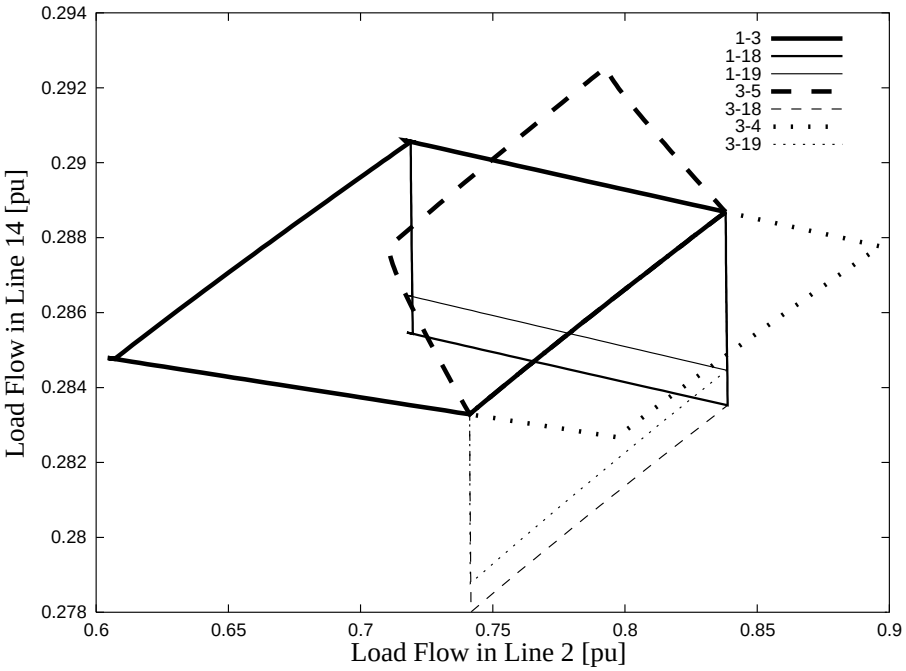

Figure 5.14. Control Areas for Lines 2- / 14-

Chapter 6

Characteristics of the UPFC

In this chapter, the benefits of using a UPFC for load flow control are discussed. There are some papers that show the characteristics of a UPFC in a system where no parallel lines to the controlled line exist [44, 45, 46]. Here, some characteristics for a larger, more realistic system, namely the IEEE 30 bus system, will be shown.

The series part of the UPFC has two control parameters, r and γ, which are the magnitude and the phase angle of the injected voltage respectively. Thus, it is in principle feasible to control quantities other than load flow. Here, the controllability of the magnitude of the bus voltages, from here on simply called bus voltages, at the buses that are connected by the line is investigated. Controlling the bus voltages is approximately equivalent to controlling the reactive power flow, just like controlling the load flow is approximately equivalent to controlling the voltage angle at the buses. The feasibility of controlling the bus voltages and the load flow simultaneously is discussed.

6.1 Load Flow

Figure 6.1 shows the load flow in line 14 with a UPFC in that line. γ is kept constant at various values while r varies from 0 to 0.1. From this figure follows

- that the controllability of the load flow with r is maximal when $\gamma = \pi/2$ for increasing load flow and when $\gamma = 3/2 \cdot \pi$ for decreasing load flow.
- that the controllability of the load flow with r is minimal when $\gamma = 0$ and when $\gamma = \pi$.
- that the relationship between r and load flow is strictly monotonic for fixed γ.

It should be noted that the monotonicity is preserved if r is varied from $-r_{max}$ to r_{max}, while γ is held at $\pi/2$. The characteristics are then the same as those obtained when regulating r from r_{max} to 0 with $\gamma = 3/2 \cdot \pi$, then switching γ to $\pi/2$ and regulating r from 0 to r_{max}.

Figure 6.2 again shows the load flow in line 14 with a UPFC in that line. In this case, r is kept constant at various values and γ is varies from 0 to 2π. Again, some conclusions can be drawn:

- The controllability of the load flow is maximal if r is maximal.
- There are two regions where the relationship between γ and the load flow are monotonic: From about $\pi/2$ to about $3/2 \cdot \pi$, the load flow is monotonically decreasing with γ, and from about $3/2 \cdot \pi$ to about $\pi/2$, the load flow is monotonically increasing with γ. However, these values are approximate since the extrema are not exactly at $\pi/2$ and $3/2 \cdot \pi$. This is somewhat more pronounced in Figure 6.3, where the same relations are shown for a UPFC in line 33. The easiest place where this is visible is at the crossings with the uncontrolled load flow (the line $r = 0$), which are not exactly at 0 and π.

Figure 6.4 shows these relations in one single three–dimensional picture.

Hence, if load flow control is the only concern, γ should be kept at $\pi/2$ and r should be varied from $-r_{max}$ to r_{max}. Even though the maximal controllability is not exactly at $\pi/2$, only little of the controllability is lost since the characteristic curve is quite flat around this value. With these settings, the relationship between the control variable r and the load flow is monotonic, and the control scheme with independent integral controllers can again be used.

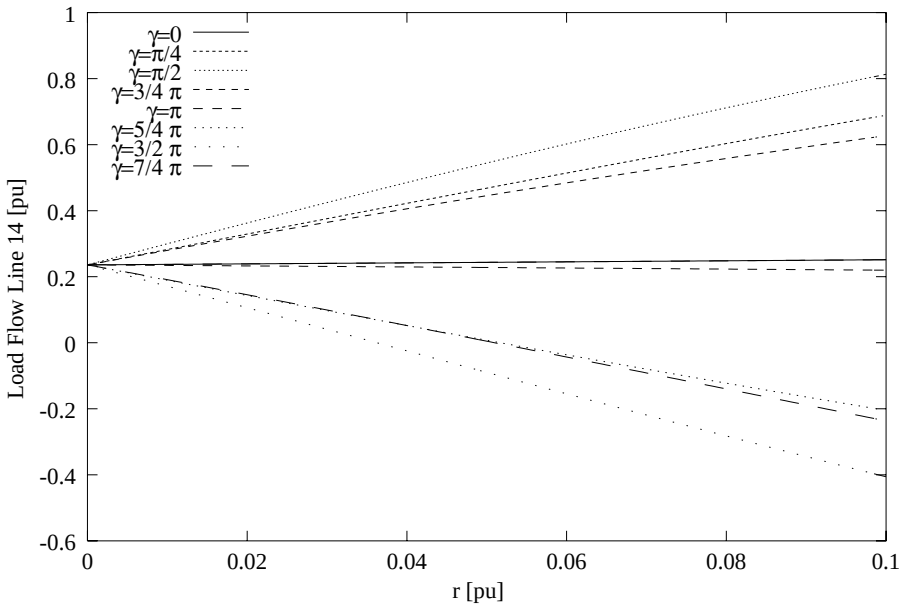

Figure 6.1. UPFC in Line 14; = const; Load Flow in Line 14

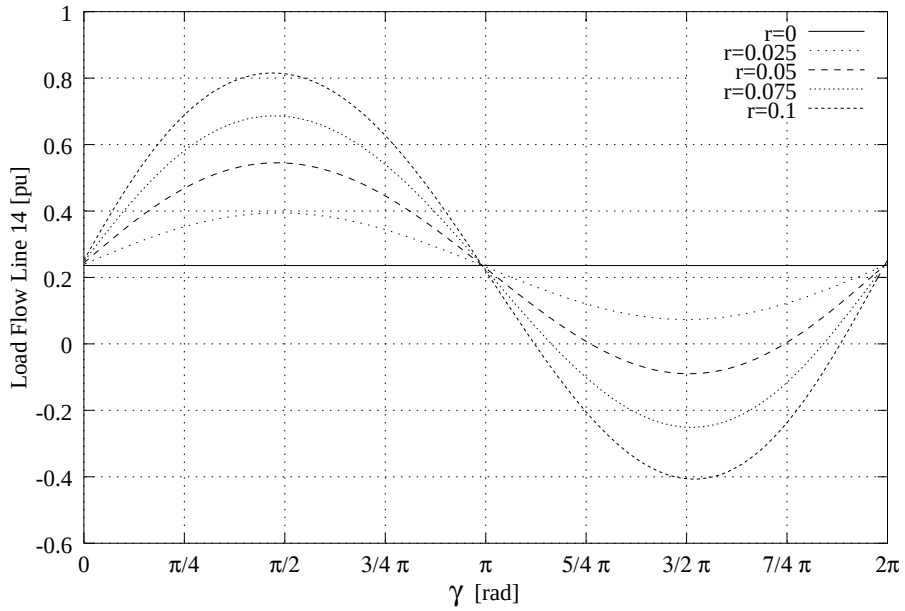

Figure 6.2. UPFC in Line 14; = const; Load Flow in Line 14

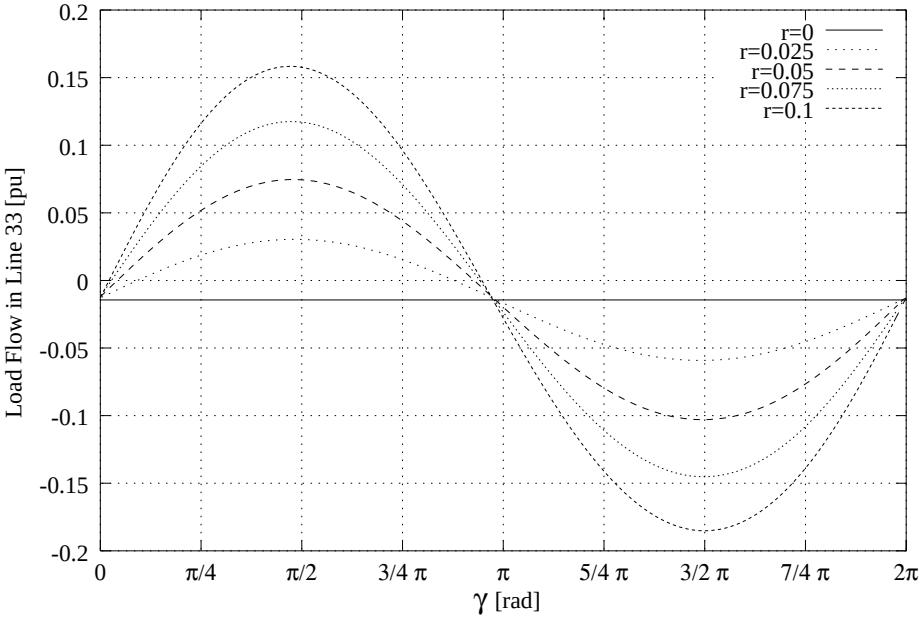

Figure 6.3. UPFC in Line 33; = const; Load Flow in Line 33

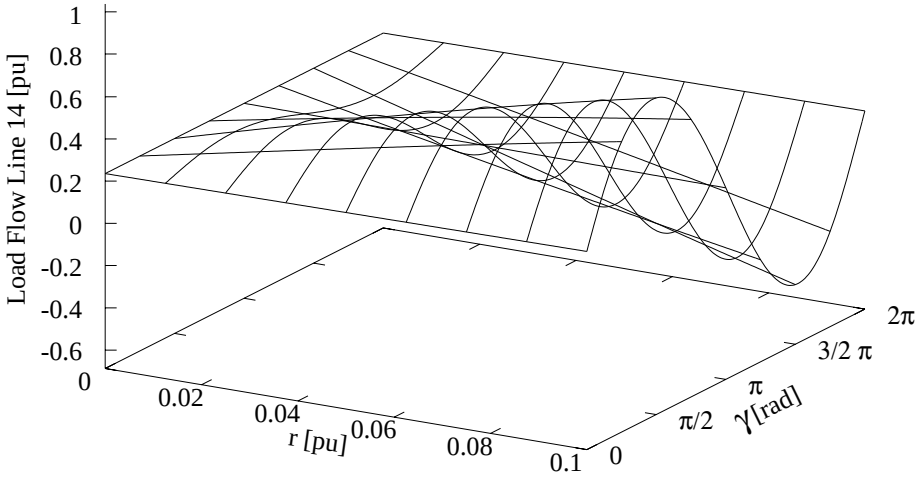

Figure 6.4. UPFC in Line 14; Load Flow in Line 14

6.2 Bus Voltages

A UPFC in a line influences the voltages at both ends of that line. Therefore, the investigation on the dependency of the bus voltages has to be carried out for both buses at the ends of the line.

Figures 6.5 and 6.6 show the voltages at the respective buses when γ is kept constant at various values and r is varied from 0 to 0.1. From these figures, it can be concluded

- that the maximum controllability is near $\gamma = 0$ and $\gamma = \pi$. The relation between the voltages at both ends is such that the voltage in one bus increases while the voltage in the other bus decreases.
- The relationship between the voltage and r is not necessarily monotonic. This is visible from the curves where $\gamma = \pi$.

Figures 6.5 and 6.6 show the bus voltages if r is kept constant at some values and γ is varied from 0 to 2π. The following observations can be made:

- The controllability of the voltages is maximal when r is maximal.
- The voltages at the buses have their maxima and minima respectively around 0 and π. Again, the voltage in one bus increases when the voltage in the other bus decreases.

Figures 6.7 and 6.8 show the voltages versus r and γ in three dimensions.

Figures 6.11 and 6.12 show the voltages at the buses as a locus curve. Depicted are the endpoints of the voltage vectors at the buses when $r = 0.1$ and $0 \leq \gamma \leq 2\pi$. The reference voltage with an angle of 0° is the voltage at the slack bus. These curves are fairly close to circles, arising from the fact that voltage that is injected by the UPFC moves in a circle when γ is varied between 0 and 2π. However, this circle–like shape can be severely deformed: Figure 6.13 depicts the movement of the bus voltage at bus 10 for a UPFC in line 27. The main difference between line 14 and line 27 is that line 14 is heavily loaded while line 27 is a fairly lightly loaded line.

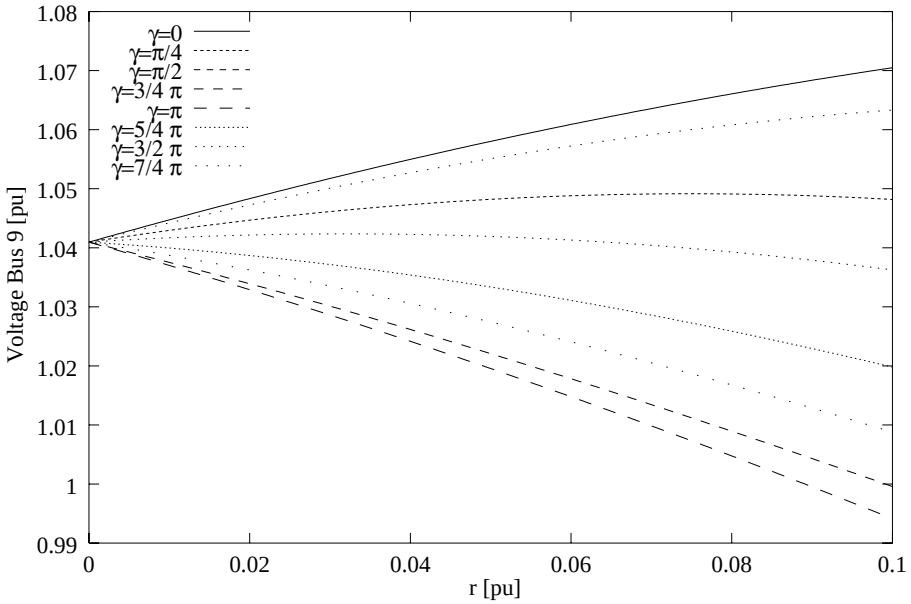

Figure 6.5. UPFC in Line 14; = const; Voltage at Bus 9

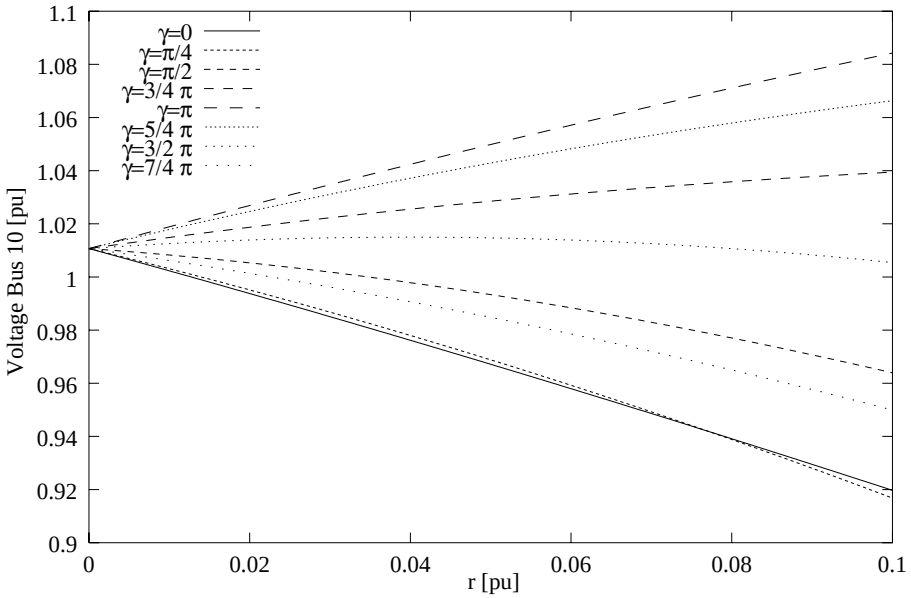

Figure 6.6. UPFC in Line 14; = const; Voltage at Bus 10

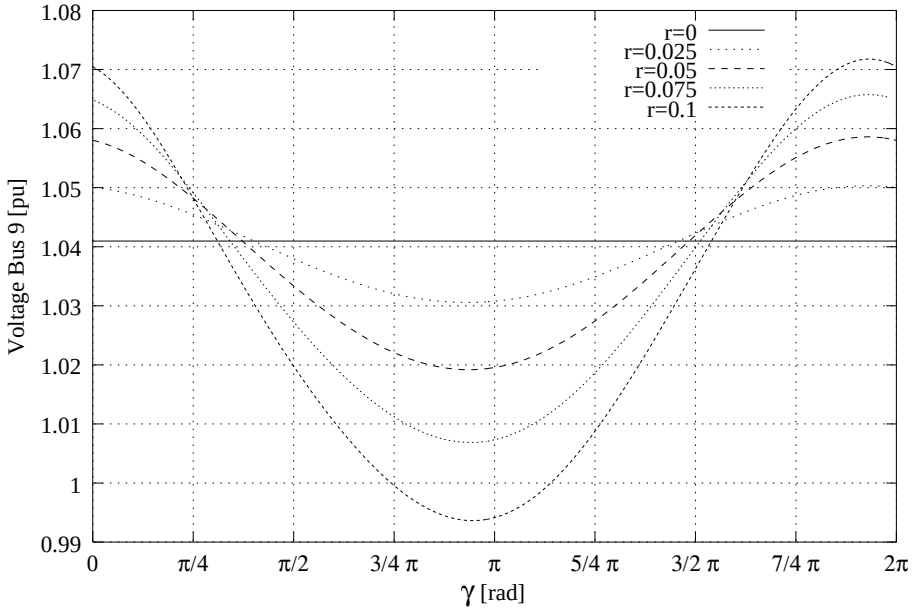

Figure 6.7. UPFC in Line 14; = const; Voltage at Bus 9

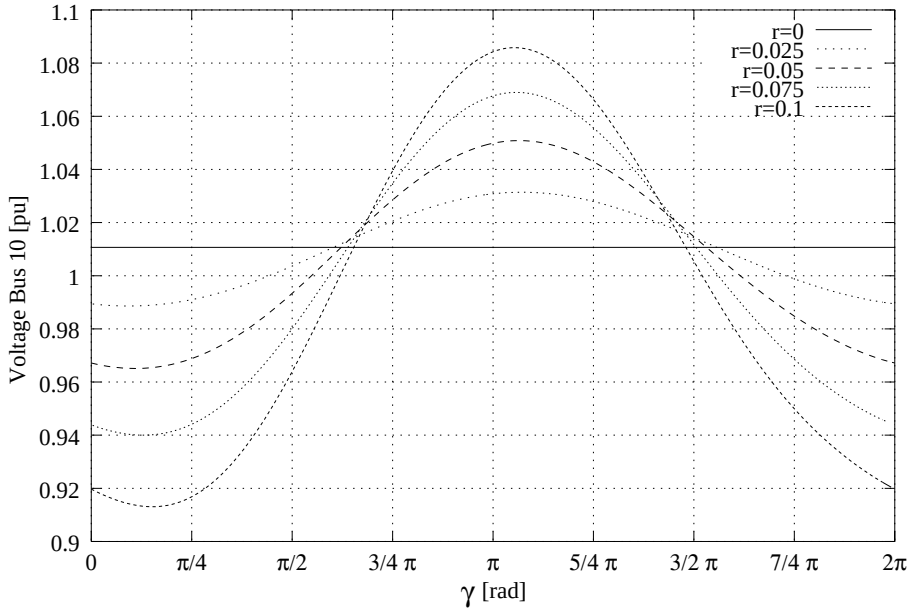

Figure 6.8. UPFC in Line 14; = const; Voltage at Bus 10

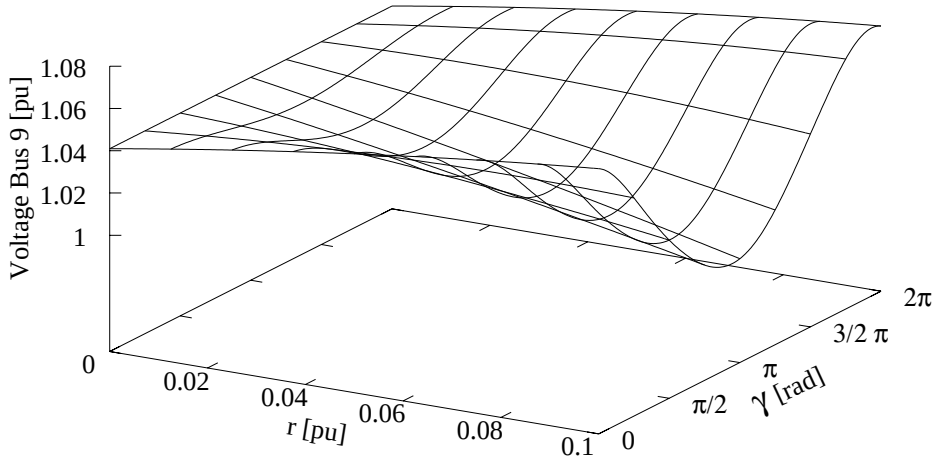

Figure 6.9. UPFC in Line 14; Voltage at Bus 9

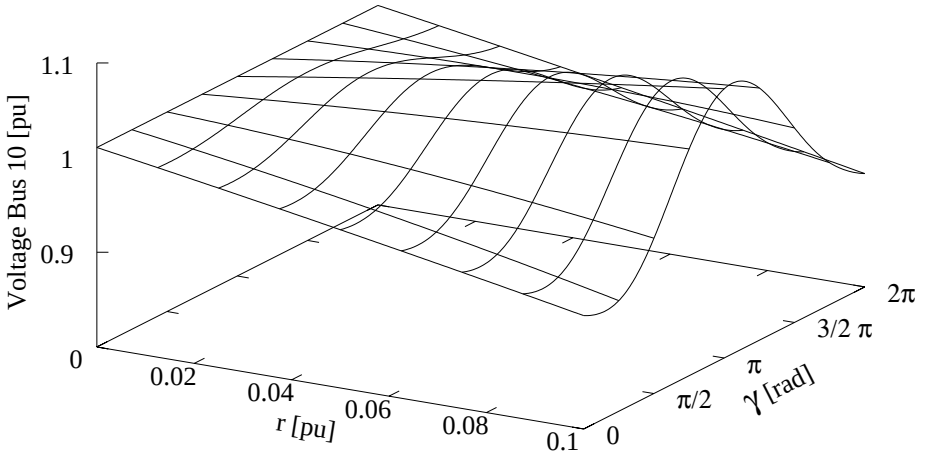

Figure 6.10. UPFC in Line 14; Voltage at Bus 10

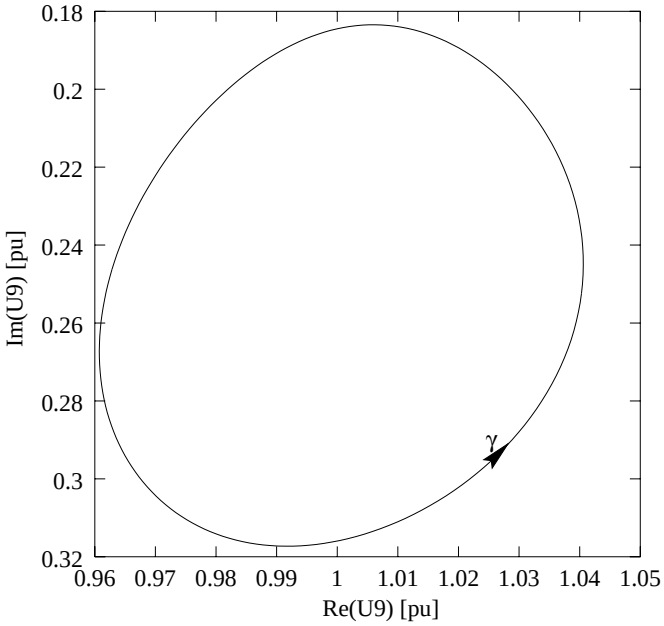

Figure 6.11. UPFC in Line 14; = 0.1; Voltage at Bus 9

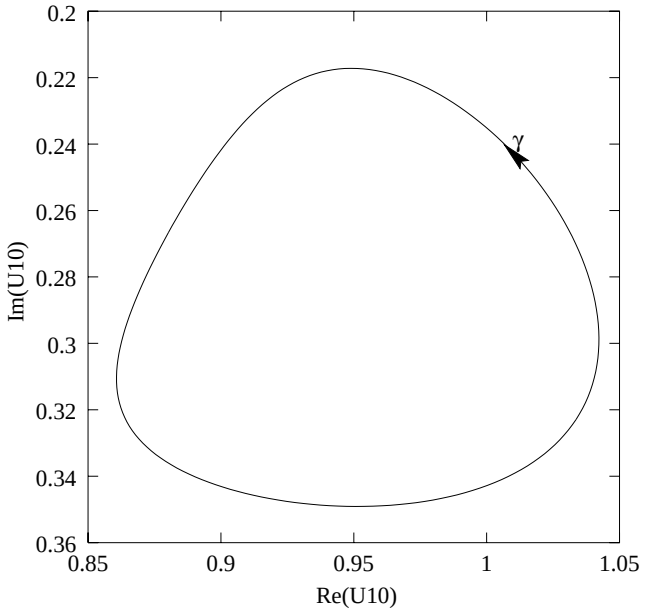

Figure 6.12. UPFC in Line 14; = 0.1; Voltage at Bus 10

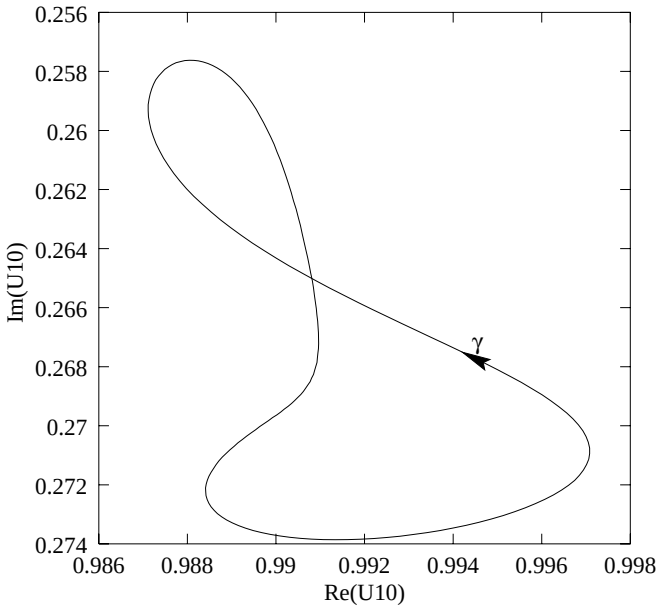

Figure 6.13. UPFC in Line 27; = 0.1; Voltage at Bus 10

6.3 Simultaneous Voltage and Load Flow Control

Is it feasible to use the UPFC to control load flow and bus voltages at the same time? From the observations in the previous section, it is clear that r is the best choice for the load flow control. Figure 6.14 depicts the load flow and the bus voltages when $r = const$ in one diagram. From this and the observations in the last section, several points can be made that are against combining load flow and bus voltage control:

- The controllability of the bus voltages is maximal when the controllability of the load flow is minimal.
- To enable voltage control, a large part of the controllability of the load flow must be sacrificed by setting γ to a value different from $\pi/2$.
- The controllability and the characteristic curves for voltage control depend on the system and the location of the UPFC in the system.

However, there is a different possibility for controlling the bus voltages: The shunt part of the UPFC can be used to inject or extract reactive power from the bus. This will be discussed further in the next chapter.

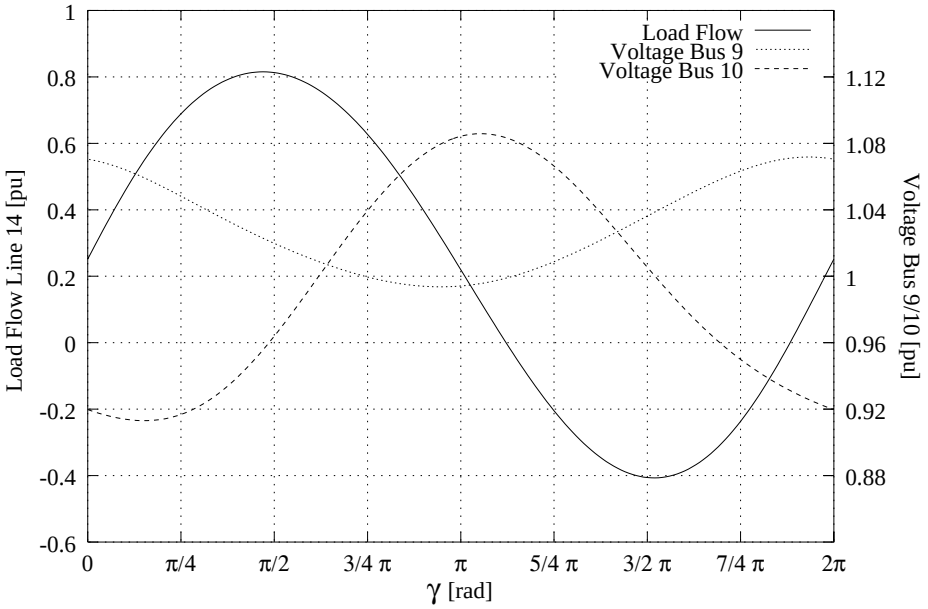

Figure 6.14. UPFC in Line 14; = 0.1; Load Flow and Voltages

Chapter 7

Load Flow Control Using the UPFC

Now that the characteristics of the UPFC have been established in the last chapter, this chapter deals with the use of the UPFC for power flow control. Since the UPFC, if used with a constant γ, is a monotonic device, the control scheme is expected to work in the same way as for CSCs and PARs. This is confirmed in the first section. In the second section, the ability of the UPFC to independently inject or absorb reactive power at a bus independently of the load flow control is investigated.

7.1 Load Flow Control Only

If the UPFC is operated with r as the control variable and γ fixed at $\pi/2$, the controllability of the load flow in the line where UPFC is located is maximized. For reasonably small values of r, the UPFC acts in this control mode very similar to a PAR. Further, with $\gamma = \text{const.}$, the UPFC has a monotonic characteristic. The load flow increases with r, just like the line flow increases with the series capacitance in case of the CSC and the phase angle in case of the phase shifter. Thus, the same control scheme can be used, and neither oscillation problems nor stability problems are expected in the control of power flows.

This is verified by the simulation results in Figure 7.1 and 7.2. Figure 7.1 shows the result for controlling the load flow in lines 2, 6, and 14. The

simulation starts in the corners of the control volume, and the setpoint of the controllers is 0.55 pu, 0.4 pu, and 0.25 pu in lines 2, 6, and 14 respectively. Figure 7.2 shows on principle the same simulation, only for lines 2, 6, and 7, and with setpoints of 0.55, 0.5, and 0.75 pu. In both cases, the convergence is smooth and unproblematic.

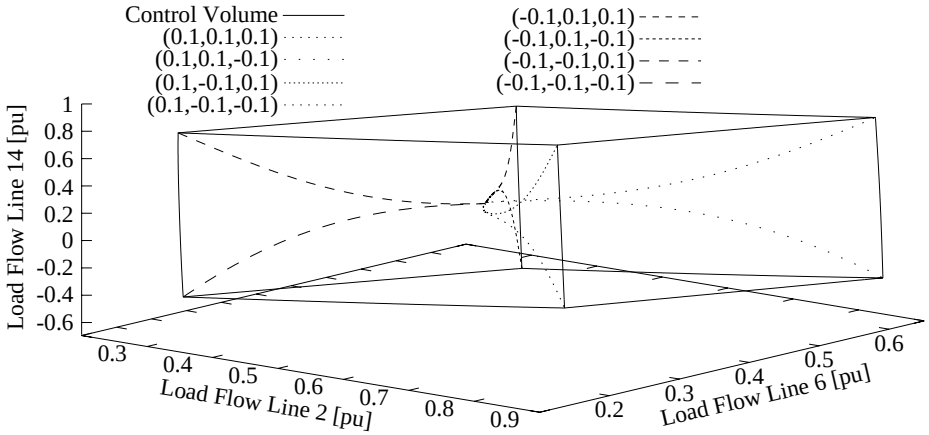

Figure 7.1. Load Flow Control in Lines 2, 6, and 14

7.2 Load Flow Control and Bus Voltage Control

As mentioned in the previous chapter, the UPFC has one control parameter that has not been investigated yet: The parallel branch of the UPFC can be used to inject reactive power into or absorb reactive power from the bus it is located at. In other words, the parallel branch of the UPFC can be used as an independent controllable shunt reactive power source. In this section, one possible application of this feature is discussed: the voltage at the bus with the parallel branch of the UPFC is kept constant at the value it has when $r = 0$.

As examples, three different lines are used: line 2, which ends in the slack bus; line 14, which is close to a PU–bus; and line 30, which is far from any PU–bus and has PQ–buses at both ends. Further, it is assumed that the voltage control is instantaneous compared to the load flow control; this can be achieved by an appropriate fast controller.

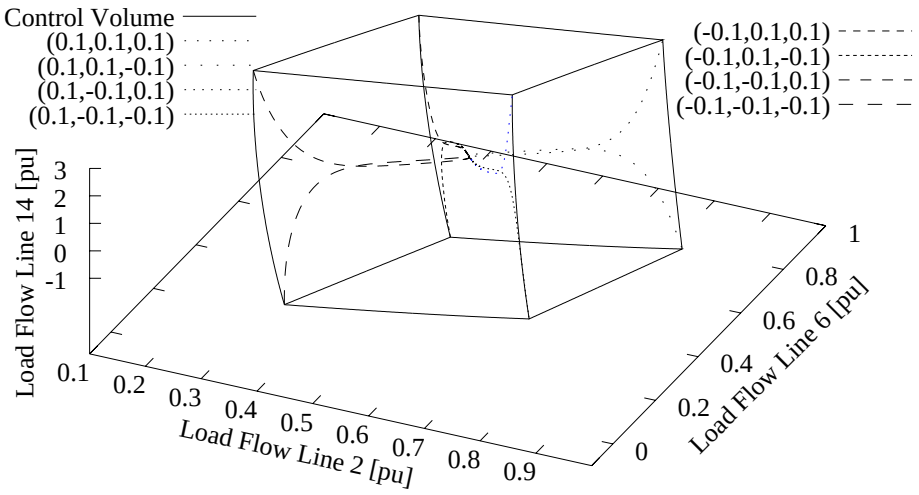

Figure 7.2. Load Flow Control in Lines 2, 6, and 7

First, a look at the bus voltages is provided. Figures 7.3, 7.4, and 7.5 show the voltages at both ends of the three lines when

- the voltages at both buses are not controlled.
- the voltage at the first bus is controlled.
- the voltage at the second bus is controlled.

For line 2, it obviously does not make sense to regulate the voltage at the slack bus: the voltage at the slack bus is by definition constant; the same is valid at PU buses. For lines 14 and 30, results for voltage control of both buses, one at a time, when r is varied from -0.1 to 0.1, are provided. A couple of observations can be made:

- For line 14, when the voltage at bus 10 is controlled, the voltage at bus 9 changes only very little. This can be explained with the proximity of bus 9 to a PU–bus.
- Controlling the voltage at one bus has, as one would expect, a strong influence on the voltage at the other bus. In general, a pattern is not recognizable.

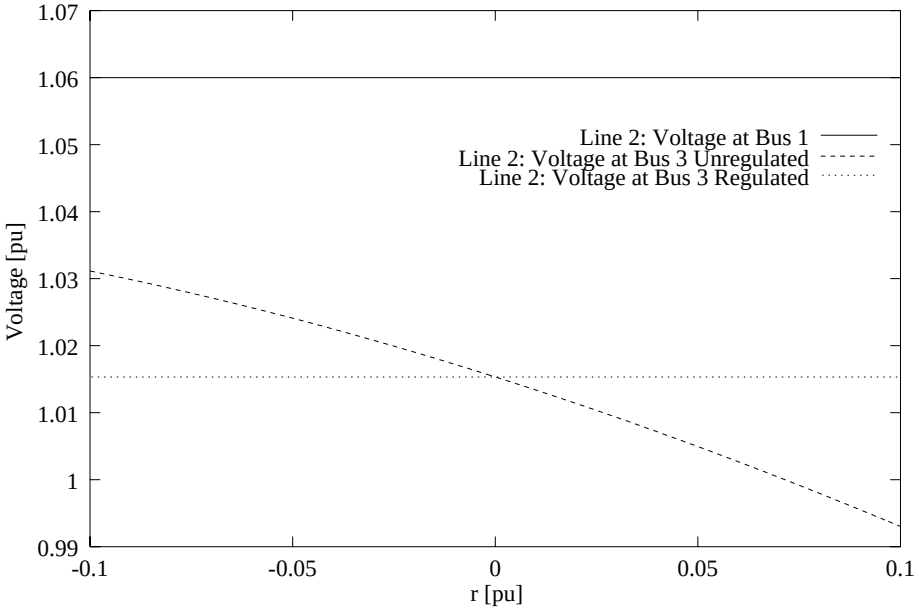

Figure 7.3. Voltages at Buses in Line 2

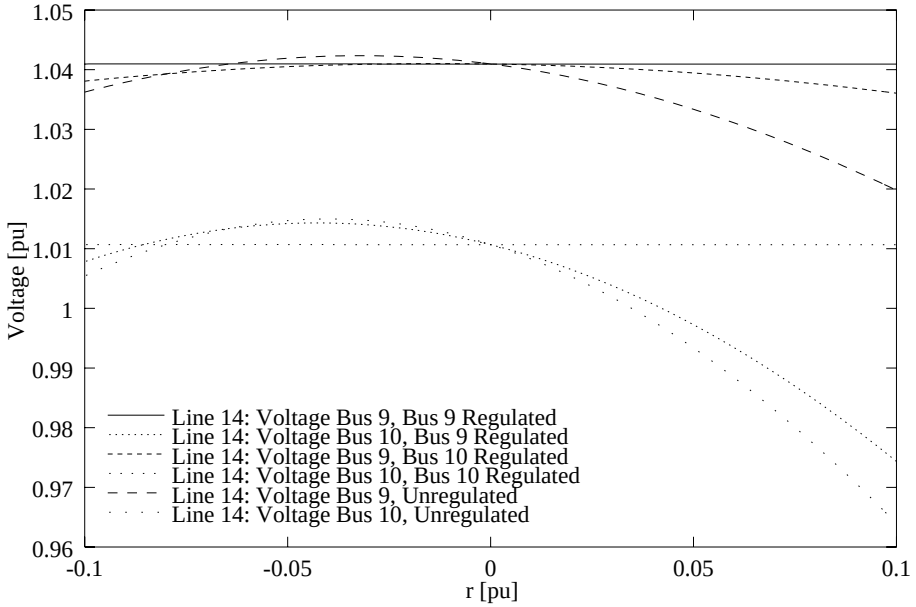

Figure 7.4. Voltages at Buses in Line 14

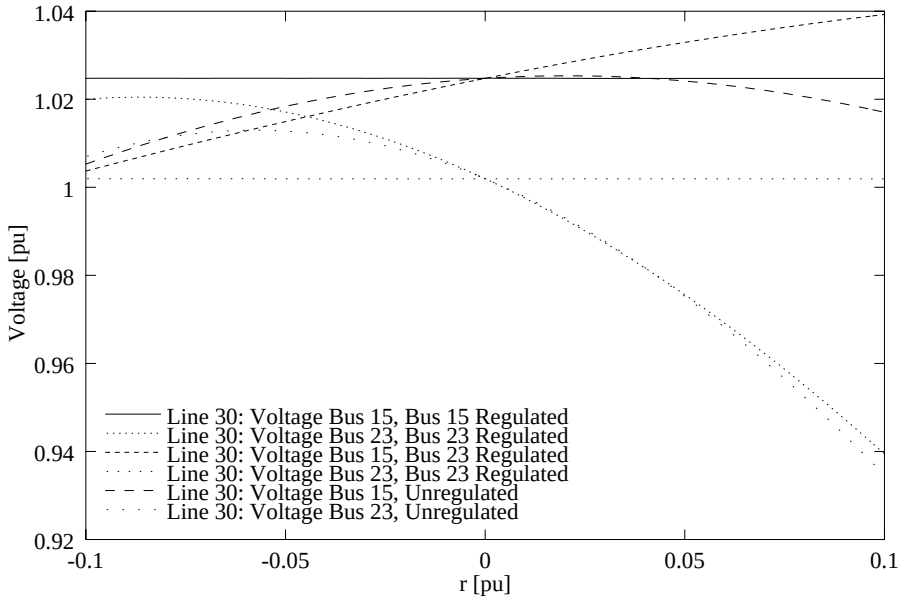

Figure 7.5. Voltages at Buses in Line 30

Next, the influence of the voltage control on the load flow control is investigated. No large influence is expected, since the load flow though a line mainly depends on the difference of the voltage angles at the ends of the line. Figures 7.6, 7.7, and 7.8 show the load flow in the three lines when r is varied from -0.1 to 0.1, again, without voltage control, with voltage control at the first bus, and with voltage control at the second bus. For line 2, the same exception as above applies.

For all lines, in Figures 7.7 the load flow varies slightly depending on the voltage control. However, the variations are very small.

Of course, the control of the bus voltages comes at a cost. Without bus voltage control, the parallel branch of the UPFC, that is, converter 1, only has to transfer the active power that is injected into the line by the series branch, that is, converter 2. When the bus voltages are controlled by injecting reactive power into the buses, the power rating of converter 1 and the series transformer changes from $S_{conv1} = P_{conv1} = P_{conv2}$ to $S_{conv1} = \sqrt{P_{conv1}^2 + Q_{conv1}^2}$. To give an idea of the relative magnitude of P_{conv2} and Q_{conv2}, Figures 7.9, 7.10, and 7.11 are provided. In these figures, the active power injected by the series branch and the reactive

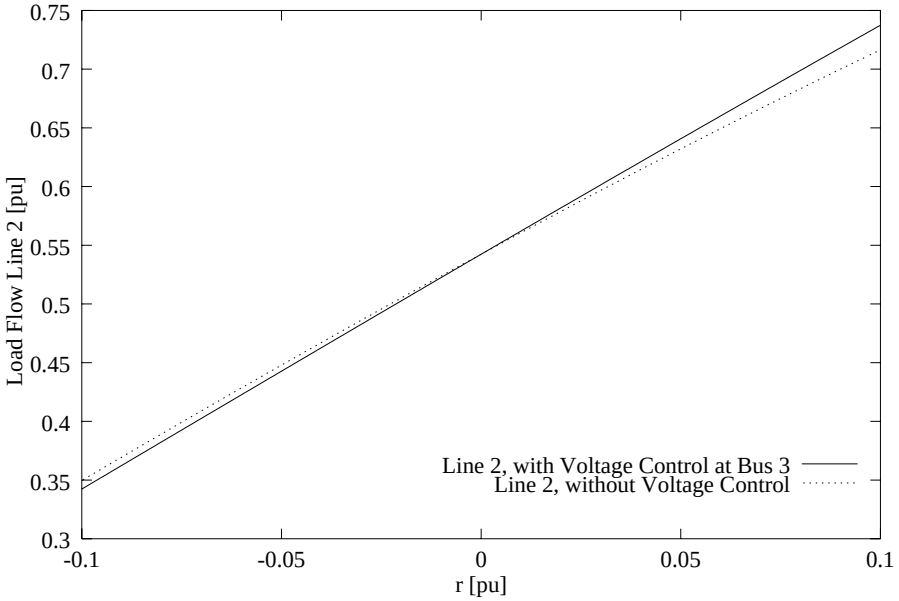

Figure 7.6. Load Flow in Line 2

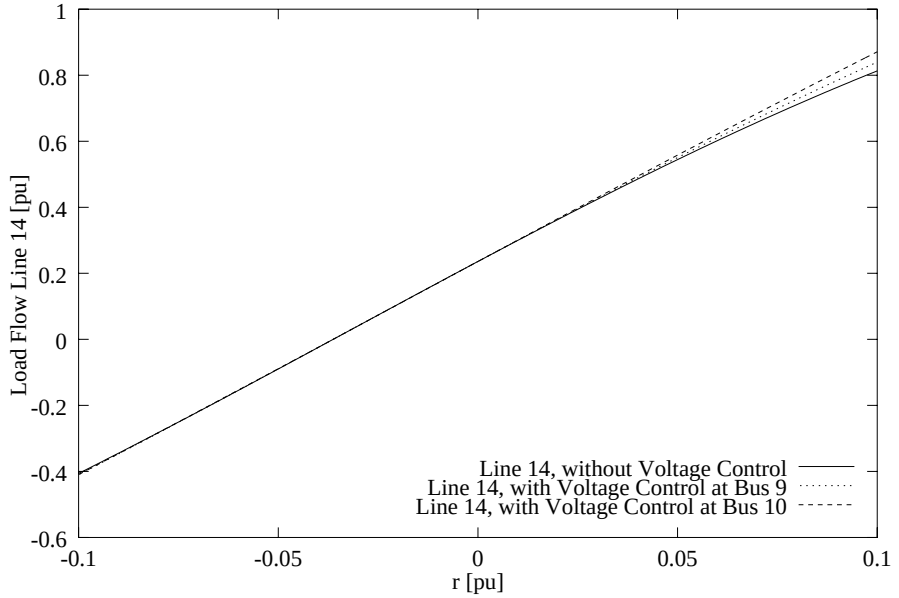

Figure 7.7. Load Flow in Line 14

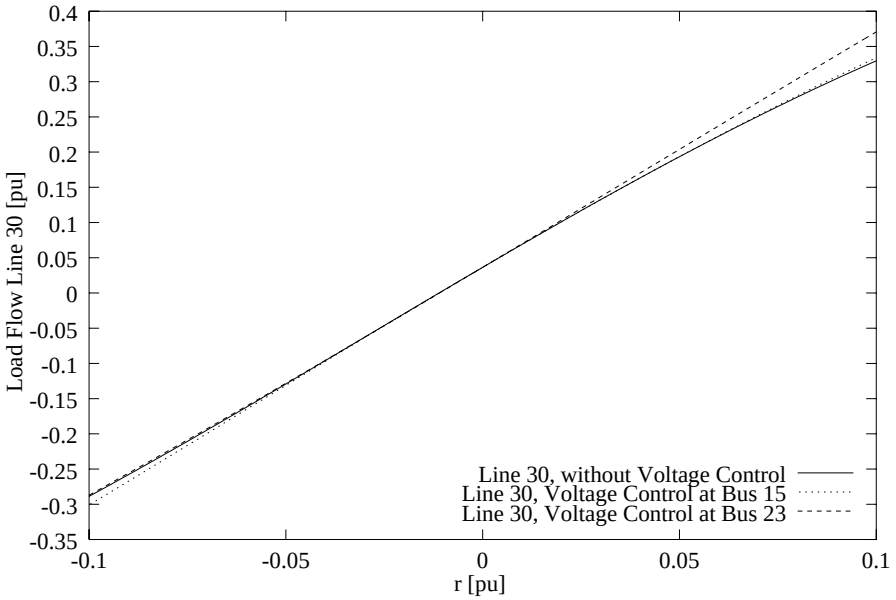

Figure 7.8. Load Flow in Line 30

power injected into the controlled bus are plotted with the same scale. In all five cases, the maximum reactive power injected to keep the bus voltage constant is considerably larger than the active power injected for load flow control. The rating of converter 1 therefore has to be increased considerably for the bus voltage control. Table 7.1 shows the ratings for converter 1 with and without bus voltage control.

Line	Controlled Bus	$\|P\|_{max}$	$\overline{\|P\|^2_{max} + \|Q\|^2_{max}}$
2	3	0.045	0.347
14	9	0.078	0.259
14	10	0.040	0.364
30	15	0.096	0.170
30	23	0.050	0.251

Table 7.1. Ratings for Converter 1 With and Without Bus Voltage Control

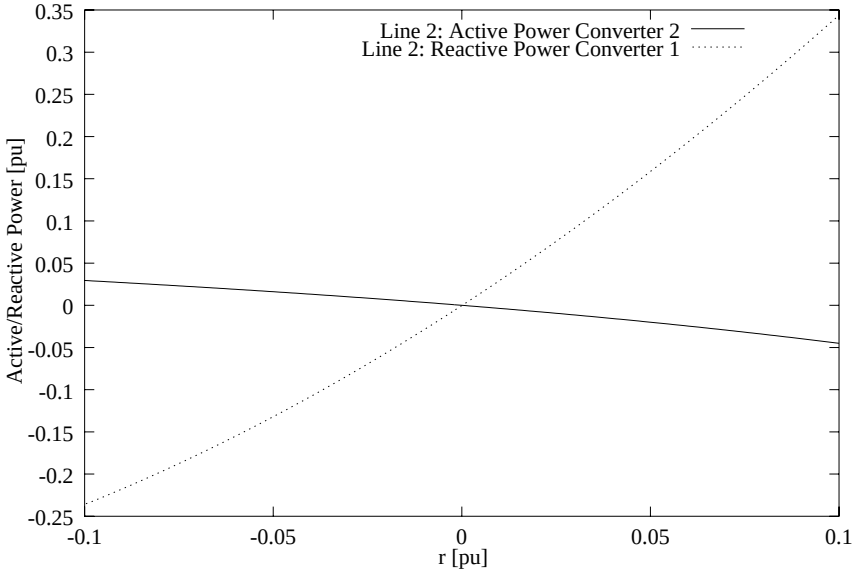

Figure 7.9. Line 2: Active and Reactive Power in Converters 1 and 2 respectively

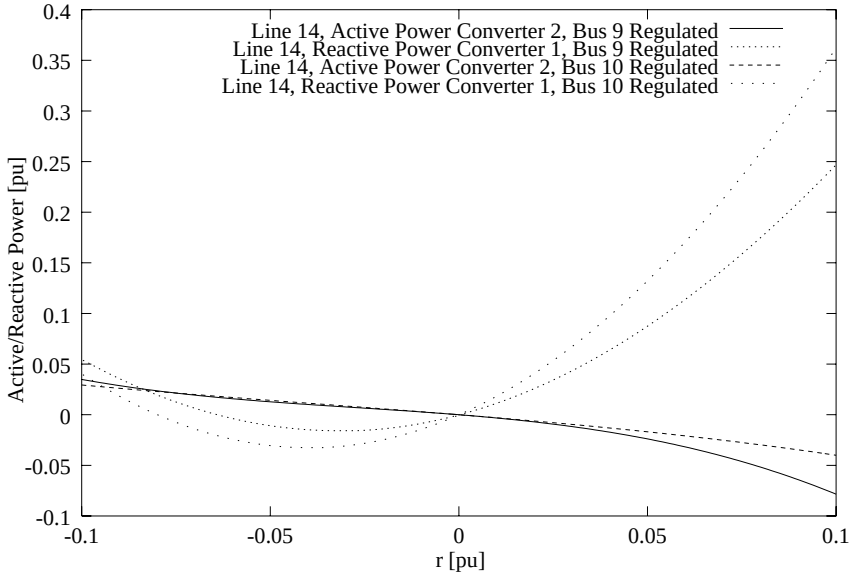

Figure 7.10. Line 14: Active and Reactive Power in Converters 1 and 2 respectively

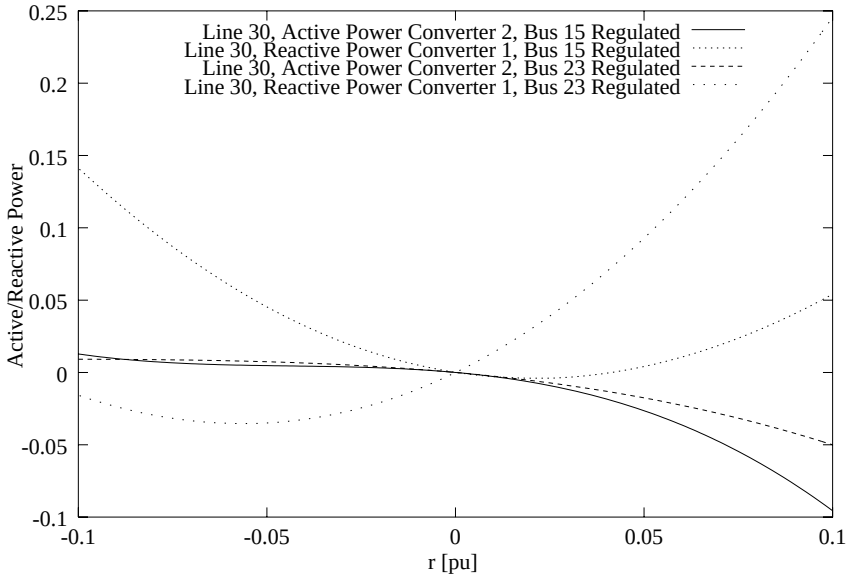

Figure 7.11. Line 30: Active and Reactive Power in Converters 1 and 2 respectively

7.3 Summary

As expected, if γ is kept constant and r is varied, the proposed control scheme can be used. Further, the bus voltages can be controlled with the parallel branch of the UPFC. This, however, comes at a cost: the ratings of the parallel transformer and the corresponding converter have to be increased considerably.

Chapter 8

On the Large Signal Stability of the Control Scheme

In this chapter, the large signal stability of the control scheme is investigated. A concise description of some methods and their background, mainly from [47] and [48] for determining the input–output stability of feedback systems is given. Then, the input–output stability of the control system is discussed, and arguments for stability of the controlled system are given. The chapter concludes with a description and simulation of an unstable situation.

8.1 Preliminaries

Before the large signal stability of the load flow controller is investigated, some definitions and theorems and their background are described in this section.

8.1.1 The Nonlinear Nyquist Criterion

The nonlinear Nyquist criterion [49], also called circle criterion, is valid for single–input single–output systems when one component of the feedback loop is linear and the other component is nonlinear; see Figure 8.1. The idea is to put bounds on the nonlinearity of $f(\cdot)$, that is, to limit the gain of the nonlinear function; see Figure 8.2. Once these bounds are

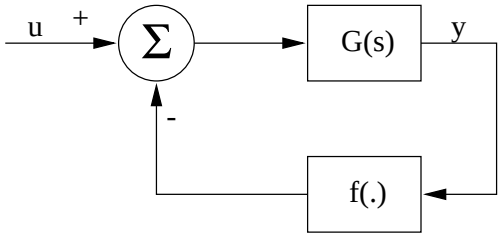

Figure 8.1. Feedback Loop with Linear Block ( ) and Nonlinear Block ( )

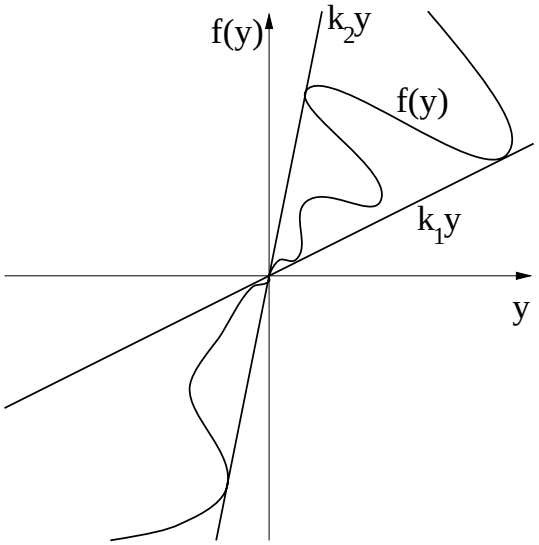

Figure 8.2. Bounds on the Nonlinearity

established, the nonlinear Nyquist criterion can be used:

Nonlinear Nyquist criterion: *Let $\mathcal{C}$ be a circle in the complex plane with the center on the real axis and passing through the points $-1/k_1$ and $-1/k_2$. The configuration in Figure 8.1 is stable if $G(s)$ has no poles in the right half plane and its Nyquist plot does not intersect or encircle $\mathcal{C}$.*

An example for the nonlinear Nyquist criterion with a stable system is given in Figure 8.3.

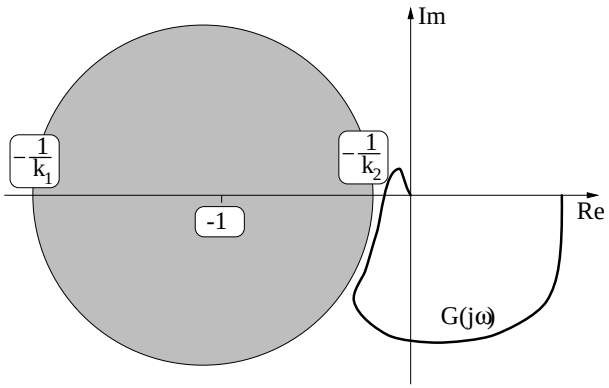

Figure 8.3. Conditions on the Nyquist Curve

8.1.2 Dynamical Systems, Graphs and Input–Output Stability

A dynamical system is an object that produces an output signal for each input signal. A signal is a "reasonable" (for example, piecewise continuous) vector–valued function $u : t \longrightarrow \mathbb{R}^n$ defined on an interval of time t of the form $[0, T)$, where T is either a strictly positive real number or infinity.

The norm $||\cdot||$ of a signal captures the "size" of signals on the semi–infinite time interval. Examples of norm functions are the p-norms. For any positive real number $p > 1$, the p–norm of a signal u is defined as

$$||u||_p = \left(\int_0^\infty \sum_i |u_i(t)|^p \, dt \right)^{\frac{1}{p}} \tag{8.1}$$

For $p = \infty$,

$$||u||_\infty = \sup_{t \geq 0} |u(t)| \tag{8.2}$$

is defined.

Often, truncated versions of signals are of interest. Given a signal u defined on $[0, T)$ and a strictly positive real number τ, u_τ denotes the truncated signal that is equal to the original signal u on the interval $[0, \tau]$ and is equal to zero on the interval (τ, ∞).

A dynamical system is stable with respect to the norm $||\cdot||$ if there is a gain function γ that gives a bound on the norm of the truncated output signals y as a function of the norm of the truncated input signals u,

$$||y_\tau|| \leq \gamma(||u_\tau||) \quad \text{for all } \tau. \tag{8.3}$$

In the special case when the gain function is linear, which means that there is at most an amplification by a constant factor, the system is finite gain stable.

Of interest for this work is the stability analysis of interconnected system as shown in Figure 8.4. The composite system in Figure 8.4 is called a

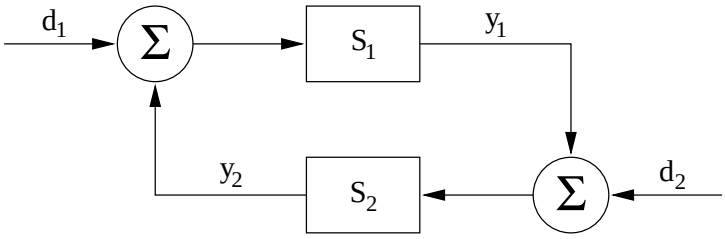

Figure 8.4. Standard Feedback Configuration

well–defined interconnection if it is a dynamical system with the inputs d_1 and d_2 and the outputs y_1 and y_2. That means that for a combination of input signals d_1 and d_2, a combination of output signals y_1 and y_2 exists such that the dynamical system S_1 has the output signal y_1 given the input signal $d_1 + y_2$ and the dynamical system S_2 has the output signal y_2 given an input signal $d_2 + y_1$. The systems that make up a well–defined interconnection are called feedback components.

For a given dynamical system with input signals u and output signals y, the set of its ordered input–output pairs (u, y) is referred to as the graph of the dynamical system and is denoted $\mathcal{G}_S$. The set of the exchanged ordered input–output pairs (y, u) is called the inverse graph of the system $\mathcal{G}_S^I$. For the system in Figure 8.4, the graph of S_1 and the inverse graph of S_2 lie in the same Cartesian product space.

The basic observation regarding input–output stability for a feedback configuration like in Figure 8.4 states that if a signal in the inverse graph of S_2 is near any signal in the graph of S_1, then it must be small. To formalize this idea, a distance d_τ from signals x to the graph of S_1 must be defined:

$$d_\tau(x, \mathcal{G}_{S_1}) = \inf_{z \in \mathcal{G}_{S_1}} ||(x - z)_\tau|| \tag{8.4}$$

With d_τ, the graph separation theorem is:

Graph separation theorem: *A well–defined interconnection is stable if and only if a gain function γ exists that gives a bound on the norm of truncated signals in the inverse graph of S_2 as a function of the truncated distance from the signals to the graph of S_1:*

$$x \in \mathcal{G}_{S_2}^I \Longrightarrow ||x_\tau|| \leq \gamma(d_\tau(x, \mathcal{G}_{S_1})) \text{ for all } \tau \tag{8.5}$$

If γ is a linear function, the well–defined interconnection is finite gain stable.

To understand the idea behind this observation, consider the signals that arise in the closed loop belonging to the inverse graph of S_2, $(y_2, y_1 + d_2)$. The signals belonging to the graph of S_1 have the form $(y_2 + d_1, y_1)$. Thus, signals $x \in \mathcal{G}_{S_2}^I$ and $z \in \mathcal{G}_{S_1}$ that satisfy the feedback equations also satisfy

$$(x - z)_\tau = (d_1, -d_2)_\tau \tag{8.6}$$

and

$$||(x - z)_\tau|| = ||(d_1, d_2)_\tau|| \tag{8.7}$$

for truncations in the defined interval. Now, if there are signals x with large truncated norm but small truncated distance to the graph of S_1, then (d_1, d_2) can according to (8.6) be chosen small but produce a large output. This contradicts the stability definition.

To present some other theorems that are based on the graph separation theorem, a few more definitions are needed:

- A dynamical system is passive if, for each input–output pair (u, y) and each $\tau > 0$, the inner product

$$\langle u, y \rangle = \int_0^\infty u^T(t) y(t)\, dt \tag{8.8}$$

is positive. For the inner product, $\langle u, y \rangle = \langle y, u \rangle$ and $\langle u, u \rangle = ||u||_2^2$.

- A dynamical system is input and output strictly passive if a strictly positive real number ε exists such that for each input–output pair (u, y) and each $\tau > 0$

$$\langle u_\tau, y_\tau \rangle \geq \varepsilon(||u_\tau||_2^2 + ||y_\tau||_2^2)\ . \tag{8.9}$$

- A dynamical system is input strictly passive if a strictly positive real number ε exists such that for each input–output pair (u, y) and each $\tau > 0$

$$\langle u_\tau, y_\tau \rangle \geq \varepsilon||u_\tau||_2^2\ . \tag{8.10}$$

- A dynamical system is output strictly passive if a strictly positive real number ε exists such that for each input–output pair (u, y) and each $\tau > 0$

$$\langle u_\tau, y_\tau \rangle \geq \varepsilon||y_\tau||_2^2\ . \tag{8.11}$$

It is worth noting that a dynamical system is input and output strictly passive if it is both finite gain stable and input strictly passive.

With these definitions, two important theorems can be stated:

Small gain theorem: *If each feedback component is finite gain stable and the product of the gains, that is, the coefficients of the linear gain functions, is less than one, then the well–defined interconnection is finite gain stable.*

A graphical interpretation of the small gain theorem is given in Figure 8.5.

Passivity theorem: *If one dynamical system and the other dynamical system followed by the scaling '-1' are one of*

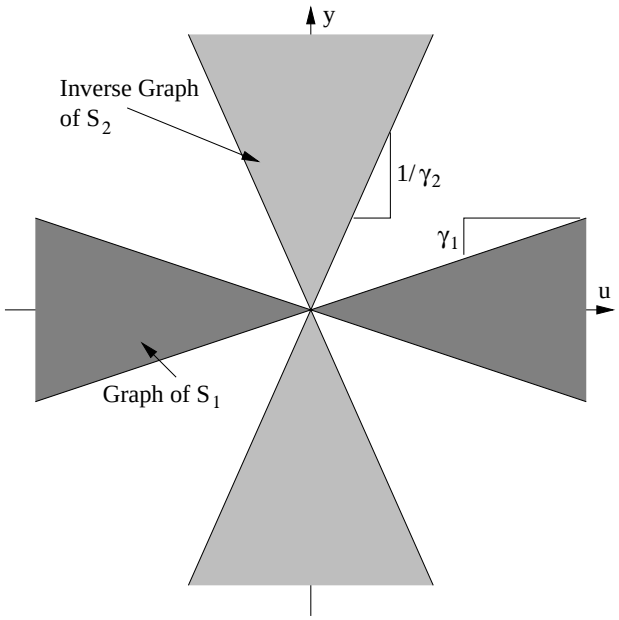

Figure 8.5. Small Gain Theorem

- *both input strictly passive,*
- *both output strictly passive,*
- *respectively, passive and input and output strictly passive,*

then the well-defined interconnection is finite gain stable using the 2–norm.

Two cases of the passivity theorem are illustrated in Figures 8.6 and 8.7.

8.2 Stability of the Controlled System

In the previous section, some theorems on input–output stability were presented, namely the nonlinear Nyquist criterion, the small gain theorem, and the passivity theorem. Here, these theorems are applied to the control system with the proposed load flow controller.

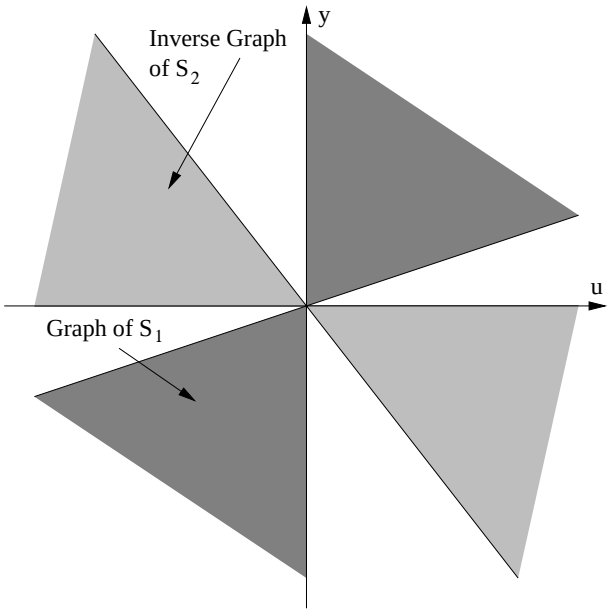

Figure 8.6. Interconnection of Input Strictly Passive Systems

8.2.1 Circle Criterion for One Controllable Device

All devices discussed in this thesis have strictly monotonic characteristics for the function F connecting the control input to the achieved load flow in the line. Thus, the nonlinearities are bounded such that F has values only in the upper right and lower left quadrant of a representation similar to Figure 8.2. Assuming, without loss of generality, that $k_1 \leq k_2$,

$$0 < k_1 \leq k_2 < \infty \tag{8.12}$$

holds. The circle that is obtained for any such k_1 and k_2 never touches or includes the origin; it can, however, come arbitrarily close for small values of k_1.

Since the Nyquist curve for an integral controller is a straight line along the imaginary axis ending in the origin, this circle is never intersected or encircled and the control system is stable; see Figure 8.8.

This stability investigation is strictly valid only for the single–input single–output system, that is, for one controllable device in the system. Of course,

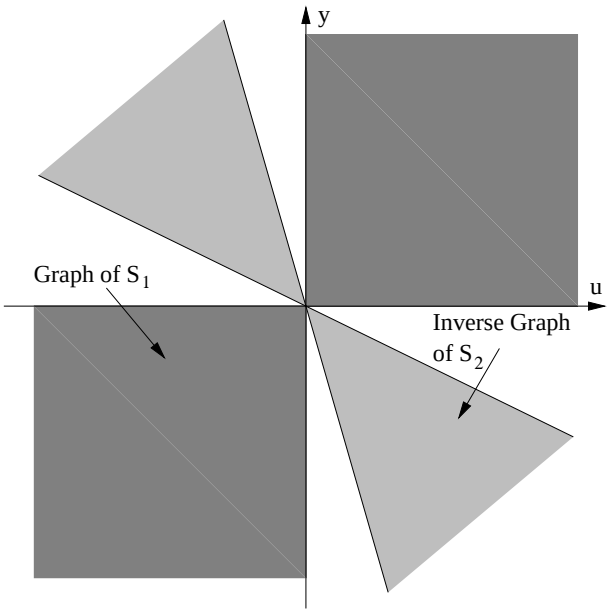

Figure 8.7. Interconnection of Passive and Input Output Strictly Passive System

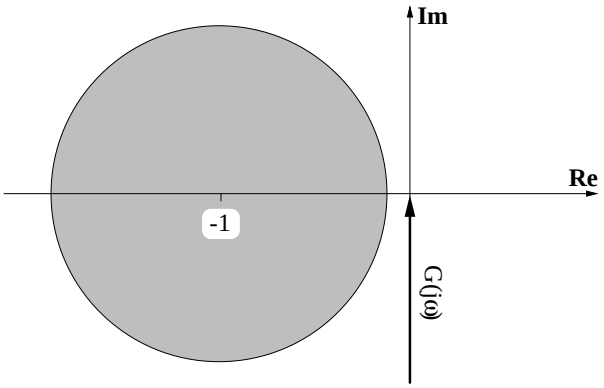

Figure 8.8. Nonlinear Nyquist Criterion for Load Flow Control

it can be argued that this criterion can be applied to several controlled devices if those are sufficiently de–coupled.

8.2.2 Small Gain Theorem

The load flow equations are finite–gain stable by definition: The methods in this thesis are explicitly valid only if the power system is inherently stable, which implies that a limited change in the control settings of the controllable devices causes a limited change in the load flows. For the integrator with input u and output y,

$$y = K \int_0^\tau u(t)\, dt \; . \tag{8.13}$$

Unfortunately, the integral controller is not finite–gain stable for all possible input signals $u(t)$. Thus, the small gain theorem cannot be used to determine the stability of the controlled system for all signals that can possibly occur.

However, if the input signals $u(t)$ for the integrator are in the set $u(t) \in \{t \longrightarrow \mathbb{R}^n) : || \int_0^\tau u(t)dt|| < c\}$ where c is a finite constant, and if in addition an upper bound b for the gain of the load flow equations is known, then it is trivial to make the elements of K small enough so that the product of $||K|| \cdot c \cdot b < 1$. Then, the feedback system is stable. Usually, the input of the integrator is a step function from which the output of the load flow is subtracted. Due to the monotonic characteristic of the control devices, the input signal of the integrator becomes smaller than the amplitude of the step function.

8.2.3 Passivity Theorem

The state equations of the integrator are

$$\begin{aligned} \dot{x} &= u \quad x(0) = 0 \\ y &= Kx \; . \end{aligned} \tag{8.14}$$

The integrator is passive because, with $K = \mathrm{diag}[k_1, k_2, \ldots, k_n]; k_i > 0$,

$$\begin{aligned} 0 \le \frac{1}{2}x(t)^T K x(t) &= \int_0^\tau \frac{d}{dt}\left[\frac{1}{2}x(t)^T K x(t)\right] dt \\ &= \int_0^\tau \dot{x}(t)^T K x(t)\, dt \\ &= \int_0^\tau u(t)^T y(t)\, dt \\ &= \langle u_\tau, y_\tau \rangle \end{aligned} \tag{8.15}$$

For the load flow, the "state equations" have no dynamical part. The load flow, together with the negative feedback, is given by

$$y = -F(u) \tag{8.16}$$

where $F(u)$ is the function connecting the settings of the controllable devices with the line flow in the lines. The inner product determining the passivity of this system is then given by

$$\begin{aligned} \langle u_\tau, -y_\tau \rangle &= \int_0^\tau u(t)^T y(t)\, dt \\ &= \int_0^\tau u(t)^T F(u(t))\, dt\ . \end{aligned} \tag{8.17}$$

The problem here is obviously the function $F(u)$. This function is given by purely algebraic equations, that is, it is memoryless. Therefore, it can be replaced with a gain matrix G for any $u_0 = u(t_0)$. Of course, this gain matrix varies with u and thus with t. Equation (8.16) can then be rewritten as

$$y = G(u) \cdot u\ , \tag{8.18}$$

and the inner product becomes

$$\langle u_\tau, -y_\tau \rangle = \int_0^\tau u(t)^T G(u(t)) u(t)\, dt\ . \tag{8.19}$$

In Equation (8.19), the expression in the integral, $u(t)^T G(u(t))u(t)$, is a quadratic form. If it can be shown that $G(u(t))$ is positive definite for all

t_0, it follows that the dynamical system (8.16) is at least passive, since then $\langle u_\tau, -y_\tau \rangle > 0$. There is indeed an argument for positive definiteness of $G(u(t))$: If the diagonal elements of G are positive and large compared to the off–diagonal elements, Gershgorin's theorem, as discussed in Section 4.3.1, states that G has only positive eigenvalues and is thus positive definite. Physically, that corresponds to positive load flow in all controlled lines and a high independence of the load flows in these lines. However, passivity is not sufficient: for the interconnected system to be stable, strict input and output passivity must be shown.

Since the load flow equations are finite–gain stable (see Section 8.2.2) it is sufficient to show strict input passivity. The load flow equations are input strictly passive, if

$$\int_0^\tau \langle u_\tau, -y_\tau \rangle \geq \epsilon \int_0^\tau ||u_\tau||_2^2 \,, \tag{8.20}$$

$$\int_0^\tau u(t)^T G(u(t)) u(t)\, dt \geq \epsilon \int_0^\tau u(t)^T u(t)\, dt \,. \tag{8.21}$$

The $\epsilon \in \mathbb{R}^+$ that is required here must be smaller or equal to a *lower* bound on the nonlinear gain. If such a lower bound can be determined, the feedback connection is stable.

8.2.4 Observations on the Investigation

The three theorems that have been discussed in the previous three sections are conservative, that is, they give sufficient, not necessary conditions for the stability of the feedback system. Therefore, the limitation on certain signals in Section 8.2.2 does not necessarily imply that the feedback system is unstable for other signals.

The circle criterion has shown stability for the case of a single–input single–output system. If the control loops are sufficiently decoupled, an argument for stability of a multi–input multi–output system can be made. It is interesting that under the same assumption of decoupled control loops, passivity of the load flow equations can be shown.

To summarize, while a general proof of input–output stability was not found, there are a number of results that indicate that there are circumstances where the controlled system is almost certainly stable, namely when the lines are sufficiently decoupled.

8.2.5 Worst Case Scenario – Unstable Controller

Despite all arguments for stability of this control system, there are clearly situations where the controlled system is not stable. Consider, for example, the simple test system in Figure 8.9, which is the same as Figure 4.1. The total load flow transported through lines 5, 7, and 8 is 1 pu. Since these lines have the same data and the conditions are almost equivalent each line carries a load flow of about 1/3 pu. If the load flow is controlled with a CSC so that lines 7 and 8 carry a slightly higher load of about 0.36 pu, then the CSCs compensate 35% of the line reactance in both lines.

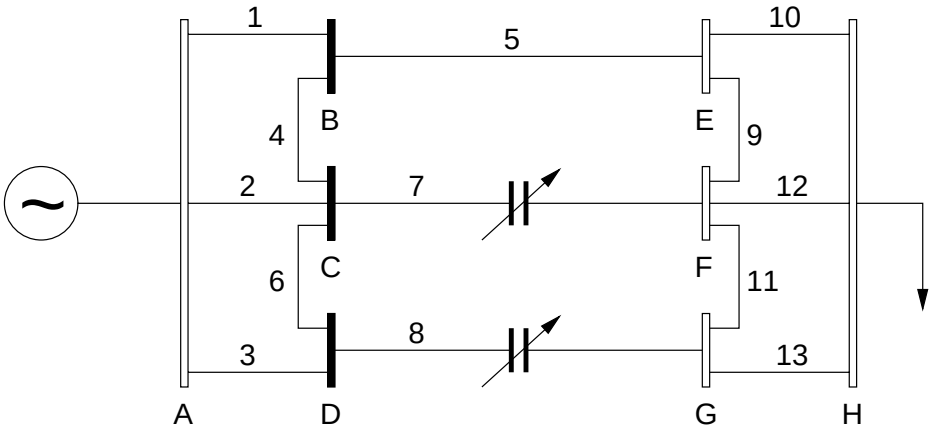

Figure 8.9. Simple Test System

Now, if line 5 is lost, the setpoint of the controllers is clearly not reachable, since the sum of load flows through the two lines must be 1 pu. The integrators will try to reach their respective setpoints anyway and decrease the capacitance to lower the line flows. If, for the sake of the argument, there were no limits on the apparatus and the controller, the series capacitor would become an ever rising series inductor.

However, the control range of the devices is limited. Without limits on the integrator, these limits are windup limits. The control input to the devices falls while the capacitors are stuck at zero compensation. To avoid this windup behavior, there are non–windup limits on the integrators. Thus, one can expect that the series capacitance of both CSCs decreases to zero, where the limits are reached. Simulation results shown in Figure 8.10 confirm this reasoning.

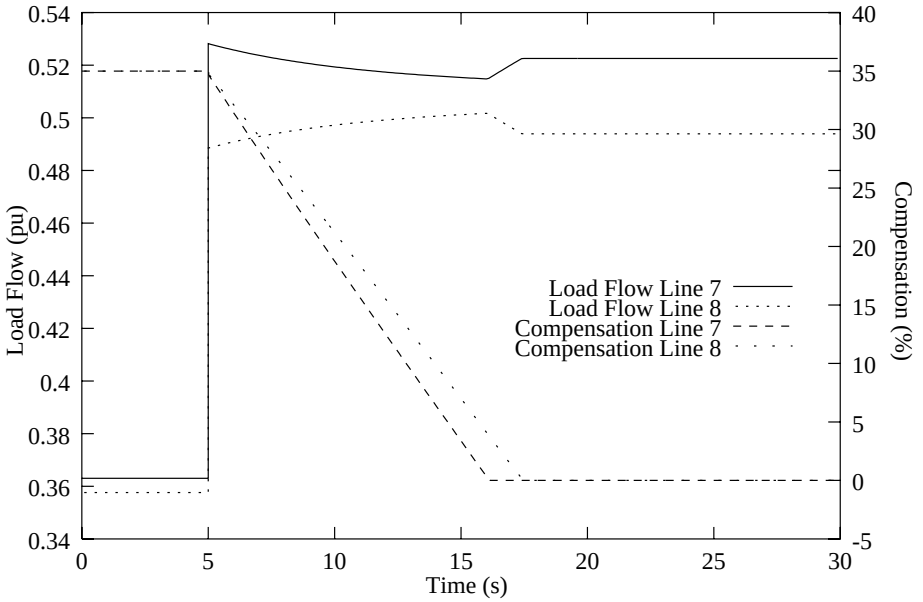

Figure 8.10. Unstable Controller with Non–Windup Limits

In the situation described above, it is clear that the load flow in the two remaining lines cannot be controlled independently. With the total load flow from the generation area to the load area at 1 pu load flow control so that line 7 carries a load flow of P_7, line 8 must carry a load flow of 1 pu $- P_7$. To get the controllability back, one controller must be blocked.

Chapter 9

Influence of Load Flow Control on Inter–Area Oscillations

So far, the model that has been used for the study of load flow control is the purely algebraic load flow equation model. In this chapter the influence of load flow control using an integral controller on a comparatively fast dynamic phenomenon, namely inter–area oscillations, is studied. First, a short description of inter–area oscillations is given. Then, the influence of the controller is investigated in a test system.

9.1 Inter–Area Oscillations

In an electric power system, oscillations between interconnected synchronous generators are an inherent phenomenon. Oscillations associated with a single generator or a single plant are called local modes or plant modes, and their frequency is usually in the range of 0.7 to 2.0 Hz. Those oscillations can be analyzed and controlled comparatively easily [50].

A different type of oscillations involves groups of generators. These oscillations are called inter–area oscillations or inter–area modes. Their frequency is usually in the range from 0.1 to 0.8 Hz. To study these oscillations, generally a detailed model of the whole interconnected power

system is required [51]. In large interconnected systems, there can generally be many such modes, each involving a number of generators.

9.2 A Case Study

Figure 9.1 shows a four–machine test system that is often used for investigating inter–area oscillations. The system data can be found in [52] on page 813. A CSC is introduced in the upper line between buses 8 and 9. The system model was implemented in ABB's power system analysis software SIMPOW [53].

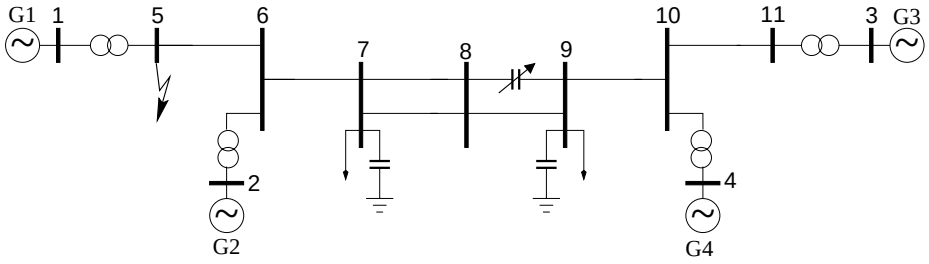

Figure 9.1. Two area test system

If a solid three–phase short circuit fault with a fault duration of 150 ms is applied at bus 5 at $t = 1$ s, the system shows damped oscillations. The dominant mode is an inter–area mode where generators G1 and G2 oscillate against generators G3 and G4 with a frequency of about 0.56 Hz. Figure 9.2 shows these oscillations, as seen in the load flow through the upper line between buses 8 and 9, for two cases: the original system and the system with a series capacitance that compensates 35% of the line reactance of the upper line between bus 8 and bus 9. The series capacitor increases the load flow in the line, but qualitatively, the oscillations have changed very little. Figure 9.3 shows the eigenvalues of the system with and without the series capacitor. The series capacitor has little influence on the eigenvalues.

Now, the series capacitor is controlled with an integral controller. The load flow in the line with the capacitor is controlled to 2.35 pu, where 35% of the line reactance is compensated, and the gain K of the controller is set to two different values, 0.015 and 0.127. The non-windup limits on the

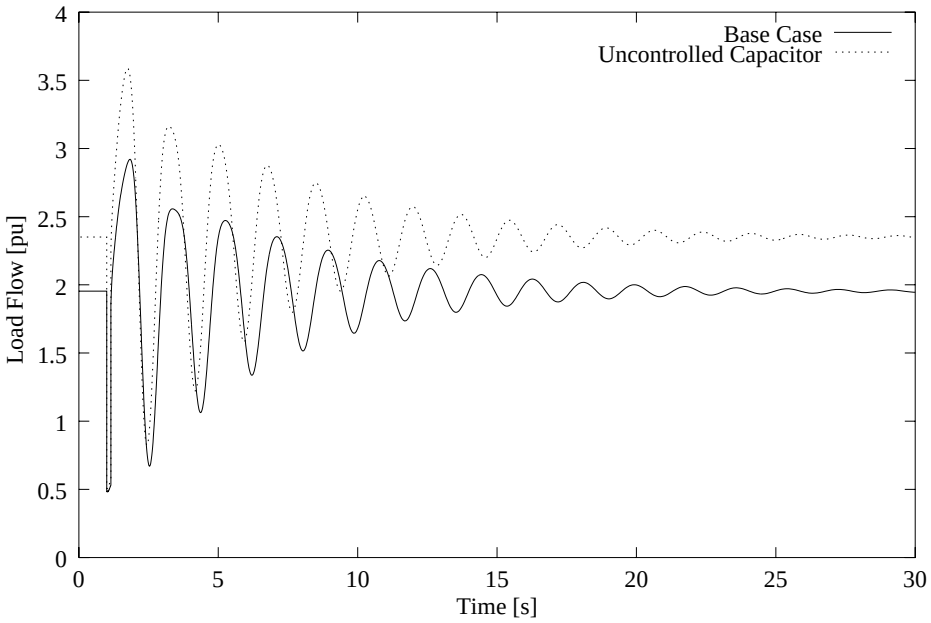

Figure 9.2. Base Case With and Without Series Capacitor

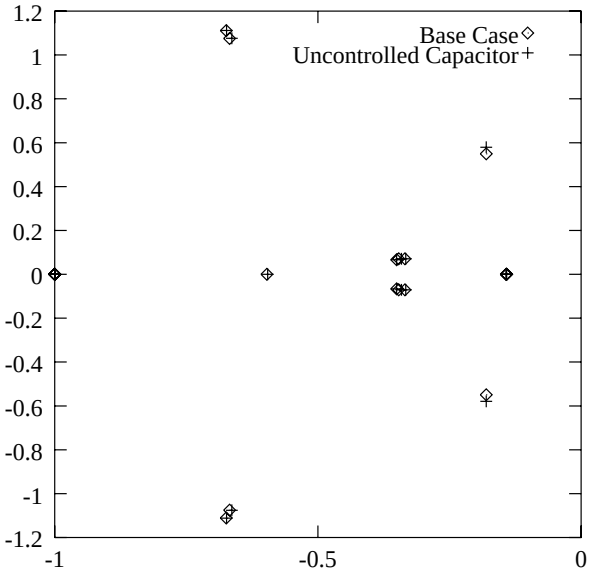

Figure 9.3. Eigenvalues With and Without Series Capacitor

integrator are set to such values that the CSC can compensate between 0 and 70% of the line reactance. The same fault is applied, and the results are shown in Figures 9.4 and 9.5. Figure 9.4 depicts the load flow in the line where the controllable device is located, that is, the upper line between buses 8 and 9 in Figure 9.1. Figure 9.5 shows the load flow between buses 8 and 9, that is, the sum of the load flows through both lines between these buses. The oscillations are slightly damped for the case with a controller gain of $K = 0.015$. In Figure 9.4, the oscillations actually seem to be worse immediately after the fault. This can be explained by the behavior of the CSC during the fault: The series compensation rises significantly, which decreases the line impedance and leads to the line taking a bigger share of the load flow. In Figure 9.5, the overall damping effect is visible. The oscillations are noticeably damped when the controller gain is set to $K = 0.127$. In this case, the effect is clearly visible in both figures.

These observations are also reflected in the eigenvalues, shown in Figure 9.6. The eigenvalue corresponding to the 0.56 Hz mode moves slightly to the left in the case of $K = 0.015$ and noticeably to the left when $K = 0.127$. Thus, the load flow control does not destabilize the system; it even has a beneficial effect on the damping of the oscillations.

However, there is a drawback to setting the gain of the controller to a high value. Figure 9.7 shows the response to a step in the set value of the load flow that is specified in the controller input. The simulation starts with a specified and actual load flow of 1.94 pu in the line. At $t = 1$ s, the specified load flow changes to 2.35 pu. With the low gain ($K = 0.015$) in the controller, the specified load flow is reached after about 30 s and no oscillations appear. With the high gain ($K = 0.127$), the specified load flow is reached much faster, but there are some oscillations present. These oscillations have a frequency of approx. 0.6 Hz; the change of the load flow in the line has excited the inter–area mode. With an intermediate gain ($K = 0.030$), the adjustment of the line load becomes more "wavy" than with the low gain.

9.3 Conclusions from the Case Study

The investigation of the integral controller in a model that takes the faster dynamics in a power system into account has shown, by example, that a slow control of load flow only has marginal influence on the fast dynamics.

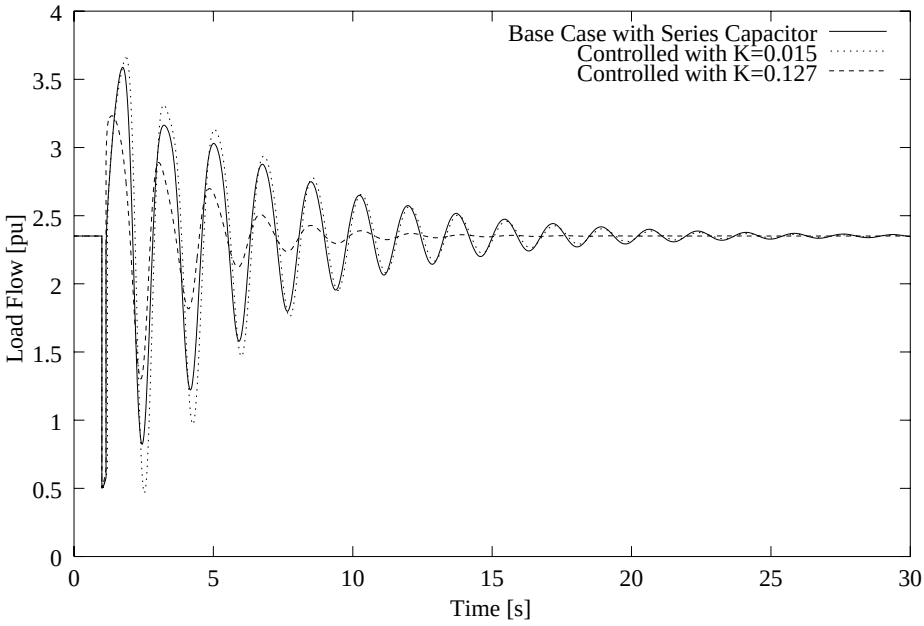

Figure 9.4. Oscillations With Controller

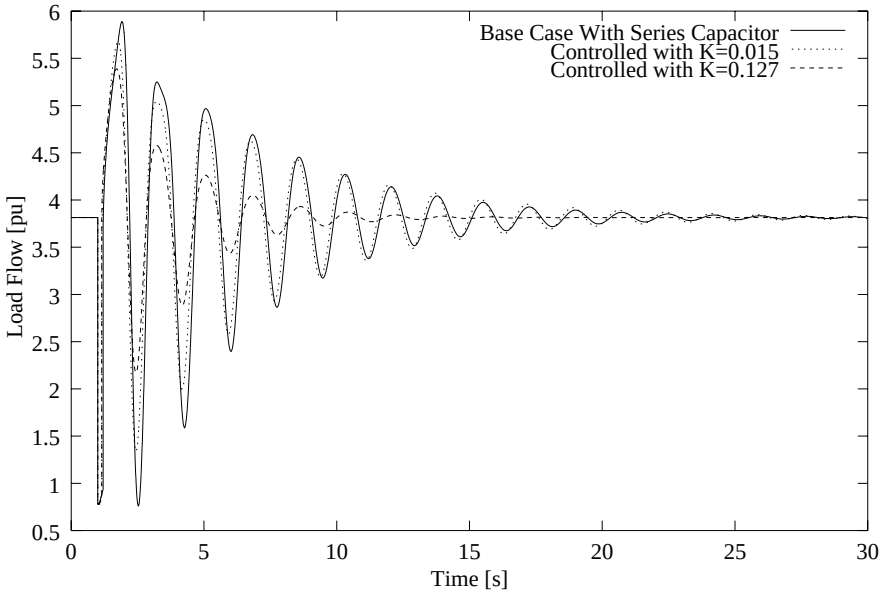

Figure 9.5. Oscillations with Controller — Load Flow Between Buses 8 and 9

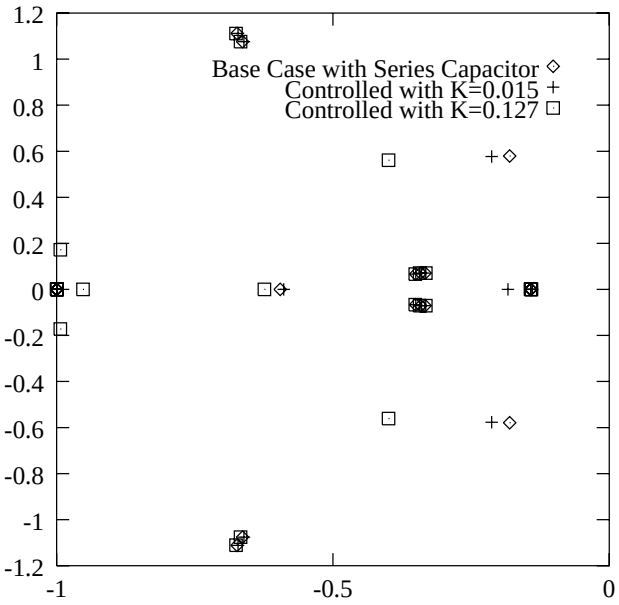

Figure 9.6. Eigenvalues with Controller

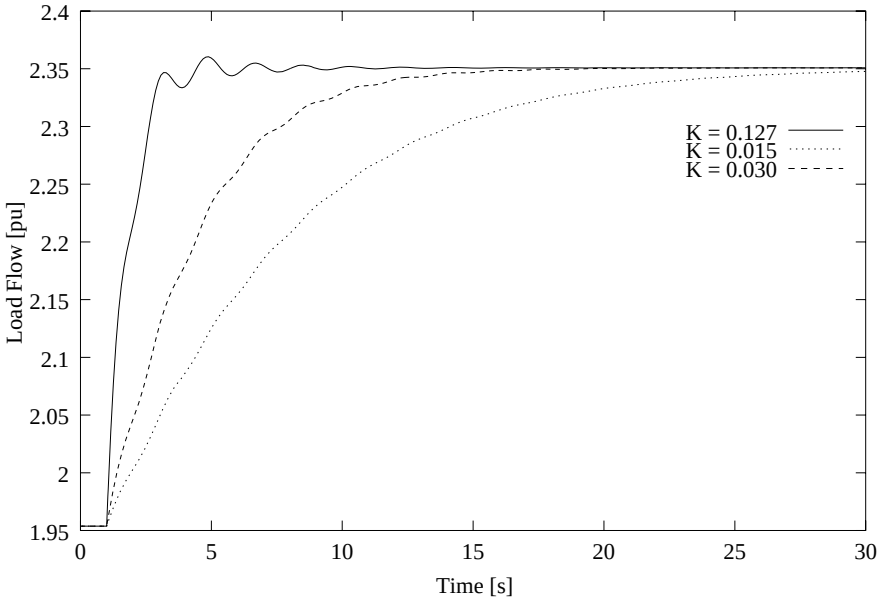

Figure 9.7. Load Flow Control Step Response

While this has only been investigated for inter–area oscillations, there is no reason to anticipate larger interactions with other fast dynamics.

It was also shown that fast load flow control interacts with these faster dynamics, for better or worse. For the inter–area oscillations, the fast load flow controller actually contributes to the damping; on the other hand, the inter–area mode can be excited by a change in the set value of the controller.

Chapter 10

Phase Root Locus Approach to Design Robust Controllers

This chapter is different from the other chapters in this thesis: it does not treat load flow control, but introduces a way to determine the robustness of control systems using a new graphical tool called the phase root locus. First, measures of robustness and relative stability are briefly discussed. A short description on how phase root locus plots can be drawn is provided. Then, an example that illustrates how the phase root locus can be used in the design and analysis of a controller based on HVDC modulation is presented.

10.1 Introduction

Robust utilization of controllable devices to enhance the stability of power systems has become an issue of concern in the engineering and operation of these systems [54]. This has been actuated by the variation in the fundamental dynamics as a result of structural changes, complex load patterns, and the increasing risk of unexpected interaction between control devices. The power system is continuously subjected to predictable and unpredictable, large and small disturbances that constantly change the operating conditions.

One of the main concerns in the field of control theory is the ability of a system to remain stable and perform its task in the presence of unknown

perturbations. A well–designed controller must be able to tolerate such uncertainties without destabilizing the system. Consequently, the ability to be able to measure the relative stability of systems is essential. Only then can it be determined whether they are robust, that is, whether they will remain stable when subject to disturbances.

In classical control design, quantitative measures of relative stability are the gain and phase margins based on Nyquist stability criteria. This information can be extracted from a Nyquist curve or the well–known Bode magnitude and phase plots. Gain margins can also be obtained by considering conventional root locus, or gain root locus, in which the closed–loop poles of the system are plotted in the complex s–plane as the gain is varied. The study of how the phase margin is affected by adding phase to the closed loop system has led to the introduction of the concept of phase root locus [8]; it is the dual to the conventional root locus.

10.2 Measures of Robustness and Relative Stability

In control systems design, not only stability, but also a certain robustness is required. Gain margin and phase margin are two criteria commonly used to measure the system's relative stability. Neither margin alone is sufficient to characterize relative stability; one margin can be large, indicating a robust system, while the other margin is extremely small, which makes the system not robust. Gain margin and phase margin provide an indication of the closeness of the Nyquist plot of the system's open–loop frequency response $L(j\omega)$ to the critical point, -1, in the complex plane (Figure 10.1). The gain margin is the amount of gain in dB that can be introduced into the loop, with unchanged open loop phase shift, before the closed loop system reaches instability. The phase margin is the change of open loop phase shift required to make the system unstable if the gain remains unchanged.

Gain margin and phase margin are dependent on the design gain K_m (see Figure 10.4) since K_m affects the location of the closed-loop system poles, from which the gain margin and phase margin are determined. This can be made explicit by introducing the notation $\mathrm{GM}(K_m)$ and $\mathrm{PM}(K_m)$ with obvious meanings.

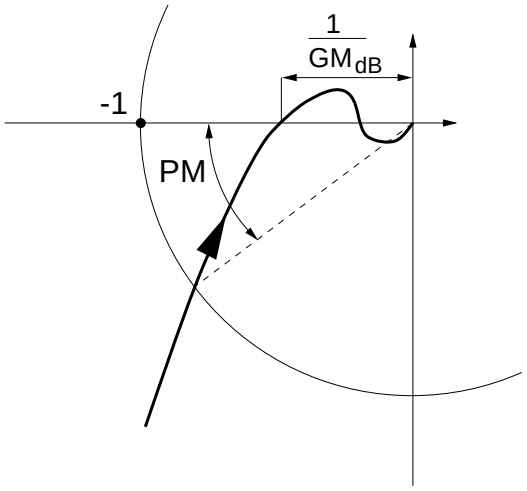

Figure 10.1. Nyquist Diagram with Gain and Phase Margin

It is also possible to determine gain margin and phase margin from the Bode–Diagram (Figure 10.2). The gain margin is the distance of the gain from 0 dB at the phase crossover frequency ω_{pc}, where the phase crosses the $-180°$–line from above; the phase margin is the distance of the phase to $-180°$ at the gain crossover frequency where the gain crosses 0 dB from above.

10.3 Gain Root Locus and Phase Root Locus

Conventional Evans root locus depicts the locus of the closed loop poles of a system in the complex s–plane when the gain of the open loop transfer function is varied, while the phase shift is held at zero. This concept can be generalized for phase shifts not equal to zero, resulting in a family of curves for different open loop transfer function phase angles, like in Figure 10.5. Such a family of curves can be computed as the isocontours of

$$\angle G(s)H(s) \quad . \tag{10.1}$$

This family of curves is the gain root locus.

Obviously, it is possible to depict a dual to the gain root locus by keeping the gain of the open loop transfer function constant and varying the phase

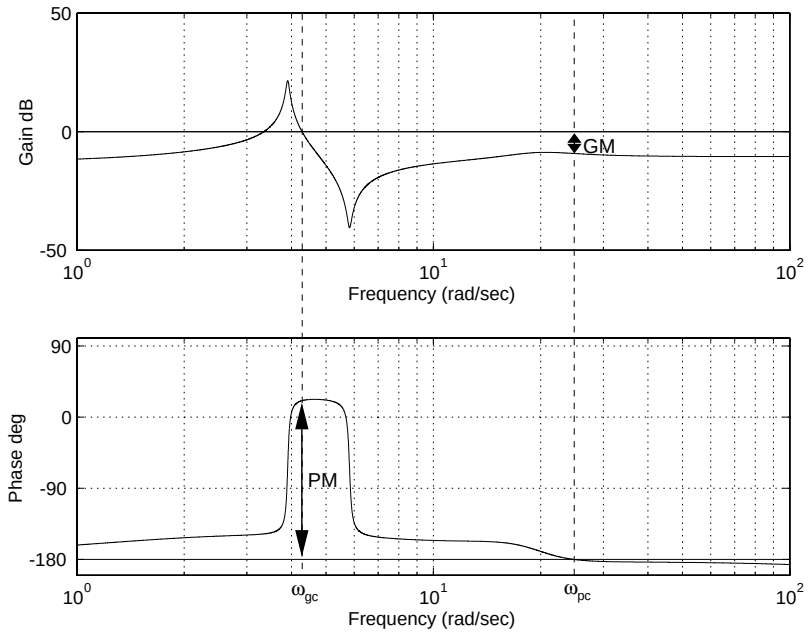

Figure 10.2. Bode Diagram for the Test System with Controller

angle. The analogue of the Evans root locus in this family of curves is the curve depicting

$$|K_m G(s)H(s)| = 1, \tag{10.2}$$

and curves like that can be computed as isocontours of

$$|K_m G(s)H(s)| \ . \tag{10.3}$$

These curves are the phase root locus, and an example is Figure 10.6.

The closed–loop poles for a certain gain and a certain phase shift of the open loop transfer function are found at the intersection of the appropriate gain root locus and phase root locus curves; see Figure 10.7. In the next section, the use of gain root locus and phase root locus for controller design will be explained, showing the benefits of using this particular method.

10.4 Illustrative Example

The AC/DC test system [52] shown in Figure 10.3 is used to illustrate the use of phase root locus in conjunction with gain root locus in control design. It is well known that the stability of an interconnected AC/DC system can be enhanced by modulating the power flowing through the HVDC link [3]. Eigenanalysis of the test system at the studied operating point indicates a pair of unstable complex conjugated eigenvalues that are found to be associated with an interarea mode of oscillation. The machines in area 1 swing against those in area 2. The complete system data can be found in [52].

In this example, a 6^{th} order reduced single–input single–output transfer function of the test system, linearized around a given operating point, is used to design a power modulation controller. The controller should also provide sufficient robustness margin. This will be determined by examining the distance of the closed loop poles to the point where the gain root locus and the phase root locus cross the imaginary axis. The input to the controller is the AC power on the line between bus 7 and bus 8. After appropriate amplification and phase compensation, the output of the controller is the modulating signal that is added to the DC power reference.

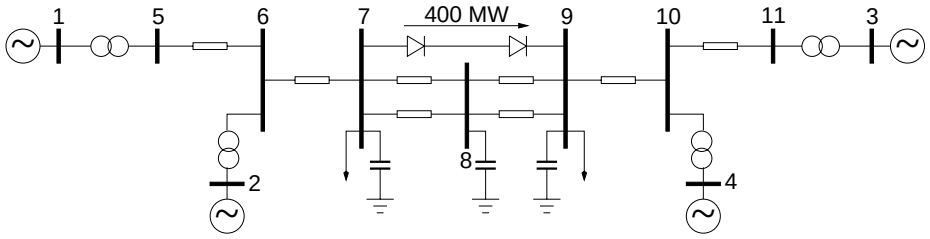

Figure 10.3. Test System

The plant is given by

$$G(s) = \frac{\Delta P_{ac-78}}{\Delta P_{dc}} \tag{10.4}$$

with the controller given by

$$K_m \cdot H(s) = \frac{\Delta P_{mod}}{\Delta P_{ac-78}} = 0.25 \cdot \frac{1 + 0.55s}{1 + T_2 s} \; . \tag{10.5}$$

Thus, the open loop transfer function is given by

$$L(s) = K_m \cdot G(s) \cdot H(s) \; . \tag{10.6}$$

In this example, we assume that the gain and the phase of $L(s)$ do not change simultaneously.

The curves labeled '1' in Figure 10.7 correspond to the gain root locus and phase root locus for the plant $G(s)$ with K_m and $H(s)$ equal to unity. The actual pole of the closed loop system is the intersection of gain root locus and phase root locus. It is clear that the root locus will never cross the imaginary axis into the complex left–half plane for any amount of added log-magnitude gain to $G(s) = L(s)$. The phase root locus, however, crosses the stability boundary. Part of it is in both planes, which indicates that, by adding phase angle to the open loop transfer function, the system can be stabilized or become more unstable. Phase addition is, in fact, what is achieved through the well–known phase compensation technique. Phase root locus makes it possible to determine the location of the closed loop poles when phase is added. Another interesting point of the phase root locus '1' in Figure 10.7 is that it crosses the stability boundary at two points. This means that the closed–loop system will remain stable only for phase addition within a finite region. This is a case of 'conditional stability' which may also arise when gain is added to the loop transfer function.

Figure 10.5 shows several constant-phase contours for the open loop transfer function $L(s)$. Contours of constant magnitude are shown in Figure 10.6.

To further understand the usefulness of phase root locus in control design and analysis, phase is added to the transfer function by changing the parameter T_2 in $H(s)$. Figure 10.8 shows the phase plot for different values of T_2.

The gain root loci and phase root loci for the series connection of the plant and $H(s)$ with $K_m = 1$ are labeled in Figure 10.7 above. In all cases, the phase root locus is primarily horizontal at the designed closed–loop pole. This indicates that the damping of the eigenvalue will be most affected when phase is added to the open loop transfer function. The frequency of oscillation will not vary significantly. This visualization of the temporal response for phase addition is not obvious when looking at Bode diagrams.

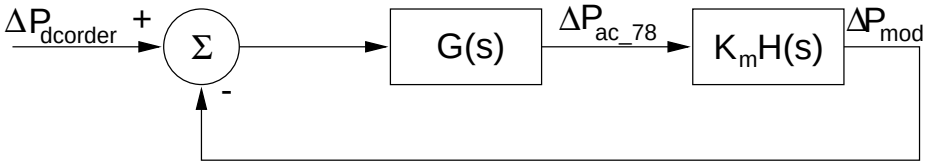

Figure 10.4. Controller Structure

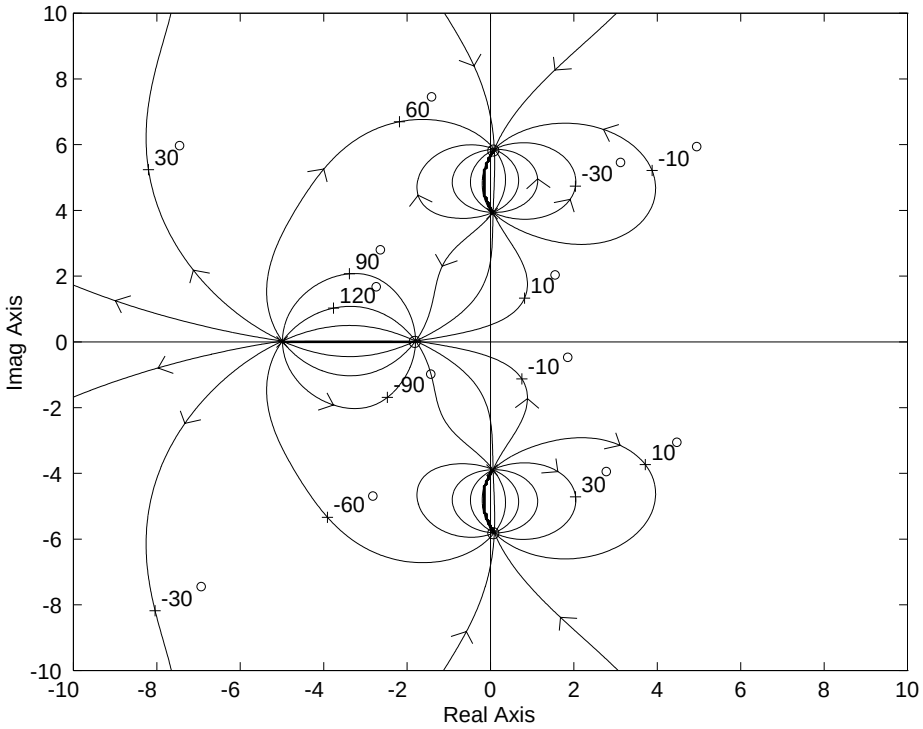

Figure 10.5. Phase Contours (Gain Root Locus)

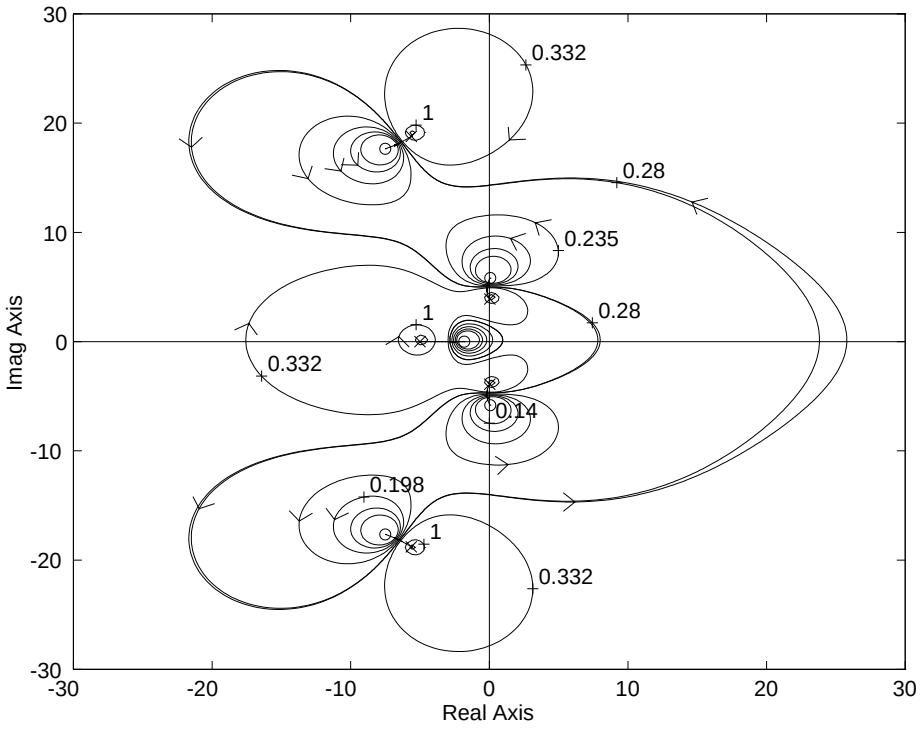

Figure 10.6. Contours of Constant Magnitude (Phase Root Locus)

The closed loop pole P given by the intersection of the gain root locus and the corresponding phase root locus indicates that the system will be stable for the chosen values. It is, however, almost marginally stable at $T_2 = 0.40$, which gives a maximum added phase of about 10°. The stability margins can be obtained as the points where gain root locus and phase root locus cross the imaginary axis. The root loci in Figure 10.7 also indicate conditional stability due to multiple crossings of the stability boundary.

The transfer function of the plant has a pair of unstable complex conjugate zeros, which will attract the poles of the closed loop system as the gain is increased. This zero pair constrains the movement of the closed loop pole into the left half plane, so that there will always be a maximum amount of damping that can be achieved irrespective of phase addition [55].

Eigenvalue analysis validates that the closed loop poles are those values indicated by the intersection of the two loci for the different T_2. Figure

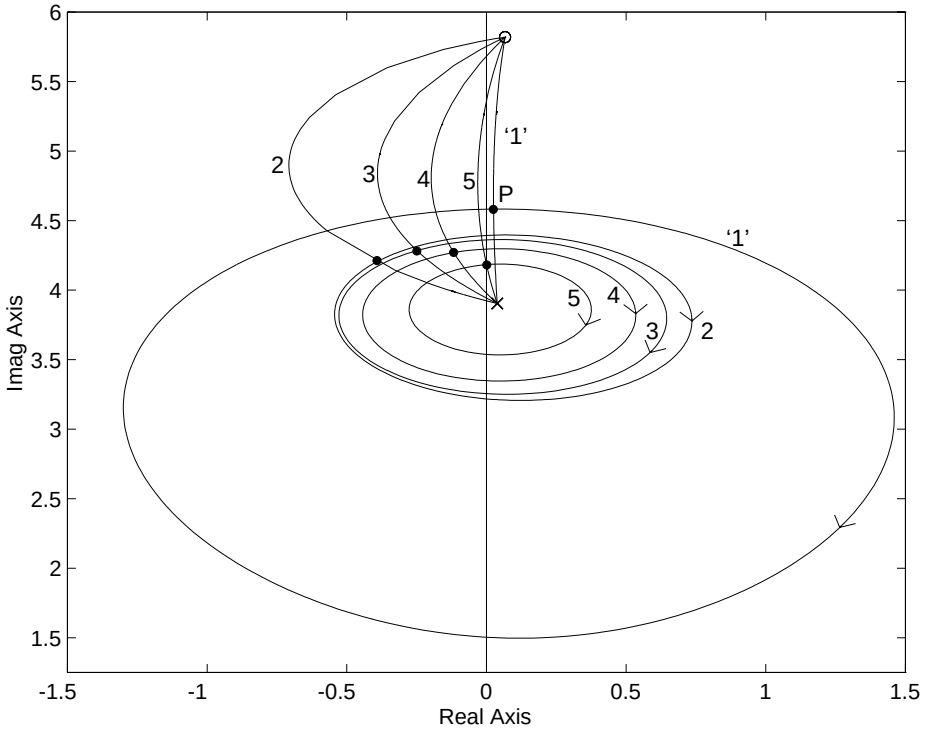

Figure 10.7. Root Locus / Phase Root Locus

10.9 shows the response to a 1% step in the DC power order for the test power system with the DC power modulation control for several values of T_2. '-' (solid), '- -', '·', '–·' correspond to $T_2 = 0.01$, 0.1, 0.20 and 0.40 respectively.

By simultaneously studying the gain root locus and phase root locus plots, the motion of the actual closed–loop poles can be tracked when phase is added to the open loop transfer function. This knowledge on the location of the new closed–loop poles is not provided by the Nyquist diagram, nor can it be extracted from the Bode diagram. It should be pointed out that Nyquist and phase root locus plots give clear information about relative and absolute stability for both minimum-phase and non-minimum-phase systems.

Also, the Bode plot relates to gain root locus and phase root locus as follows: when $\omega_{pc} = \infty$, no gain root locus branch crosses the imaginary

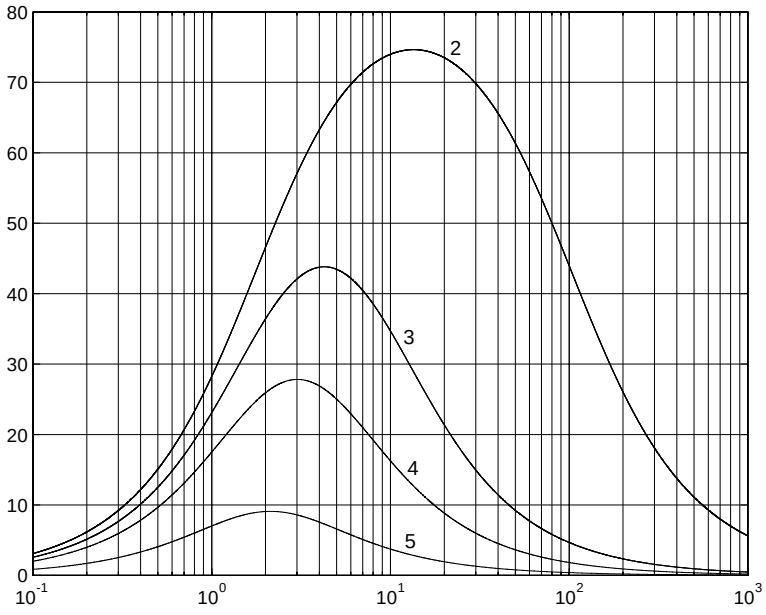

Figure 10.8. Phase Diagram for ( ) with different $_2$

axis; when $\omega_{gc} = \infty$, no phase root locus branch crosses the imaginary axis.

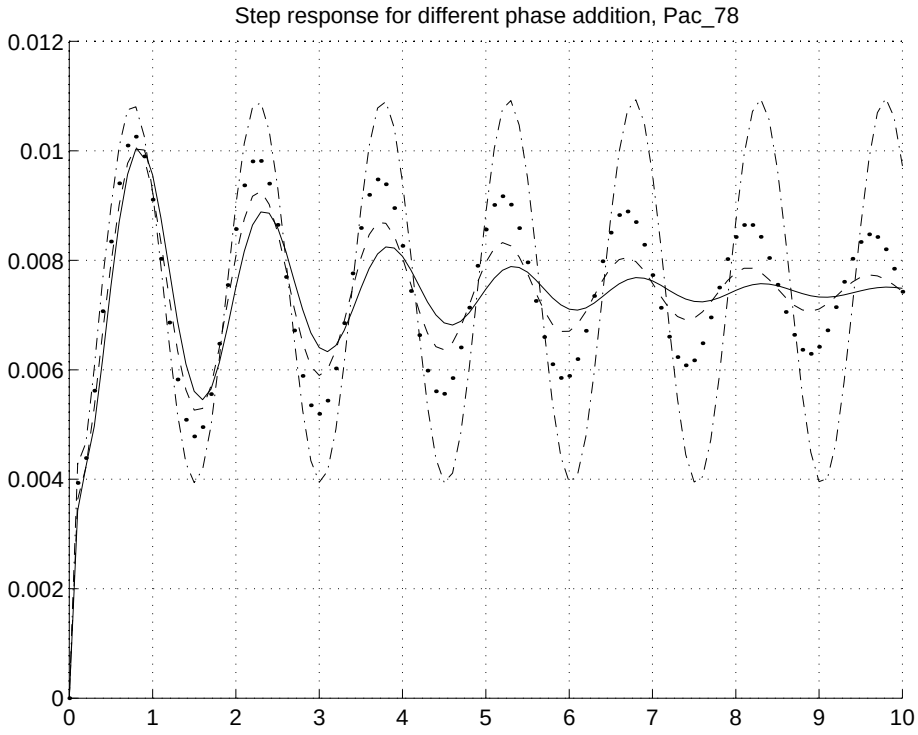

Figure 10.9. Step Response for Different Phase Addition, See Text

Chapter 11

Closure

11.1 Conclusions

This thesis has focused on the control of load flow, or active power flow, with three different FACTS devices, the controllable series capacitor (CSC), the phase angle regulator (PAR), and the unified power flow controller (UPFC).

It was shown that independent integral controllers can be used for load flow control as long as the device that controls the load flow maps the control input to the load flow in the line in a monotonic way. The controllable series capacitor and the phase angle regulator are monotonic devices in that sense; the unified power flow controller is monotonic if the magnitude of the injected voltage is used as the control variable while the angle of the injected voltage is kept constant.

The control scheme has a number of advantages:

- It is easy to implement, physically as well as in software packages like voltage stability assessment or dynamic security assessment programs.
- Since only local signals are used, it is robust with respect to the system topology. The exception to that rule is the loss of all paths parallel to the implemented devices. However, since the loss of all parallel paths implies that one degree of freedom is lost, no controller can maintain its full capabilities under these circumstances.

- Small-signal stability can be shown analytically.
- If the time constants are chosen large enough, the control scheme can be used in conjunction with methods to control dynamic phenomena.

The usability of the sensitivity matrix for determining the optimal location of controllable series capacitors in an electric power system has been investigated and examples for its use were given. Verification by simulations matched the predictions.

The influence of the UPFC on the load flow and the bus voltages in lines that are in a realistic meshed system was explored. It was shown how the control variables of the UPFC affect the load flow and the bus voltages, and the use of these variables for load flow control and bus voltage control was discussed.

The input–output stability of the controlled system was discussed. While a general proof of input–output stability was not achieved, indicators for the circumstances under which problems can arise were given.

The control scheme was implemented in a four–machine system with detailed generator models. The influence of the load flow control on a dynamic phenomenon, namely inter–area oscillations, was investigated for different controller gains. Advantages and disadvantages of high and low controller gains are discussed.

The phase root locus approach was introduced and compared to more traditional graphical tools. The usefulness of this approach for stability analysis and controller design was demonstrated with an example.

11.2 Suggestions for Future Work

Costing

Currently, estimates for the cost of the controllable series devices are extremely hard to come by. That will probably change once more of these devices are in service. It would then be meaningful to compare the capabilities and necessary ratings for these devices. Then, recommendations for these devices in different situations could be made on an economical basis.

Voltage Stability Issues

It has been shown that the devices discussed in this thesis can improve the loadability margin of electric power systems [43]. It stands to reason that it is possible to decrease the loadability margin as well. An implementation of the control scheme discussed in this thesis in a system that is prone to voltage instabilities might provide interesting insights.

Emergency Damping Control

A study of an implementation of slow integral controllers together with fast controllers designed for emergency damping control, for example, the non-linear control methods in [56], would be useful to confirm that the slow integral controllers can indeed be used together with fast stability controllers.

Generalized Root Locus

Gain root locus and phase root locus plots are qualitatively similar to plots for the electric and magnetic field [8]. In [57], the root locus analogy to potential fields leads to the introduction of a generalized root locus. Gain root locus and phase root locus are obtained as special cases of the generalized root locus. An application of the generalized root locus on controller design in electric power systems could show which additional insights on stability and robustness can be gained from the generalized root locus.

Appendix A

Modeling of the FACTS–Devices

A.1 Controllable Series Capacitor

The controllable series capacitor is simply modeled as a change in the line impedance:

$$X_{Line,new} = X_{Line,old} - |X_C| = X_{Line,old} + X_C \tag{A.1}$$

A.2 Phase Angle Regulator

A phase shifter changes the voltage magnitude and the angle of the voltage on its primary side by a factor t and an angle ϕ respectively. With designations according to Figure A.1,

$$\begin{aligned} \bar{U}_i' &= te^{j\phi}\bar{U}_i \ , \\ \bar{I}_i' &= \frac{1}{t}e^{j\phi}\bar{I}_i \ . \end{aligned} \tag{A.2}$$

The currents at the two ends of the line are given by

$$\begin{aligned} \bar{I}_i' &= (\bar{U}_i' - \bar{U}_j)\bar{y}_s + \bar{U}_i'\bar{y}_p \\ \bar{I}_j &= (\bar{U}_j - \bar{U}_i')\bar{y}_s + \bar{U}_j\bar{y}_p \ . \end{aligned} \tag{A.3}$$

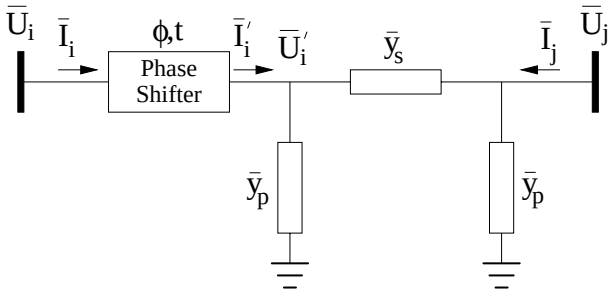

Figure A.1. Transmission Line with Phase Shifter

With (A.2),

$$\begin{aligned} \bar{I}_i &= t^2(\bar{y}_p + \bar{y}_s)\bar{U}_i - t(\bar{y}_s e^{-j\phi})\bar{U}_j \\ \bar{I}_j &= (-t\bar{y}_s e^{j\phi})\bar{U}_i + (\bar{y}_p + \bar{y}_s)\bar{U}_j \end{aligned} \tag{A.4}$$

is obtained. The bus incidence matrix changes from

$$Y_{bus} = \begin{matrix} \bar{y}_p + \bar{y}_s & \bar{y}_s \\ \bar{y}_s & \bar{y}_p + \bar{y}_s \end{matrix} \tag{A.5}$$

to

$$Y_{bus} = \begin{matrix} t^2(\bar{y}_p + \bar{y}_s) & -t\bar{y}_s e^{-j\phi} \\ -t\bar{y}_s e^{j\phi} & \bar{y}_p + \bar{y}_s \end{matrix} \quad . \tag{A.6}$$

The phase shifter changes the bus incidence matrix to a non–symmetrical matrix.

A.3 Unified Power Flow Controller

The converter in the series branch of the UPFC can be modeled as a series–connected voltage source between the buses i and j in a power system. The series voltage source can be modeled as an ideal series voltage source in line with a reactance x_s; see Figure A.2. $\bar{U}_s$ is the ideal voltage source

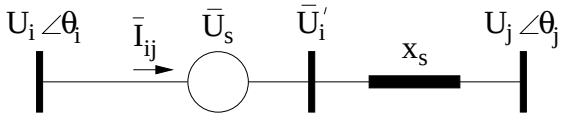

Figure A.2. Series Voltage Source

and $\bar{U}_i'$ is a fictitious voltage behind the series reactance. Obviously,

$$\bar{U}_i' = \bar{U}_s + \bar{U}_i \ . \tag{A.7}$$

The ideal series voltage source is controllable in phase and magnitude, that is,

$$\bar{U}_s = r\bar{U}_i e^{j\gamma} \text{ with } 0 < r < r_{max} \text{ and } 0 < \gamma < 2\pi \ . \tag{A.8}$$

The voltage source $\bar{U}_s$ can be replaced by a current source $\bar{I}_s = jb_s\bar{U}_s$ parallel to the admittance $b_s = 1/x_s$; see Figure A.3. The injected current

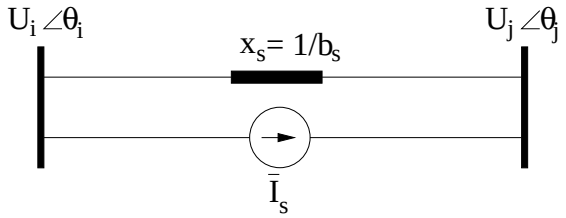

Figure A.3. Current Source Replacing Voltage Source

corresponds to injected powers $\bar{S}_{is}$ and $\bar{S}_{js}$, with

$$\bar{S}_{is} = \bar{U}_i(-\bar{I}_s)^* \ , \tag{A.9}$$

$$\bar{S}_{js} = \bar{U}_j\bar{I}_s^* \ . \tag{A.10}$$

With $\theta_{ij} = \theta_i - \theta_j$, the injected power can be expressed in terms of voltages, angles, the control parameters r and γ, and the line admittance:

$$\begin{aligned} \bar{S}_{is} &= \bar{U}_i(jrb_s\bar{U}_i e^{j\gamma})^* \\ &= -rb_sU_i^2\sin\gamma - jrb_sU_i^2\cos\gamma \end{aligned} \tag{A.11}$$

$$\begin{aligned} \bar{S}_{js} &= \bar{U}_j(-jrb_s\bar{U}_i e^{j\gamma})^* \\ &= rb_sU_iU_j\sin(\theta_{ij}+\gamma) + jrb_sU_iU_j\cos(\theta_{ij}+\gamma) \end{aligned} \tag{A.12}$$

Now, the series voltage source can be modeled with injections of active and reactive power at the buses i and j; see Figure A.4. The injected

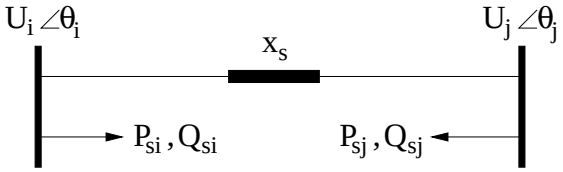

Figure A.4. Injection model

active and reactive power at buses i and j for the series branch are

$$P_{si} = rb_s U_i^2 \sin\gamma \,, \tag{A.13}$$
$$Q_{si} = rb_s U_i^2 \cos\gamma \,, \tag{A.14}$$
$$P_{sj} = -rb_s U_i U_j \sin(\theta_{ij} + \gamma) \,, \tag{A.15}$$
$$Q_{sj} = -rb_s U_i U_j \cos(\theta_{ij} + \gamma) \,. \tag{A.16}$$

For the parallel branch, the reactive power can be modeled as a separate controllable shunt reactive source. Thus, for this model, it can be assumed that the reactive power from the parallel branch is zero, and the parallel branch provides only the active power that is injected to the network via the series branch. In a lossless UPFC,

$$P_{parallel} = P_{series} \,. \tag{A.17}$$

The apparent power supplied by the series branch is

$$\bar{S}_{series} = \bar{U}_s \bar{I}_{ij}^* = re^{j\gamma}\bar{U}_i \left(\frac{\bar{U}_i' - \bar{U}_j}{jx_s} \right)^* \,, \tag{A.18}$$

which leads to the active and reactive power supplied by the series branch:

$$P_{series} = rb_s U_i U_j \sin(\theta_{ij} + \gamma) - rb_s U_i^2 \sin\gamma \tag{A.19}$$
$$Q_{series} = -rb_s U_i U_j \cos(\theta_{ij} + \gamma) + rb_s U_i^2 \cos\gamma + r^2 b_s U_i^2 \tag{A.20}$$

To get the injection model for the full UPFC, P_{si} has to be corrected to account for the active power in the parallel branch; that is, equations

(A.13) and (A.13) have to be added to get P_{si}. The injected powers for the full UPFC are then given by

$$P_{si} = rb_s U_i U_j \sin(\theta_{ij} + \gamma) \,, \tag{A.21}$$

$$Q_{si} = rb_s U_i^2 \cos\gamma \,, \tag{A.22}$$

$$P_{sj} = -rb_s U_i U_j \sin(\theta_{ij} + \gamma) \,, \tag{A.23}$$

$$Q_{sj} = -rb_s U_i U_j \cos(\theta_{ij} + \gamma) \,. \tag{A.24}$$

As expected for a lossless UPFC, the active power exchange balance with the network is zero.

This injection model can easily be incorporated in a load flow program. If a UPFC is located in the line between buses i and j, the bus incidence matrix is modified by adding a reactance equivalent to x_s between bus i and j. The Jacobian matrix is modified by addition of the appropriate injection powers. For the linearized load flow model

$$\begin{array}{c} \Delta P \\ \Delta Q \end{array} = \begin{array}{cc} H & N \\ J & L \end{array} \begin{array}{c} \Delta\theta \\ \Delta U/U \end{array} \,, \tag{A.25}$$

the Jacobian is modified as described in Table A.1, where the superscript o denotes the Jacobian matrix elements without the UPFC.

$H_{(i,i)} = H^o_{(i,i)} - Q_{sj}$	$N_{(i,i)} = N^o_{(i,i)} - P_{sj}$
$H_{(i,j)} = H^o_{(i,j)} + Q_{sj}$	$N_{(i,j)} = N^o_{(i,j)} - P_{sj}$
$H_{(j,i)} = H^o_{(j,i)} + Q_{sj}$	$N_{(j,i)} = N^o_{(j,i)} + P_{sj}$
$H_{(j,j)} = H^o_{(j,j)} - Q_{sj}$	$N_{(j,j)} = N^o_{(j,j)} + P_{sj}$
$J_{(i,i)} = J^o_{(i,i)}$	$L_{(i,i)} = L^o_{(i,i)} + 2Q_{si}$
$J_{(i,j)} = J^o_{(i,j)}$	$L_{(i,j)} = L^o_{(i,j)}$
$J_{(j,i)} = J^o_{(j,i)} - P_{sj}$	$L_{(j,i)} = L^o_{(j,i)} + Q_{sj}$
$J_{(j,j)} = J^o_{(j,j)} + P_{sj}$	$L_{(j,j)} = L^o_{(j,j)} + Q_{sj}$

Table A.1. Modification of Jacobian Matrix for UPFC

Appendix B

IEEE 30 Bus Test System – System Data

The topology of the system is shown in Figure 4.9. All data here are in pu with a base power of 100 MVA.

B.1 Bus Data

Table B.1: Bus Data for IEEE 30 Bus Test System

Nr.	Type	ϑ	U_{fix}	P_{load}	Q_{load}	P_{gen}	Q_{gen}	B_{shunt}	U_{base}
1	Slack	0	1.060	-	-	-	-	0.000	132
2	PU	-	1.045	0.217	0.000	0.4	-	0.000	132
3	PQ	-	-	0.024	0.012	0.0	0	0.000	132
4	PQ	-	-	0.076	0.016	0.0	0	0.000	132
5	PU	-	1.010	0.942	0.000	0.0	-	0.000	132
6	PQ	-	-	0.000	0.000	0.0	0	0.000	132
7	PQ	-	-	0.228	0.109	0.0	0	0.000	132
8	PU	-	1.010	0.300	0.000	0.0	-	0.000	132
9	PQ	-	-	0.000	0.000	0.0	0	0.000	1
10	PQ	-	-	0.058	0.020	0.0	0	0.190	33
11	PU	-	1.082	0.000	0.000	0.0	-	0.000	11

continued ⟶

Table B.1: (Bus Data Continued)

Nr.	Type	ϑ	U_{fix}	P_{load}	Q_{load}	P_{gen}	Q_{gen}	B_{shunt}	U_{base}
12	PQ	-	-	0.112	0.075	0.0	0	0.000	33
13	PU	-	1.071	0.000	0.000	0.0	-	0.000	11
14	PQ	-	-	0.062	0.016	0.0	0	0.000	33
15	PQ	-	-	0.082	0.025	0.0	0	0.000	33
16	PQ	-	-	0.035	0.018	0.0	0	0.000	33
17	PQ	-	-	0.090	0.058	0.0	0	0.000	33
18	PQ	-	-	0.032	0.009	0.0	0	0.000	33
19	PQ	-	-	0.095	0.034	0.0	0	0.000	33
20	PQ	-	-	0.022	0.007	0.0	0	0.000	33
21	PQ	-	-	0.175	0.112	0.0	0	0.000	33
22	PQ	-	-	0.000	0.000	0.0	0	0.000	33
23	PQ	-	-	0.032	0.016	0.0	0	0.000	33
24	PQ	-	-	0.087	0.067	0.0	0	0.043	33
25	PQ	-	-	0.000	0.000	0.0	0	0.000	33
26	PQ	-	-	0.035	0.023	0.0	0	0.000	33
27	PQ	-	-	0.000	0.000	0.0	0	0.000	33
28	PQ	-	-	0.000	0.000	0.0	0	0.000	132
29	PQ	-	-	0.024	0.009	0.0	0	0.000	33
30	PQ	-	-	0.106	0.019	0.0	0	0.000	33

B.2 Branch Data

Table B.2: Branch Data for IEEE 30 Bus Test System

Nr.	Type	Bus1	Bus2	R	X	$B/2$	n_1/n_2
1	Line	1	2	0.0192	0.0575	0.0264	0
2	Line	1	3	0.0452	0.1852	0.0204	0
3	Line	2	4	0.0570	0.1737	0.0184	0
4	Line	3	4	0.0132	0.0379	0.0042	0
5	Line	2	5	0.0472	0.1983	0.0209	0
6	Line	2	6	0.0581	0.1763	0.0187	0
7	Line	4	6	0.0119	0.0414	0.0045	0
8	Line	5	7	0.0460	0.1160	0.0102	0

continued ⟶

Table B.2: Branch Data (Continued)

Nr.	Type	Bus1	Bus2	R	X	$B/2$	n_1/n_2
9	Line	6	7	0.0267	0.0820	0.0085	0
10	Line	6	8	0.0120	0.0420	0.0045	0
11	Trafo	6	9	0	0.2080	0	0.978
12	Trafo	6	10	0	0.5560	0	0.969
13	Line	9	11	0	0.2080	0	0
14	Line	9	10	0	0.1100	0	0
15	Trafo	4	12	0	0.2560	0	0.932
16	Line	12	13	0	0.1400	0	0
17	Line	12	14	0.1231	0.2559	0	0
18	Line	12	15	0.0662	0.1304	0	0
19	Line	12	16	0.0945	0.1987	0	0
20	Line	14	15	0.2210	0.1997	0	0
21	Line	16	17	0.0824	0.1923	0	0
22	Line	15	18	0.1073	0.2185	0	0
23	Line	18	19	0.0639	0.1292	0	0
24	Line	19	20	0.0340	0.0680	0	0
25	Line	10	20	0.0936	0.2090	0	0
26	Line	10	17	0.0324	0.0845	0	0
27	Line	10	21	0.0348	0.0749	0	0
28	Line	10	22	0.0727	0.1499	0	0
29	Line	21	22	0.0116	0.0236	0	0
30	Line	15	23	0.1000	0.2020	0	0
31	Line	22	24	0.1150	0.1790	0	0
32	Line	23	24	0.132	0.27	0	0
33	Line	24	25	0.1885	0.3292	0	0
34	Line	25	26	0.2544	0.3800	0	0
35	Line	25	27	0.1093	0.2087	0	0
36	Trafo	28	27	0	0.3960	0	0.968
37	Line	27	29	0.2198	0.4153	0	0
38	Line	27	30	0.3202	0.6027	0	0
39	Line	29	30	0.2399	0.4533	0	0
40	Line	8	28	0.0636	0.2000	0.0214	0
41	Line	6	28	0.0169	0.0599	0.0065	0

Appendix C

Sensitivity Matrix for CSC

A power system in the steady state is modeled by the load flow equations

$$F(X, Z, D) = 0\,, \tag{C.1}$$

with the vector of state variables X, the vector of control variables Z, and the vector of parameters D.

The sensitivity of the states X to the inputs Z determines changes ΔX that result from small changes ΔZ around a nominal point Z^0, assuming that a solution X^0 for the nominal control vector Z^0 and the nominal parameter D^0 exists, that is,

$$F(X_0, Z_0, D_0) = 0\,. \tag{C.2}$$

The first order Taylor series expansion of Equation (C.1) in the neighborhood of (X^0, Z^0, D^0) is

$$\begin{aligned} 0 = F(X^0 + \Delta X, Z^0 + \Delta Z, D^0 + \Delta D) \approx \\ F(X^0, Z^0, D^0) + F_X \Delta X + F_Z \Delta Z + F_D \Delta D\,, \end{aligned} \tag{C.3}$$

with the Jacobian matrices F_X, F_Z, and F_D that are computed at the nominal operating point (X^0, Z^0, D^0). If the approximation is accurate, then Equations (C.2) and (C.3) imply

$$F_X \Delta X + F_Z \Delta Z + F_D \Delta D = 0\,. \tag{C.4}$$

Assuming that F_X is invertible,

$$\Delta X = -F_X^{-1} F_Z \Delta Z - F_X^{-1} F_D \Delta D \tag{C.5}$$

follows.

At the equilibrium, the load flow vector W^0 is determined by a function H, that is,

$$W^0 = H(X^0, Z^0) \,, \tag{C.6}$$

which with a preturbation ΔZ becomes

$$W^0 + \Delta W = H(X^0 + \Delta X, Z^0 + \Delta Z) \,. \tag{C.7}$$

Linearization yields

$$\Delta W \approx W_X \Delta X + W_Z \Delta Z \,. \tag{C.8}$$

Expanding (C.5) into (C.8) delivers

$$\Delta W = \ -W_X F_X^{-1} F_Z + W_Z \ \ \Delta Z + \ -W_X F_X^{-1} F_D \ \ \Delta D \,, \tag{C.9}$$

which, assuming $\Delta D = 0$, leads to

$$\Delta W = \ -W_X F_X^{-1} F_Z + W_Z \ \ \Delta Z \,. \tag{C.10}$$

F_X is the Jacobian matrix that is known from standard Newton–Raphson load flow computations. The Jacobian matrices F_Z, W_X, and W_Z are given below.

C.1 Notation

In this part, the following notations and definitions are used:

- n_ℓ: number of transmission lines
- ℓ, ℓ': indices for transmission lines
- $z_\ell = r_\ell + j(x_l - x_C\ )$: series impedance of line ℓ
- $y_\ell = g_\ell + jb_\ell$: series admittance of line ℓ.
- Z_C: vector of series capacitive resistances
- P: vector of active power injections at all nodes except slack node
- Q: vector of reactive power injections at PQ–nodes

- $\mathcal{S}^{L(i)}$: set of lines connected to bus i
- $\mathcal{S}^{PU}$: set of PU–nodes
- $\mathcal{S}^{PQ}$: set of PQ–nodes
- SLK: slack node
- $\theta_{ij} = \theta_i - \theta_j$
- $\gamma_\ell = \dfrac{\partial g_\ell}{\partial x_C} = \dfrac{2r_\ell(x_l - x_C\,)}{r_\ell^2 + (x_\ell - x_C\,)^{2\ 2}}$
- $\beta_\ell = \dfrac{\partial b_\ell}{\partial x_C} = \dfrac{r_\ell^2 - (x_\ell - x_C\,)^2}{r_\ell^2 + (x_\ell - x_C\,)^{2\ 2}}$

C.2 Jacobian Matrix $\boldsymbol{F_Z}$

$$F_Z = \begin{matrix} P_Z \\ Q_Z \end{matrix} \tag{C.11}$$

$$\frac{\partial P_i}{\partial Z_{C\ell}} = \begin{matrix} -\gamma_\ell(U_i^2 - U_iU_j\cos\theta_{ij}) + \beta_\ell U_iU_j\sin\theta_{ij} & i \neq SLK, \ell \in \mathcal{S}^{L(i)} \\ 0 & \text{otherwise} \end{matrix} \tag{C.12}$$

$$\frac{\partial Q_i}{\partial Z_{C\ell}} = \begin{matrix} \beta_\ell(-U_i^2 + U_iU_j\cos\theta_{ij}) + \gamma_\ell U_iU_j\sin\theta_{ij} & i \in \mathcal{S}^{PQ}, \ell \in \mathcal{S}^{L(i)} \\ 0 & \text{otherwise} \end{matrix} \tag{C.13}$$

C.3 Jacobian Matrix W_X

$$W_X = \begin{matrix} W_\theta & W_U \end{matrix} \tag{C.14}$$

$$\frac{\partial W_\ell}{\partial \theta_i} = \begin{matrix} g_\ell U_i U_j \sin\theta_{ij} - b_\ell U_i U_j \cos\theta_{ij} & i \neq SLK \ i,j \in \ell \\ 0 & \text{otherwise} \end{matrix} \tag{C.15}$$

$$\frac{\partial W_\ell}{\partial \theta_j} = \begin{matrix} -g_\ell U_i U_j \sin\theta_{ij} + b_\ell U_i U_j \cos\theta_{ij} & i \neq SLK \ i,j \in \ell \\ 0 & \text{otherwise} \end{matrix} \tag{C.16}$$

$$\frac{\partial W_\ell}{\partial U_i} = \begin{matrix} 2g_\ell U_i - g_\ell U_j \cos\theta_{ij} - b_\ell U_j \sin\theta_{ij} & i \in \mathcal{S}^{PU} \ i,j \in \ell \\ 0 & \text{otherwise} \end{matrix} \tag{C.17}$$

$$\frac{\partial W_\ell}{\partial U_j} = \begin{matrix} -g_\ell U_i \cos\theta_{ij} - b_\ell U_j \sin\theta_{ij} & i \in \mathcal{S}^{PU} \ i,j \in \ell \\ 0 & \text{otherwise} \end{matrix} \tag{C.18}$$

C.4 Jacobian Matrix W_Z

$$W_Z = \begin{matrix} W_Z \end{matrix} \tag{C.19}$$

$$\frac{\partial W_\ell}{\partial Z_{C\,\ell'}} = \begin{matrix} -\gamma_\ell (U_i^2 - U_i U_j \cos\theta_{ij}) + \beta_\ell U_i U_j \sin\theta_{ij} & \ell = \ell' \\ 0 & \ell \neq \ell' \end{matrix} \tag{C.20}$$

References

[1] Arnim Herbig and Göran Andersson. Control of power flows in transmission systems. In *Proceedings of the International Power Engineering Conference*, pages 431–435. Nanyang Technological University, May 1997.

[2] Arnim Herbig and Göran Andersson. Optimal placement of controllable series capacitors in an electric power system. In *Proceedings of the 1998 Large Engineering Systems Conference on Power Engineering*, pages 167 – 170, June 1998.

[3] Arnim Herbig, Mehrdad Ghandhari, Lawrence Jones, Denis Lee, and Göran Andersson. Power flow and stability control in power systems. In *Bulk Power Systems Dynamics and Control IV – Restructuring. Symposium Proceedings*, pages 91–104. International Institute for Research and Education in Power System Dynamics, August 1998.

[4] L. E. Jones, Arnim Herbig, and Göran Andersson. Phase root locus approach to design robust controllers for power systems. In *Proceedings of the 32nd Universities Power Engineering Conference*, volume 1, pages 519 – 522, 1997.

[5] Sally Hunt and Graham Shuttleworth. Unlocking the grid. *IEEE Spectrum*, pages 20–25, July 1996.

[6] Jeff Donahue. The role of HVDC transmission for independent transmission projects. In *Proceedings of the IEEE Power Engineering 1999 Winter Meeting*, pages 125–126, 1999.

[7] W.R. Evans. Graphical analysis of control systems. *AIEE Transactions*, 67:547–551, 1948.

[8] T.J. Cavicci. Phase root locus and relative stability. *IEEE Control Systems Magazine*, 16(4):69–77, August 1996.

[9] Lawrence Markus. *Differential Equations, Dynamical Systems and Control Science*, volume 152 of *Lecture Notes in Pure and Applied Mathematics*, chapter "A Brief History of Control", pages xxv – xl. Marcel Dekker, Inc., New York · Basel · Hong Kong, 1994.

[10] H.S. Black. Inventing the negative feedback amplifier. *IEEE Spectrum*, pages 55–60, December 1977.

[11] H. Nyquist. Regeneration theory. *Bell System Technical Journal*, 11:126–147, 1932.

[12] H.W. Bode. *Network Analysis and Feedback Amplifier Design.* D, Van Nostrand, Princeton, New Jersey, 1945.

[13] C. G. Moore C. J. Harris and M. Brown. *Intelligent Control - Aspects of Fuzzy Logic and Neural Nets*, volume 6 of *World Scientific Series in Robotics and Automated Systems.* World Scientific Publishing Co. Pte. Ltd., Signapore · New Jersey · London · Hong Kong, 1993.

[14] Michael Green and David J. N. Limebeer. *Linear Robust Control.* Prentice Hall Information and System Sciences Series. Prentice–Hall Inc., 1995.

[15] Peter M. Young, Matthew P. Newlin, and John C. Doyle. μ analysis with real parametric uncertainty. In *Proceedings of the 30th Conference on Decision and Control*, pages 1251–1256, December 1991.

[16] Chuen Chien Lee. Fuzzy logic in control systems: Fuzzy logic controller—Part I. *IEEE Transactions on Systems, Man, and Cybernetics*, 20(2):404–418, 1990.

[17] Chuen Chien Lee. Fuzzy logic in control systems: Fuzzy logic controller—Part II. *IEEE Transactions on Systems, Man, and Cybernetics*, 20(2):419–435, 1990.

[18] E. H. Mamdani. Twenty years of fuzzy control: Experiences gained and lessons learnt. In *Second IEEE International Conference on Fuzzy Systems*, volume 1, pages 339–344, 1993.

[19] D. A. Linkens and M. F. Abbod. Self–organizing fuzzy logic control for real–time processes. In *Proceedings of the International Conference on Control 1991*, volume 2, pages 971–976, 1991.

[20] D. A. Linkens and J. S. Shieh. Self–organizing fuzzy modeling for nonlinear system control. In *Proceedings of the 1992 IEEE International Symphosium on Intelligent Control*, pages 210–215, 1992.

[21] Andreas Zell. *Simulation neuronaler Netze.* Addison–Wesley Publishing Company, Bonn · Paris · Reading, Massachusetts [et al.], first edition, 1994.

[22] Philip Klahr and Donald A. Waterman, editors. *Expert Systems — Techniques, Tools and Applications.* Addison Wesley, 1986.

[23] P. Albertos, A. Crespo, F. Morant, and J.L. Navarro. Intelligent controllers issue. In *[58]*, pages 27 – 40, 1992.

[24] S.J. Corfield, R.J.C. Fraser, and C.J. Harris. Architectures for real–time intelligent control of autonomous vehicles. *Computing & Control Engineering Journal*, November 1991.

[25] Marija D. Ilić and Shell Liu. *Hierarchical Power Systems Control — Its Value in a Changing Industry.* Advances in Industrial Control. Springer–Verlag Londom, 1996.

[26] Thomas P. Hughes. *Networks of Power: Electrification in Western Society 1880 – 1930.* Johns Hopkins University Press, 1993.

[27] Statens Offentliga Utredningar. Säker elförsörjning. Betänkande av Kommisionen om elförsörjningens sårbarhet, (In Swedish), 1984.

[28] Narain G. Hingorani. Flexible AC transmission. *IEEE Spectrum*, pages 40–45, April 1993.

[29] Einar Larsen. Power flow control with rotary transformers. United States Patent 5 841 267, November 1998.

[30] Einar V. Larsen. A classical approach to constructing a power flow controller. In *Proceedings of the 1999 IEEE Power Engineering Society Summer Meeting*, volume 2, pages 1192–1195, July 1999.

[31] M. Leijon, F. Owman, T. Sörqvist, C. Parkegren, S. Lindahl, and T. Karlsson. Powerformer®: A giant step in power plant engineering. In *Electric Machines and Drives, International Conference IEMD '99*, pages 830–832, 1999.

[32] Roger Dettmer. The heart of a new machine. *IEE Review*, 44(6):255–258, November 1998.

[33] Laszlo Gyugyi. Power electronics in electric utilities: Static var compensators. *Proceedings of the IEEE*, 76(4):483–494, April 1988.

[34] Laszlo Gyugyi. Reactive power generation and control by thyristor circuits. *IEEE Transactions on Industry Applications*, 15(5), 1979.

[35] Jaques Brochu, Pierre Pelletier, François Beauregard, and Gaston Morin. The interphase power controller — a new concept for managing power flow within ac networks. *IEEE Transactions on Power Delivery*, 9(2):833–841, April 1993.

[36] César A. Luongo. Superconducting storage systems: An overview. *IEEE Transactions on Magnetics*, 32(4):2214–2223, July 1996.

[37] M. Noroozian and G. Andersson. Power flow control by use of controllable series components. *IEEE Transactions on Power Delivery*, pages 1420–1429, July 1993.

[38] Mojtaba Noroozian. *Exploring Benefits of Controllable Series Compensators in Power Systems.* PhD thesis, Department of Electric Power Engineering, Electric Power Systems, Royal Institute of Technology, Stockholm, Sweden, 1994.

[39] V. Venkatasubramanian, X. Jiang, H. Schättler, and J. Zaborsky. Current status of the taxonomy theory of large power system dynamics — DAE systems with hard limits. In *Proceedings of the NSF International Symphosium on Bulk Power System Phenomena: Voltage Stability and Security III*, pages 15–103, 1994.

[40] Thierry Van Cutsem and Costas Vournas. *Voltage Stability of Electric Power Systems.* The Kluwer International Series in Engineering and Computer Science. Kluwer Academic Publishers, Boston · London · Dordrecht, 1998.

[41] `ftp://wahoo.ee.washington.edu/pub/` (contains data for IEEE 30 bus system).

[42] E. Kreyszig. *Advanced Engineering Mathematics*. John Wiley & Sons, New York, 1983.

[43] Zeno T. Faur and Claudio A. Cañizares. Effects of FACTS devices on system lodability. In *Proceedings of the North American Power Symposium (NAPS)*, pages 520–524, Bozeman, Montana, October 1995.

[44] Dr. L. Gyugyi. Unified power–flow concept for flexible AC transmission systems. *IEE Proceedings-C*, 139(4):323–331, July 1992.

[45] M. R. Lund D. M. Hamai T. R. Rietman D. R. Torgerson A. Edris C. D. Schauder, L. Gyugyi. Operation of the unified power flow controller under practical constraints. *IEEE Transactions on Power Delivery*, 13(2):630–637, April 1998.

[46] S. L. Williams T. R. Rietman D. R. Torgerson A. Edris L. Gyugyi, C. D. Schauder. The unified power flow controller: A new approach to power transmission control. *IEEE Transactions on Power Delivery*, 10(2):1085–1097, April 1995.

[47] Andrew R. Teel. On graphs, conic relations, and input–output stability of nonlinear feedback systems. *IEEE Transactions on Automatic Control*, 41(5):702–708, May 1996.

[48] William S. Levine, editor. *The Control Handbook*. CRC Press, Inc., 1996.

[49] S. T. Glad. Nonlinear control theory. Technical Report LiTH-ISY-I-1081, Department of Electrical Engineering, Linköping University, 1990.

[50] D. C. Lee P. Kundur and H. M. Zein el din. Power system stabilizers for thermal units: Analytical techniques and on–site validation. *IEEE Transactions on Power Apperatus and Systems*, pages 614–621, 1981.

[51] P. Kundur M. Klein, G. J. Rogers. A fundamental study of inter–area oscillations in power systems. *IEEE Transactions on Power Systems*, 6(3):914–921, August 1991.

[52] P. Kundur. *Power Systems Stability and Control*. EPRI Power System Engineering Series. McGraw-Hill Inc., 1994.

[53] H. R. Fankhauser, T. Adielson, M. Aneros, A. Edris, L. Lindkvist, and S. Torseng. SIMPOW — a digital power system simulator. *ABB Review*, 3(7):27–38, 1990.

[54] IEEE Power Engineering Society. Inter–area oscillations in power systems. IEEE Catalog Number 95 TP 101, October 1994.

[55] Lawrence E. Jones. *On Zero Dynamics and Robust Control of Large AC and DC Power Systems*. PhD thesis, Royal Institute of Technology, Stockholm, Sweden, 1999.

[56] Mehrdad Ghandhari. Control of power oscillations in transmission systems using controllable series devices. Licenciate Thesis, Royal Institute of Technology, Stockholm, Sweden, 1997.

[57] Ciann-Dong Yang and Fang-Bo Yeh. On modeling root–locus behavior. In *Proceedings of the 53rd Conference on Decision and Control*, volume 3, pages 2151–2156, December 1994.

[58] A. Ollero and E.F. Camacho, editors. *Intelligent Components and Instruments for Control Applications — Selected Papers from the IFAC Symposium, Malaga, Spain, 20–22 May*. Pergamon Press, Oxford · New York · Seoul · Tokyo, 1992.